FREIE UNIVERSITÄT BERLIN

The evolution of carbonate weathering carbon sinks under climatic and anthropogenic perturbations

Dissertation

Submission for the Academic Title
Doktor der Naturwissenschaften
(Dr. rer. nat.)

Fachbereich Geowissenschaften

Freie Universität Berlin

Submitted by:
Sibo Zeng

May 2021

I hereby declare the except where specific reference is made to the work of others, the contents of this dissertation are original and have not been submitted in whole or in part for consideration for any other degree or qualification in this, or any other University. This dissertation is the results of my own work and includes nothing which is the outcome of work done in collaboration, except where specifically indicated in the text.

Sibo Zeng
Berlin, May 2021

First referee:	Prof. Dr. Georg Kaufmann
Second referee:	Prof. Dr. Nico Goldscheider
Defense:	16.07.2021

Summary

The chemical weathering processes of continental rocks are thought to be a major mechanism that control the long-term global climate. Carbonate rock on land surface is the largest carbon reservoir comparing to atmosphere and ocean. The chemical weathering products of carbonates constitutes nearly half of the dissolved loads in terrestrial water systems, although carbonates only covers 15.2% of ice-free continental surface. The aquatic photoautotroph in inland waters can utilize the carbonate weathering product HCO_3^- to produce organic carbon, thus forming a geological long-term carbon sink. This coupled biological carbon pump effect (BCP) may be responsible to a large proportion of terrestrial missing carbon sink. Due to the rapid dissolution kinetics, carbonate weathering process presents strongly sensitivity to environmental perturbations such as climate change and human land-use conversion. The better understanding of how carbonate weathering related carbon sink evolve under global change is significant to predict the future global carbon cycle and climate dynamics. This cumulative thesis consists of four scientific papers that together characterize the mechanisms and variations of carbonate weathering carbon sink under global change in terms of CO_2 capture, inorganic carbon sink transfer, and organic carbon formation.

In order to discuss the variation of carbonate weathering carbon sink in a dynamic earth system, a better understanding of the behavior of carbonate weathering process under different natural condition is essential. The first paper of this thesis selects three typical karst catchments with different geo-backgrounds to quantify the impacts of temperature, water flow and vegetation cover on carbonate weathering intensity and related carbon sink flux. Results indicate that the role of climate and vegetation may equally important, which play as a counterbalance effect in controlling the HCO_3^- concentration and carbon sink flux. Due to the chemo-statistic behavior of solutes flux, the total amount of carbon sink is depending on the water yield rate instead of HCO_3^- concentration. By comparing the results of three soil pCO_2 models with global spring records, the second study find that net primary production (*NPP*) could be the optimal predictor for evaluating carbonate weathering intensity in most areas. On account of the disproportional influence of HCO_3^- and water flow on total carbon sink budget, the spatial distribution of carbonate weathering carbon sink flux is mainly dominated by global runoff pattern. By the insight of global spring evidences and the results of global simulations, a new mixed effect model is constructed to predict the historical and future variations of carbonate weathering carbon sink. This model indicates that this carbon sink flux will experience a widespread and consistent increase, ranging from +9.8 % (RCP4.5) to +17.1 % (RCP8.5) during 1950 to 2100. This carbon sink enhancement will mostly occur in low latitudes accompanied by intense human agricultural extension, implying that will have a great potential for human land-use strategies to regulate this carbon sink in the future. Finally, the impacts of different land-use strategies on carbonate weathering coupled biological carbon pump effect (BCP) has been detected in an artificial karst simulation test. Results suggest that DIC fertilization

(high HCO_3^- input) will release the CO_2 limitation in high pH aquatic environment, promoting the ecosystem primary production and in-stream organic carbon export. The high HCO_3^- inputs in grassland and shrubland dominant spring-pond systems lead a higher organic carbon export than that in bare rock land.

In summary, the findings in this thesis indicate a considerable feedback that carbonate weathering carbon sink may response to climate and land-use change, which could have a great potential for mitigating the future global warming. Although the increasing global temperature will constrain the carbonate weathering intensity, yet human land-use activities may inversely lead a carbon sink enhancement. The carbonate weathering coupled terrestrial biological carbon pump effect is another key mechanism that can use to increase the atmospheric CO_2 remove by human land-use strategies. Results in this thesis stress the significant role of carbonate weathering carbon sink for global carbon cycle and its great potential for mitigating the global warming.

Zusammenfassung

Die chemische Verwitterung von Gesteinen ist ein wesentlicher Prozess, der die langfristige Klimaveränderung beeinflusst. Kalk- und Dolomitgesteine stellen hier die größte Quelle an Kohlenstoff dar, verglichen mit Atmosphäre und Ozean. Die chemischen Verwitterungsprodukte der Karbonate tragen fast die Hälfte der Lösungsfracht in terrestrischen Abflußsystemem bei, obwohl Karbonate nur 15.2% der eisfreien Landschaftsoberfläche ausmachen. Photoautotrophe Organismen im Süßwasser können das Verwitterungsprodukt Bikarbonat nutzen, um Kohlenstoff herzustellen, eine weitere Kohlenstoffsenke. Diese gekoppelte biologische Kohlstoffpumpe (BCP) stellt möglicherweise einen Grossteil des fehlenden Anteils an der Kohlenstoffsenke dar.Aufgrund der schnellen Lösungskinetik der Kalklösung reagiert die Karbonatverwitterung schnell auf Umwelteinflüsse wie dem Klimawandel und der Änderung der Landnutzung. Es ist daher essentiell, die Karbonatverwitterung besser zu verstehen, um zukünftige Klimaänderungen besser vorherzusagen.

Diese kumulative Doktorarbeit stellt im Zentralteil vier Veröffentlichungen vor, die Mechanismen und Variationen der Karbonatverwitterung beschreiben.

Die Karbonatverwitterung als Kohlenstoffsenke braucht ein besseres Verständnis der Reaktion des Verwitterungsprozesses aufgrund von natürlichen Änderungen im Klimasystem. In der ersten Publikation werden deshalb drei verschiedene Einzugsgebiete vorgestellt auf verschiedenen Klimabereichen. Die Ergebnisse zeigen einen Einfluss sowohl von Klima- als auch von Vegetationsänderungen, Die einen gegenteiligen Einfluss auf die Karbonatlösung haben. Vor allem die Abflussmenge kontrolliert den Betrag der Kohlenstoffsenke.

In der zweiten Publikation werden drei verschiedene Boden-CO_2-Modelle betrachtet und mit dem Chemismus von Quellschüttungen verglichen. Hier stellt sich heraus das die „net primary production“ am besten die Variabilität der Bikarbonat-Variation beschreiben kann. Demnach kontrolliert der Oberflächenabfluss den Betrag der Kohlenstoffsenke am stärksten.

In einer dritten Publikation wird mit Hilfe der Quellschüttungsdaten ein neues Modell entwickelt, dass heutige und zukünftige Karbonatverwitterung beschreiben kann. Aus dem Modell lassen sich Anstiege des Kohlenstoffflusses von +9.8% bis +17.1% ableiten für den Zeitraum 1950-2100. Dieser Anstieg findet im Wesentlichen im niedrigen Breiten statt, so dass hier eine Landnutzungsänderung als möglicher Eingriff in die zukünftige Klimaentwicklung in Betracht gezogen werden kann.

In einer vierten Publikation werden verschiedene Landnutzungsszenarien in einem Feldlabor nachgestellt. Hier lassen sich Rückschlüsse sowohl auf dem Kohlenstoffkreislauf als auch zum Effekt der biologischen Kohlenstoffpumpe quantifizieren.

Die Ergebnisse dieser Doktorarbeit zeigen ein Feedback zwischen natürlichen Klimavariationen und anthropogenen Landnutzungsänderungen einerseits und der Karbonatverwitterung andererseits. Während ein globaler Temperaturanstieg den Betrag der Karbonatverwitterung limitiert, können Landnutzungsänderungen zu einer Erhöhung der Karbonatverwitterung führen. Auch die biologische Kohlenstoffpumpe führt zu einem Anstieg der Karbonatverwitterung.

Table of Contents

1. Introduction

1.1. Motivation

A fundamental question of climate change for the scientific community is how to balance the atmospheric carbon dioxide ($CO_{2(atm)}$) budget, and central to this issue is how to tackle the missing carbon-sink problem. The terrestrial carbon cycle is thought to be a major source that accounts for this missing sink (Melniko and O'Neill; 2006; Ciais et al, 2013). The chemical weathering of continental rocks is a significant terrestrial process that regulates the geological long-term global climate (Berner et al, 1983). Continental carbonate rock is the largest carbon reservoir, covering nearly 10~15% of the global ice-free land surface (Ford and Williams, 2013; Goldscheider et al. 2020). The CO_2 in soil water produces aggressive carbonic acid, which them can dissolve carbonates on the land surface, forming the famous karst landscape (Dreybrodt, 1988; Ford and Williams, 2013). During this chemical weathering process, the dissolution of carbonate minerals liberates base cations, producing an alkalinity flux (mainly bicarbonate, HCO_3^-) to the surface water systems. Hence, the atmospheric $CO_{2(atm)}$ or soil CO_2 (which is of atmospheric origin) are converted to dissolved inorganic carbon (DIC) and is then transported to the oceans via runoff (Berner et al, 1983; Liu et al 2010; Gaillardet et al, 2019). This DIC flux contributes nearly 50-60% of the continental weathering products (Gaillardet et al,1999).

In the past, conventional views suggested that carbonate weathering processes can only act as carbon sink on geologically short time scale (<100,000 years), but for longer periods (>100,000 years), CO_2 will move back to the atmosphere by DIC out-gassing from the oceans (Berner et al, 1983; Arvidson et al, 2016).

However, recent studies have highlighted that carbonate weathering products (DIC) are used by terrestrial water aquatic biota by photosynthesis (submerged plants, plankton etc.). The DIC in surface water systems is transformed to dissolved organic matter by phototrophs and can be buried in riverine or lacustrine sediments (Yang et al, 2015; Liu et al 2018), resulting a geological long-term carbon sink. Therefore, the significance and the magnitude of this carbon-sink flux has been reevaluated and quantified in this thesis.

The chemical weathering rate of carbonate is around 10-20 times fast than for silicate (Meybeck, 1986; Liu et al 2012). This fast dissolution kinetics allows carbonate weathering to rapidly respond to environmental perturbations such as climate change and human land-use changes. In past decades, the accelerating carbonate weathering carbon-sink flux has been

mapped by many global efforts (Raymond et al, 2003; Raymond et al, 2008; Macpherson et al 2008). These studies indicate that the response of carbonate weathering to global change is fast and considerable, and it may lead a positive feedback to global warming. However, most global carbon-cycle models only treat this weathering process as constant terrestrial carbon sink, which may underestimate the significant potential of carbonate weathering to mitigate the accelerated warming climate.

The aim of this thesis is to detect the mechanisms of the carbonate weathering carbon-sink response to global change (especially climatic and land-use changes), and to present a global-scale modelling framework to evaluate the role of this carbon sink in the future global carbon cycle. Previous work on carbonate weathering carbon-sinks used mainly runoff-based empirical functions or climate-based models to evaluate the global weathering intensity (e.g. Amiotte-Suchet and Probst, 1995; Gombert et al, 2002; Romero-Mujalli et al 2019b) or focused on regional-scale variations by using high-resolution water quality logger (Zeng et al, 2015; Zeng et al, 2016). However, using only regional data or climate-based models can result in inaccuracy when applied as global estimate, because the weathering behavior may vary from site to site. In order to improve these limitations and select a better method for this task, this thesis utilizes results from different field sites and compares several soil-pCO_2 models. Additionally, a series of satellite-based data sets are used for the global estimation, providing a new high-resolution map of global carbon-weathering intensity. After evaluating the advantages of different parameters, a new model is constructed to predict the long-term response of carbonate weathering carbon sink from past decades to the near future (1950-2100). The analysis of the carbonate-weathering intensity and carbon sink in this thesis offers new insights into the structure of the global carbon-cycle model, providing a potential terrestrial carbon sink process that could help to mitigate global warming.

1.2. History and present state of carbonate-weathering carbon-sink studies

1.2.1. Behaviour of carbonate weathering under different natural conditions

The chemical dissolution intensity of carbonate minerals and the related carbon sink are controlled by numerous climatic and biologic variables. Yet, the general equation of carbonate weathering carbon sink (CCSF) can be simply expressed as: CCSF = 0.5 × DIC × Q. Where DIC [mol/m^3] is the concentration dissolved inorganic carbon and Q [m/s] is the discharge. CCSF is the carbon sink flux and 0.5 indicates that only half of the carbon in the DIC is of

atmospheric origin (Liu et al, 2010). Therefore, both DIC and Q are two key factors for estimating the carbonate carbon-sink flux. Under natural conditions, numerous environmental drivers are controlling both DIC and Q. First, temperature controls the thermodynamic constants of the calcite-water-carbon-dioxide ($CaCO_3$-H_2O-CO_2) system (e.g. Plummer et al, 1978; Dreybrodt et al, 1988; White and Blum, 1995), determining the magnitude of DIC. Within the normal global temperature range, the solubility of carbonates will decrease as the temperature is raised (Dreybrodt et al, 1988). Meanwhile, the level of the partial pressure of CO_2, pCO_2, along the soil-rock interface is also responsible for the solutes concentration. Unlike the temperature, pCO_2 is mostly depending on biological processes. Soil CO_2 is mainly produced by root respiration and the decomposition of organic matter through microorganic activities, but both processes owe their CO_2 originally from the atmosphere (Berner, 1997; Liu et al, 2010). Accounting for the close relationships between soil-biota respiration and temperature as well as soil moisture (Bond-Lamberty et al, 2010; Tang et al, 2020), the weathering intensity of carbonate rocks also can be affected by climate. On the other hand, precipitation and evapotranspiration are involved in the process of carbonate-weathering carbon-sink flux (Zeng et al, 2016), because the solute flux and the saturated state of solution are strongly affected by the discharge (Q) due to the chemo-static behaviour (Godsey et al 2009; Zeng et al 2015). The daily water balance also regulates the soil moisture. Therefore, the water availability may influence the soil respiration, thus the carbonate dissolution.

Besides, growing evidence indicates that the anthropogenic factors, which were not in the focus by geochemists in the past, may play a crucial role for the carbonate carbon-sink flux. Studies show that human land-use strategies have essentially altered the carbonate-weathering process and carbon-sink flux in past decades (Raymond et al 2008; Macpherson et al 2018; Zeng et al, 2017). Due to the build-up of vegetation cover on bare surfaces, the weathering rate of rocks increases 3-10 times owing to the high soil biomass in natural ecosystem (Cochran and Berner, 1996; Berner, 1997). However, human agricultural expansion, deforestation and urbanization have also reshaped the natural vegetation conditions. An increasing proportion of land-use changes leads a large soil organic-carbon loss and a decline in respiration rate, which may result a lower intensity of carbonate dissolution. Moreover, the change of vegetation types such as forest to crop or bare-land decreases the evapotranspiration thus enhancing the water yield (Zhang et al; 2001; Piao et al, 2007). Those anthropogenic factors are intertwined with climatic parameters, complicating the carbonate weathering behaviour in different regions. The mechanisms behind the mixed impacts of these factors are crucial for discussing the response of carbonate-weathering carbon sink to global change, yet it is still poorly understood.

I will address this question in chapter 3.

1.2.2. Estimation of carbon weathering and carbon sinks

In past three decades, researchers conducted numerous attempts to evaluate the global carbonate weathering intensity and total related carbon-sink budget. For instance, in order to quantify the variable carbon-sink flux of rocks, the relationships between runoff and solute flux have been constructed by using world-wide riverine geochemical records and soil properties (Amiotte-Suchet and Probst, 1995; Bluth and Kump et al, 1994; Hartmann et al, 2014b). However, a simple empirical function cannot capture the spatial and temporal variation of carbonate weathering intensity and detect the sensitivity of its response to global change. These runoff-based global paradigms may underestimate the impacts of other environmental drivers, ignoring the huge differences from site to site. Meanwhile, the fast kinetics of the carbonate dissolution reaction allows it to reach equilibrium state in very short time (≤3 hours, Reddy et al, 1981; Dreybrodt et al, 1996). This short response times prohibit runoff based-models to evaluate the actual value of the DIC in aquifer. Another attempt to address the carbon sink is using the potential maximum dissolution equation. This approach assumes that the dissolution of carbonate is already reaching the equilibrium state after the solute flux flows to the surface-water system. The impacts of temperature on the equilibrium constants have been detected by laboratory experiments and are well known, which makes this approach very useful. Here, the most crucial and hard-to-access parameter is soil pCO_2, which is mostly associated with biological processes. Gombert (2002) first used an evapotranspiration-(*ET*)-based pCO_2 model (Brook et al, 1983) to estimate the carbonate-weathering carbon sink on a global scale. This study suggests that carbonate-weathering carbon sinks may account for nearly 30% of the total missing carbon sink. Yet, this empirical pCO_2 model may overestimate the DIC in arid region when applied to global scale, because it fails to exclude the abiotic evapotranspiration on vegetation-free land surface. Likewise, a soil water-content based model has been constructed by using global spring data for pCO_2, but no vegetation factor is involved (Romero-Mujjali et al, 2019a). Compared these two empirical methods, a process-based soil pCO_2 model has been integrated to the carbonate equilibrium equation to obtain the carbonate weathering intensity (Beaulieu et al, 2012; Goddéris et al. 2013; Calmels et al, 2014). This model calculates the respiration rate of soil biota at different root zones. Although this method adds the role of vegetation cover, the model cannot currently be applied on a global scale because of limitations in computing power. A modified version is needed to improve this model. These three soil

pCO_2 models have their own advantages and could acquire a good match with observations in some regional studies. However, there are no related studies to compare their accuracy for a global study and verify the outcomes by using global field evidence. Therefore, a comparison study of these models for a global scale will be investigated in chapter 4.

1.2.3. Sensitivity estimation of carbon weathering to global change

The increasing greenhouse emission induced global warming has altered the balance in the earth climate system, when compared to the time before the industrial revolution. In the worst case of a fossil CO_2 emission scenario, a global warming of more than 6℃is expected till 2100. Carbonate weathering processes will be strongly influenced by this human-induced perturbation due to its fast dissolution kinetics. First, the rising global temperature will enhance the ecosystem productivity thus leading a higher soil CO_2 flux (Bond-Lamberty et al, 2010). As the atmospheric CO_2 concentration increased in past decades, the rising ground water pCO_2 and accelerating weathering rate have been found both in short-term and long-term local observations (Andrews et al, 2001; Mcpherson et al, 2008; Gislason et al, 2009). Meanwhile, the global temperature and atmospheric CO_2 increases also promote the changes in the global hydrologic cycle by altering the precipitation pattern and vegetation cover (Labat et al, 2004; Gedney et al, 2006). The variation in water balance results a considerable influence on carbonate weathering process and related carbon sink flux, because runoff is a key factor that controls the total carbon-sink flux (Zeng et al 2015; Zeng et al, 2016). Additionally, the growing population results in an increasing demand of food and society development, resulting in a large proportion of land-use changes especially in developing countries. The fast growth of cropland and agricultural activities have altered numerous continental surface processes as well as continental rocks weathering. A growing number of studies imply that the contemporary weathering flux of carbonate experiences increasing trends for decades, which at least in parts is triggered by the intense human land-use changes (Raymond et al, 2008; Drake et al, 2018; Macpherson et al, 2019). For instance, the alkalinity flux in the Mississippi River has increased nearly 50% during the past decades due to agricultural management and lime fertilization. However, these anthropogenic impacts have long been neglected in studies of carbonate-weathering carbon-sink modelling. More importantly, these new evidences have challenged the previous assumption that the feedback of rock weathering and global change is slow and only may occur on a long geological time scale. Thus, the total response of the carbonate-weathering carbon sink to global changes needs be well quantified. Yet, to capture this response requires a

further understanding of the mechanism behind, especially the sensitivity of this carbon sink response to different environmental drivers. This question will be investigated in chapter 5.

1.2.4. Terrestrial biological pump and carbon weathering

In earlier decades, the carbonate-weathering carbon flux has been seen as a geological short-term carbon sink. However, the terrestrial biological carbon pump effect (BCP) coupled to carbonate weathering has been identified in more recent studies. These findings stress the significant role of the carbonate-weathering products for controlling long-term global climate (Chen et al, 2017; Jiang et al, 2013; Yang et al, 2015). This effect suggests that the aquatic photosynthesis coupled with carbonate weathering process may result a stable carbon sink in surface waters by transforming DIC to organic carbon (Liu et al, 2018). In fresh waters, aquatic ecosystem CO_2 uptakes (photosynthesis) raise the water pH and change the principle molecular hosts of DIC (Talling, 1976; Verschoor et al, 2013). These higher pH values shift the inorganic carbon dominated by $CO_{2(aq)}$, to a HCO_3^- or CO_3^{2-} dominated system (Schulte et al, 2011). Although $CO_{2(aq)}$ is the favored substrate for aquatic ecosystem photosynthesis, some phytoplankton or submerged plants have developed an ability to utilize HCO_3^- as a carbon source by CO_2-concentration mechanisms (CCMs). This mechanism allows them to acquire additional carbon when $CO_{2(aq)}$ becomes limited in high pH environment (Van Dam et al, 2018; Verspagen et al, 2014; Morales-Williams et al, 2017), especially in karst terrains (Yang et al, 2015; Chen et al, 2016). The DIC fertilizer (high HCO_3^- inputs) effect induced by carbonate weathering on aquatic ecosystem primary production promotion has been detected in field experiments (Chen et al, 2017). On the other hand, nitrogen has been thought to be a key limiting nutrient for aquatic ecosystem productivity, while the carbon ($CO_{2(aq)}$ or DIC) has been treated as a non-limiting nutrient (Hecky and Kilham, 1988; Visser et al, 2016). However, studies discover that aquatic carbon may play an important role as a reaction rate-limiting nutrient instead of yield-limiting nutrient, which can interact with other elements (N, P, SO_4^{2-}, Si) for co-limitation of ecosystem productivity in inland waters (Low-Decarie et al, 2014). The cycling of carbon and nitrogen are closely coupled, controlling the autochthonous organic carbon export through aquatic assimilation and denitrification (Seitzinger el al, 2016; Taylor and Townsend, 2010; Trimmer et al, 2012). Meanwhile, the increasing contemporary agricultural activities have increased both DIC and nitrogen loads to the surface water system (Raymod et al, 2008; Mulholland, 2008; Taylor and Townsend, 2010). Therefore, in order to strengthen the aquatic carbon uptake through human land-use strategies, a better understanding

of the relation between nutrient inputs with aquatic OC production is crucial. The mechanisms of terrestrial carbon pump effect and C, N coupling under different land-use will be carried out in chapter 6.

1.3. Objectives and outline of thesis

The following main questions will be investigated in this study:

- **Question 1:** How do temperature, runoff and land cover control the carbonate weathering behaviour and related carbon sink flux?
- **Question 2:** Which models or parameter values can be better applied to estimate the carbonate-weathering intensity on a global scale?
- **Question 3:** How does the carbonate-weathering related carbon sink response to future global changes?
- **Question 4:** What is the influence of different human land-use strategies on the terrestrial BCP effect in surface water system?

This thesis is arranged into 7 chapters. Chapter 2 describes the methods and the data applied in this research. Chapter 3 focuses on question 1, which summarizes the carbonate weathering behaviour of three typical karst catchments, and discusses the role of temperature, runoff and vegetation cover on carbon-sink flux export. Chapter 4 discusses the question 2, and applies three different parameterized soil pCO_2 models to explore the best environmental parameter values for estimating global carbonate-weathering intensity. Chapter 5 addresses the question 3, which used the outcomes of CMIP5 and a new mixed-effects model to predict the future changes of carbonate weathering carbon sink flux. Chapter 6 focuses on the mechanisms of BCP effect under the impacts of different human land-use strategies.

Chapter 3 to chapter 6 are presented by three published articles (chapter 3, 5, 6) and one article submitted (chapter 4). Chapter 3 to Chapter 6 generally describe an overview of the progresses of carbonate-weathering carbon cycle studies, from the mechanisms of atmospheric CO_2 capture on land rock surface to the organic carbon storage in terrestrial aquatic ecosystem.

The conclusions of this thesis and the future perspectives of this topic are finally presented in chapter 7.

1.4. List of abbreviations

AOC	Autochthonous organic carbon
APAR	Absorbed photo-synthetically active radiation
BCP	Biological carbon pump
DBL	Diffusion boundary-layer theory
DIC	Dissolved inorganic carbon
CCMs	CO_2-concentration mechanisms
CCSF	Carbonate weathering carbon sink flux
CMIP5	The fifth phase of Coupled Model Intercomparison Project
ET	Evapotranspiration
GM-CO2	Global Erosion Model for CO_2 flux
MPD	Maximal potential dissolution formula
NPP	Net primary production
OC	Organic carbon
RCP	Representative CO_2-concentration pathway
SWC	Soil volumetric water content
TOC	Total organic carbon

2. Theory and Methods

Due to the cumulative nature of this thesis, the individual topics are presented in the form of four published articles, resulting in concise theoretical explanations. Therefore, this chapter provides more in-depth insight into the fundamental theory and methods, upon which the individual topics are based.

All four studies discuss carbonate-weathering carbon-sink evolution under global changes. In section 2.1, the basic processes how carbonate weathering captures CO_2 (carbon dioxide) from atmosphere and transforms it to a long-term carbon sink have not been discussed in detail in the articles, yet they constitute the basis for carbon-sink flux calculations. The calculation of the equilibrium concentration of HCO_3^-(bicarbonate), using temperature-depended reaction constants and soil pCO_2 is described in section 2.2. Section 2.3 then discusses the three prevailing soil pCO_2 models, which are used in the papers. Finally, in section 2.4, the *Shawan* karst simulation test site is described, our natural laboratory of carbonate-weathering in the field.

2.1. Theory of carbonate weathering

As one of the main continental weathering processes, the weathering products of carbonate are a significant carbon sink for the global carbon cycle (e.g. Berner et al 1983; Gombert et al 2002; Liu et al, 2010). The dissolution of carbonates captures CO_2 from the atmosphere and the soil layer as a form of DIC (dissolved inorganic carbon) and delivers it from the land surface to the oceans via surface water systems. As first step of this process, CO_2 is readily soluble in water (H_2O):

$$CO_2 + H_2O \leftrightharpoons H_2CO_3 \leftrightharpoons H^+ + HCO_3^- \leftrightharpoons 2H^+ + CO_3^{2-} \quad (2.1)$$

The resulting carbonic acid (H_2CO_3) is then dissociating into hydrogen (H^+) and bicarbonate (HCO_3^-), then main constituent of the dissolved inorganic carbon (DIC), and in part further on to carbonate (CO_3^{2-}). The dissolved inorganic carbon (DIC) is the sum of $CO_{2(aq)}$, H_2CO_3, HCO_3^- and CO_3^{2-}, but for pH-values between 6.6 and 10, the freshwater pH range, HCO_3^- is dominating DIC, while $CO_{2(aq)}$ only plays a minor role. The atmospheric CO_2 is thus transformed into dissolved inorganic carbon in the form of HCO_3^- (Fig. 2.1a.)

Along the soil-rock interface of carbonate rocks, the CO_2-containing water dissolves the carbonates, which can be expressed as summation:

$Ca_xMa_{1-x}CO_3 + CO_2 + H_2O = xCa^{2+} + (1-x)Mg^{2+} + 2HCO_3^-$	(2.2)

Here, *x* represents a fractional value, with *x=1* representing calcite ($CaCO_3$), and *x=0.5* dolomite ($CaMg(CO_3)_2$).

However, due to the deposition of $CaCO_3$ in the oceans, the abiotic terrestrial weathering process only acts as a short-term rather than a long-term carbon sink, when compared to silicate weathering (Berner et al, 1983), although the DIC produced by carbonate weathering contributes nearly 50%-60% of the continental weathering products (Gaillardet et al,1999). However, $CO_{2(aq)}$ is the preferred form as nutrient for the primary production of aquatic phototrophs. Thus, the CO_2 uptake (photosynthesis) in the aquatic ecosystem will raise the pH of the water and further lower $CO_{2(aq)}$.

Some phytoplankton and submerged plants have developed the ability to utilize HCO_3^- by CO_2-concentration mechanisms (CCMs), which acts as an additional carbon source. This mechanism allows them to acquire additional carbon, when $CO_{2(aq)}$ becomes limited in high pH environments (Van Dam et al, 2018; Verspagen et al, 2014). Recent studies have found that the HCO_3^- produced by carbonate weathering in continental surface water may be utilized by aquatic phototrophs via CCMs. Thus, the DIC produced by carbonate weathering will be transformed to autochthonous organic carbon (AOC) or be captured as a form of organic matter in the sediments (Liu et al, 2010; Chen et al, 2017). The aquatic ecosystem DIC capture via photosynthesis is therefore another carbonate weathering process with great potential as geological long-term carbon sink:

$Ca^{2+} + 2HCO_3^- \rightarrow CaCO_3 + x(CO_2 + H_2O) + (1-x)(CH_2O+O_2)$	(2.3)

Here, *x* is a portioning factor between CO_2-release and O_2-erlease to the atmosphere.

As shown in Fig. 2.1a , the AOC carbon sink may occur in rivers, lakes, wetlands and reservoirs, which have been seen as carbon pipeline or CO_2 source in global carbon-cycle models. More importantly, the AOC produced by this terrestrial biological carbon pump (BCP) process is estimated to contribute nearly 30% of the terrestrial missing carbon sink (Fig. 2.1b). Hence, in an attempt to balance the global CO_2 budget, the significant role of the carbon sink flux should be reconsidered in global carbon cycle model.

Growing evidence suggests that the DIC flux is increasing in response to climate and land-use dynamics (Raymond et al, 2008; Zeng et al, 2017; Macpherson et al 2019), and these two factors are thought to change significantly in the future. Therefore, if the behavior of the DIC flux response to these environmental perturbations could be identified, the contribution and the role of this is carbon sink for the future carbon cycle can be estimated.

On the other hand, recent studies also unveil that human land-use activities may control the magnitude of aquatic organic carbon production in carbonate terrain (Jiang et al, 2013; Yang et al, 2015; Chen et al, 2017). A strong DIC fertilization effect induced by carbonate weathering is detected in surface-water ecosystems, and this extra carbon input could be managed by human land-use activities (Chen et al, 2017). Therefore, future anthropogenic land-use strategies can be applied as a $CO_{2(atm)}$ sink through additional carbonate weathering.

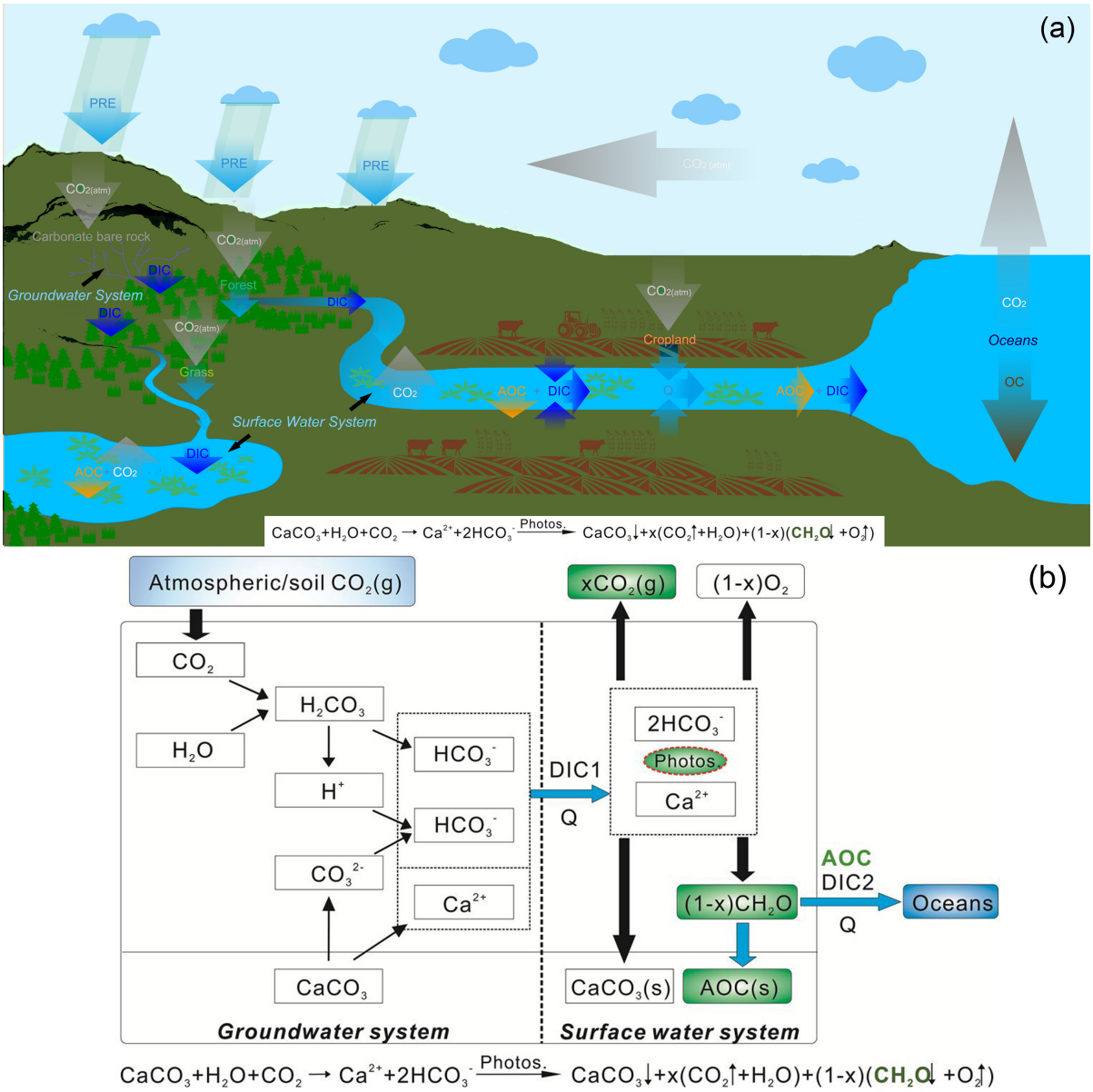

Fig. 2.1. (a) *Conceptual diagram showing the carbonate-weathering carbon cycle and the evolution of the carbonate weathering-related carbon sink.* ***(b)*** *Conceptual model of the carbonate weathering-related carbon sink formation by coupled the aquatic biochemical processes (Liu et al, 2010). Notes: DIC is the dissolved inorganic carbon producing by chemical weathering of carbonates on land surface or soil-rock interface; Q is the runoff*

through the land surface; AOC is the concentration of autochthonous organic carbon in the surface water system transformed from DIC by aquatic phototrophs photosynthesis, and OC is the sedimentary organic carbon flux in the oceans.

2.2. Global carbonate weathering carbon-sink flux (CCSF)

The concentration of HCO_3^- as carbonate weathering products, which serves as a proxy for the carbon sink intensity, is a key topic of this thesis. In previous studies, numerous approaches were applied to evaluate the carbonate dissolution intensity and the concentration of HCO_3^-:

- A common method is to place standard test tablets of calcite into the different soil layers for climatic regions and to measure the weight loss of tablets (e.g. Gabrovsek 2009; Hattanji et al, 2014). However, the secondary carbonate sedimentation and minor carbonate minerals in soils may conceal the real value by this means.
- A more accurate approach is a theoretical model of the dissolution kinetics in the carbonate system, using the diffusion boundary-layer theory (DBL). However, this method requires a detailed geological and geochemical background of the study site (e.g. Dreybrodt et al, 1996). Therefore, it is difficult to evaluate the carbonate-weathering intensity in a global context.
- Another approach uses a large amount of global river hydro-chemical data to construct an empirical model for bicarbonate concentration. For instance, the Global Erosion Model for CO_2 flux (GM-CO_2) defines a relation between runoff and rock-weathering rate for different rock types (Amiotte-Suchet and Probst, 1995). Yet, this model applies fixed coefficients to evaluate the rocks weathering intensity while neglecting the impacts from other environmental drivers except water flow.

To eliminate the disadvantages of the above-mentioned models for evaluating the carbonate weathering intensity on a global scale, Gombert (2020) first introduced a theoretical approach that assumes the dissolution rate will reach an optimized level (Maximal Potential Dissolution, MPD). Then, the carbonate weathering intensity can be simply calculated, if temperature and soil-pCO_2 are known. The following outline summarises the calculation.

CCSF

The *carbonate-weathering carbon-sink flux* CCSF [g/m^2/s] is defined as (e.g. Liu et al., 2010):

$$CCSF = \frac{Q}{A} n m_r [DIC] \quad (2.4)$$

with q [m^3/s] the discharge, A [m^2] the catchment area, $[DIC]$ [mol/ m^3] the concentration of dissolved inorganic carbon, n a dimensional partioning coefficient, which is $n = 0.5$ for limestone of dolostone weathering (only half of the carbon is of atmospheric origin), and $n = 1$ for silicate weathering (all carbon is of atmospheric origin), and m_r [g/mol] the molar mass (12 g/mol for carbon).

We need to address both runoff and chemistry next.

Runoff

We derive runoff N [m/s] from satellite-based data sets, and then use

$$N = \frac{Q}{A} \tag{2.5}$$

to account for runoff when calculating CCSF.

DIC

The concentration of the dissolved inorganic carbon, $[DIC]$, is the sum of the concentrations of carbon dioxide, carbonic acid, bicarbonate, and carbonate:

$$[\mathrm{DIC}] = [\mathrm{CO_2}] + [\mathrm{H_2CO_3}] + [\mathrm{HCO_3^-}] + [\mathrm{CO_3^{2-}}] \tag{2.6}$$

For a wide range of pH values, the different contributions are often summarized as Bjerrum plot (Fig. 2.2).

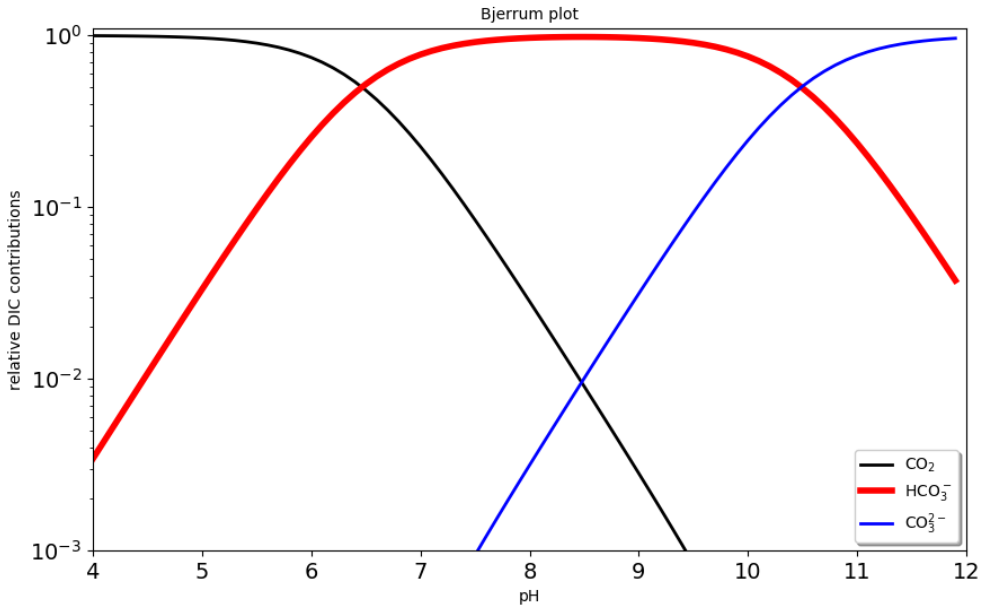

Fig. 2.2: *Contribution of dissolved inorganic carbon (DIC) as a function of pH (Bjerrum plot).*

For the pH range between 6 and 8 (most natural water systems), bicarbonate dominates. Thus we can safely assume that the relation

$$[\mathrm{DIC}] \simeq [\mathrm{HCO_3^-}] \tag{2.7}$$

holds, and that the majority of DIC is represented by bicarbonates.

We use the electro-neutrality relation:

$$\begin{aligned} & [H^+] + [Na^+] + [K^+] + 2[Ca^{2+}] + 2[Mg^{2+}] \\ = \; & [Cl^-] + 2[SO_4^{2-}] + [NO_3^-] + [HCO_3^-] + 2[CO_3^{2-}] + [OH^-] \end{aligned} \tag{2.8}$$

and solve it for the calcium concentration in the pH range $pH \in [6.5,8.5]$:

$$2[\mathrm{Ca^{2+}}] = [\mathrm{HCO_3^-}] + Rb \tag{2.9}$$

with Rb the reduced alkalinity. If we assume that Rb is small is relation to bicarbonate then

$$2[\mathrm{Ca^{2+}}] = [\mathrm{HCO_3^-}] \tag{2.10}$$

holds. We then can relate the DIC concentration directly to the calcium concentration:

$$[\mathrm{DIC}] = 2[\mathrm{Ca^{2+}}] \tag{2.11}$$

Calcium concentration

We now follow the MPD approach and assume that the calcium concentration can be derived from the calcium equilibrium concentration, which for given temperature T [°C] and soil-$p\mathrm{CO_2}$ pressure can be approximated, to excellent accuracy, by (e.g. Dreybrodt, 1988):

$$[\mathrm{Ca^{2+}}]_{eq}^3 = \frac{K_1(T)K_C(T)K_H(T)}{4K_2(T)\gamma_{Ca^{2+}}\gamma_{HCO_3^-}^2} pCO_2 \tag{2.12}$$

with $K_H(T)$ the equilibrium constant for the dissolution of atmospheric carbon dioxide into water (Henri constant), $K_0(T)$ the equilibrium constant for the reaction of water and carbon dioxide to carbonic acid, $K_1(T)$ and $K_2(T)$ the equilibrium constants for the dissociation of carbonic acid into bicarbonate, carbonate, and hydrogen, $K_C(T)$ the equilibrium constant for dissolved calcite, $\gamma_{Ca^{2+}}$ and $\gamma_{HCO_3^-}$ the activity coefficients for calcium and bicarbonate, and pCO_2 [atm] the soil carbon-dioxide partial pressure.

The calcium equilibrium concentration as a function of soil-pCO_2 and temperature is shown in Fig. 2.3. As temperature rises, the calcium equilibrium concentration decreases, if the pCO_2 is a constant. Yet, in nature with vegetation cover, the soil pCO_2 produced by root zone will rapidly increase in low temperature zone and then reaches a maximum between 15-20^{o}C. Thus, the calcium equilibrium concentration will vary non-linearly as a function of temperature (red, Fig 2.3a). Additionally, as the equilibrium concentration and temperature increase, the effect of each mole of pCO_2 for extra carbonate dissolution will be strongly constrained (Fig 2.3b).

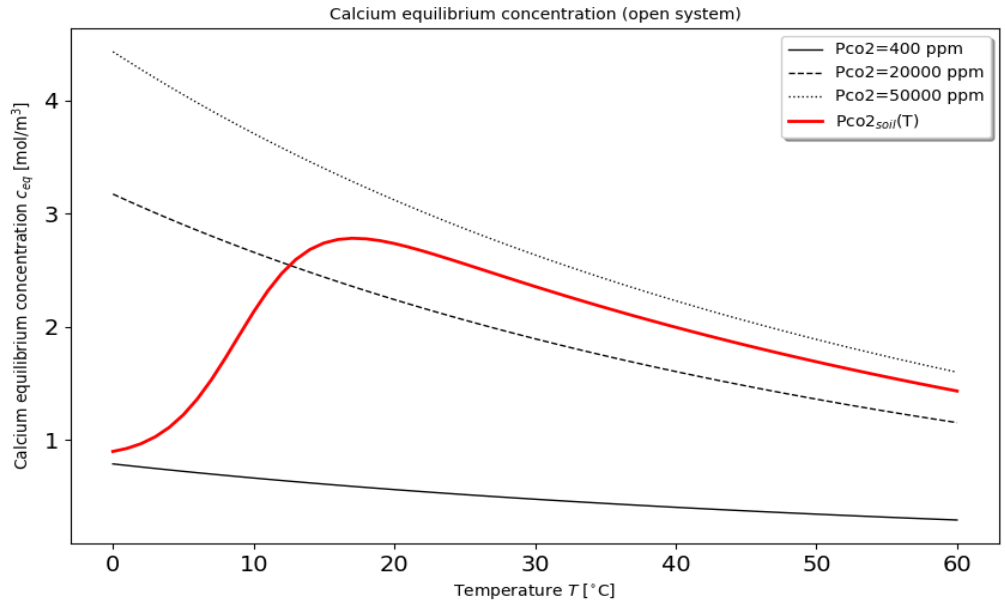

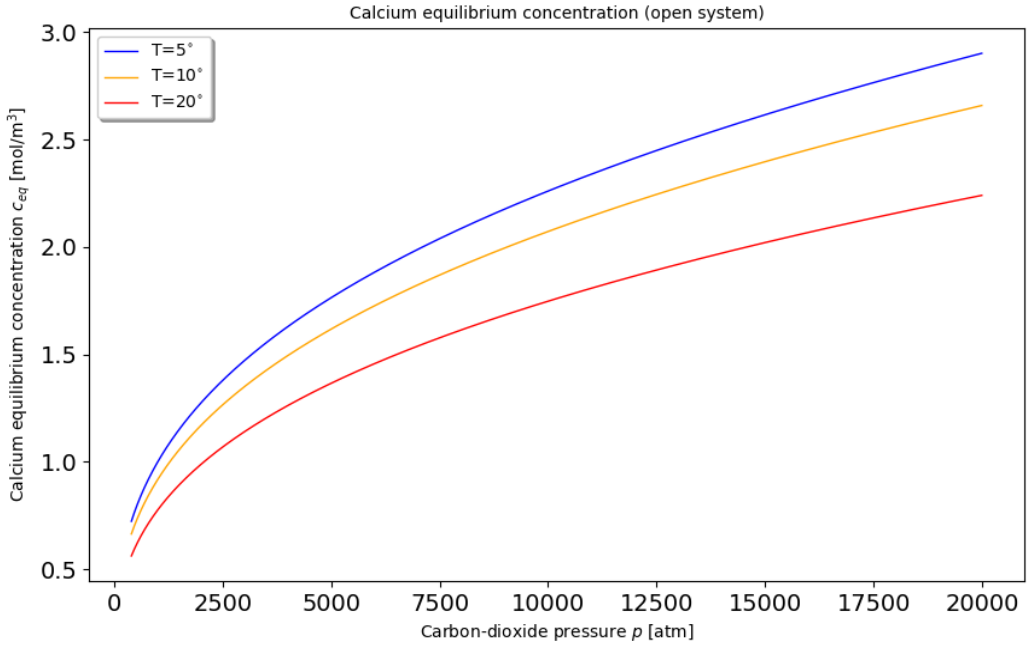

Fig. 2.3: *(a) Calcium equilibrium concentration as a function of soil- pCO_2 for three different temperatures, (b) Calcium equilibrium concentration as a function of temperature for three different pCO_2 concentrations.*

2.3. Soil carbon-dioxide concentration

In this thesis, three ecologically-based soil-pCO$_2$ models are integrated into the carbonate equilibrium equation (MPD). These soil-pCO$_2$ models are based on a series of satellite-based data, e.g. global temperature (T), net primary production (NPP), soil volumetric water content (SWC), and evapo-transpiration (ET). This section provides more details about the approaches and data used.

ET-soil- pCO$_2$

The first soil-pCO$_2$ model that has been applied to calculate the global carbonate-weathering intensity has been introduced by Gombert (2020) and Gailardet et al. (2019). This study employed an empirical model that parameterized soil-pCO$_2$ by only using temperature or evapotranspiration (T, Gailardet et al. (2019); ET, Brook et al, 1983). The ET-soil-pCO$_2$ model is based by soil-pCO$_2$ data from 19 monitoring sites worldwide, resulting in the closed-form soil-pCO$_2$ function (see Fig. 2.4):

$$\log pCO_{2(soil)} = \log pCO_{2(atm)} + \frac{1.5}{0.75 + e^{-0.12T}} \quad (2.13)$$

Here, $pCO_2^{atm} = 0.0004$ atm is used for atmospheric pCO$_2$, T is in ℃, and the resulting pCO_2^{soil} in atm.

This method has limitations for evaluating the soil-pCO$_2$ values in arid/semi-arid or desert regions, because some areas have a high evapotranspiration (even higher than precipitation), but only a small proportion can contribute to ecosystem productivity as well as soil respiration. In order to improve the quality of this estimation for better comparing with other model outcomes, a high-resolution satellite-based ET data set is employed to increase the data quality. MOD17A3 is NASA's annual 500m MODIS ET data, which is originally based on the Penman-Monteith equation. But it uses the daily meteorological re-analysis data and 8-days remotely sensed vegetation property dynamics from MODIS as input. This data incorporates the biological factors that yet have not been considered by previous studies. Therefore, this ET product is applied in second study (chapter 4), although the impacts of non-biological ET still cannot be fully excluded for some arid region.

NPP-soil- pCO_2

The second soil-pCO_2 model is a process-based model, introduced by Gwiazda and Broecker (1993) and Goddéris (2010). This model assumes that CO_2 diffuses within the soil layers. In order to acquire the full pCO_2 profile, a power function is used to solve the complete CO_2 diffusion equation. The soil-pCO_2 value at the average root depth (80cm) is set to approximately 75% of the ecosystem net primary production (*NPP*). Below, soil-pCO_2 becomes constant. Thus, soil-pCO_2 can be expressed as a function of atmospheric CO_2 concentration, temperature, and *NPP*.

The original soil-pCO_2 relation from Gwiazda and Broecker (1993) has been simplified by Gaillardet (2019) and reads (see Fig. 2.4):

$$pCO_{2(soil)} = pCO_{2(atm)} + \frac{A \cdot 0.75 \cdot NPP}{(T + 273.16)^2} \quad (2.14)$$

with the net primary production can be derived from

$$NPP = \frac{3000}{1 + e^{(1.315 - 0.119T)}} \quad (2.15)$$

Here, T is given in °C, *NPP* in g/m^2/yr, and the empirical constant $A = 1.03 \times 10^6$ is often used. Both $pCO_2^{atm} = 400$ ppm and the resulting pCO_2^{soil} are in ppm.

This simplified version *NPP*-soil-pCO_2 (eq 2.14) and a series of satellite-based global *NPP* products MOD16 are used in chapter 4. MOD16A3 is NASA's annual 500m MODIS *NPP* data. The data is based on the empirical relation between *NPP* with absorbed photo-synthetically active radiation (APAR).

SWC-soil-pCO_2

Romero-Mujalli (2018a) constructed an empirical model by fitting the water pCO_2 data taken from 26 publications with a nonlinear polynomial. This approach is a reverse-process method that predicts the soil-pCO_2 by using two parameters, temperature, and soil-water volumetric content (*SWC*). In this model, the soil-pCO_2 is described as a bell-shaped curve related to temperature. *SWC* acts as limitation factor which determines the threshold of ecosystem CO_2 production ability (see Fig. 2.4):

$$\log pCO_{2(soil)} = \log pCO_{2(atm)} + \frac{e^{(b_1\theta - \frac{b_2}{\theta})}}{b_3 + e^{b_4 T}} \quad (2.16)$$

Here, T is given in ℃, θ is the soil-volumetic water content in m^3/m^3, $pCO_2^{atm} = 0.0004$ atm and the resulting pCO_2^{soil} is also in atm. The constants are $b_1 = -3$, $b_2 = 0.25$, $b_3 = 0.09$, and $b_4 = -0.34$.

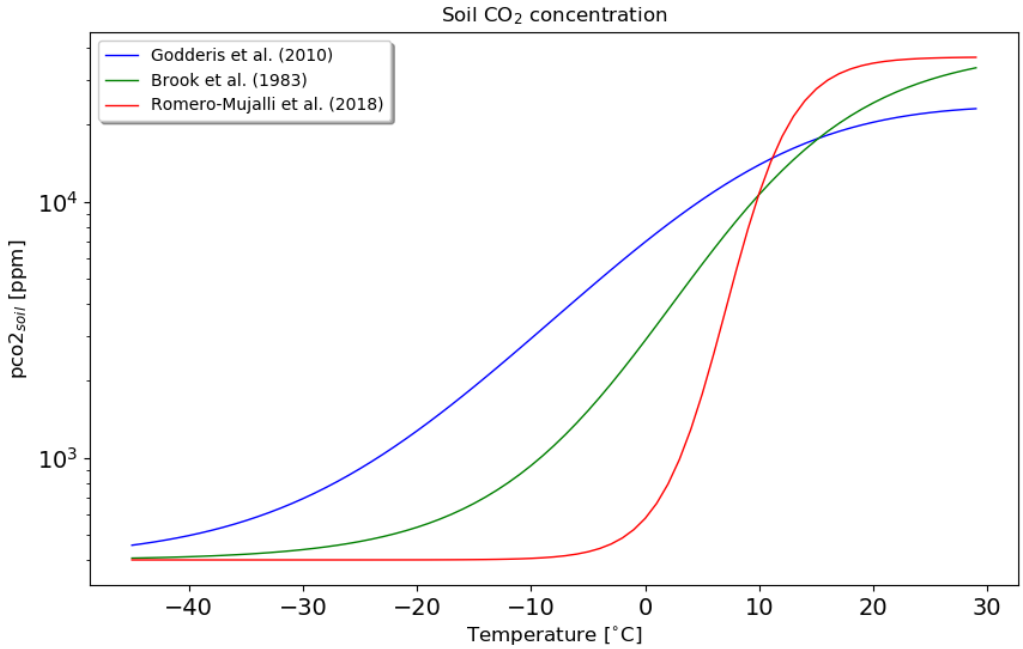

Fig. 2.4: *Different soil-pCO_2 models as a function of temperature. ET- pCO_2-green, NPP-pCO_2-blue, SWC- pCO_2-red.*

2.4. Shawan test site

In the third and fourth study (chapter 5 and chapter 6), data from the karst simulation test site *Shawan* in southwestern China are used to discuss the impact of human land-use strategies on CCSF and the BCP effect. The field test site simulates the basic hydrochemical and biochemical processes that control the carbonate-weathering carbon-sink evolution by using an artificial spring-pond system.

The *Shawan* karst test site (26°14′-26°15′, 105°42′-105°43′) is located in the Puding comprehensive karst research and experimental station in Guizhou, China. The field experiment intents to trace the evolution pathway of a carbon sink on karst terrain and estimates the impact of human land use changes (Fig. 2.5a). As shown in Fig. 2.5b, five concrete tanks have been built and filled with broken limestone along the bottom. Each concrete tank is 20 m long, 5 m wide, and 3 m deep. In order to avoid the influence of possible concrete erosion on the tank

inside, the walls are covered with epoxy resin. A 50 cm thick soil layer is then filled above the rock layer, while one tank is left without soil cover to mimic bare-land cover. The remaining three tanks are planted with grass (Alfalfa), shrub (Roxburgh roses), and crop (corn), respectively (Fig. 2.5b). A hole at the bottom is used to capture drainage from each, thus simulating a karst spring. The holes are connected to five artificial ponds that are planted with flourished algae (the algae are collected from a nearby karst river), as shown in Fig. 2.5c. These spring-fed ponds simulate five typical inland-water systems, which are controlled by different land use types.

The unique advantage of this simulation test site is having strictly controlled boundaries conditions and a clear separation between each tank. By running a three-year water balance experiment within each tank, chapter 5 extends the *ET* equation introduced by Zhang (2001) to five land-cover types and calculates global runoff pattern. In chapter 6, the diurnal and seasonal biogeochemistry measurements in five spring-fed ponds are conducted to detect the role of land-use strategies on BCP effect.

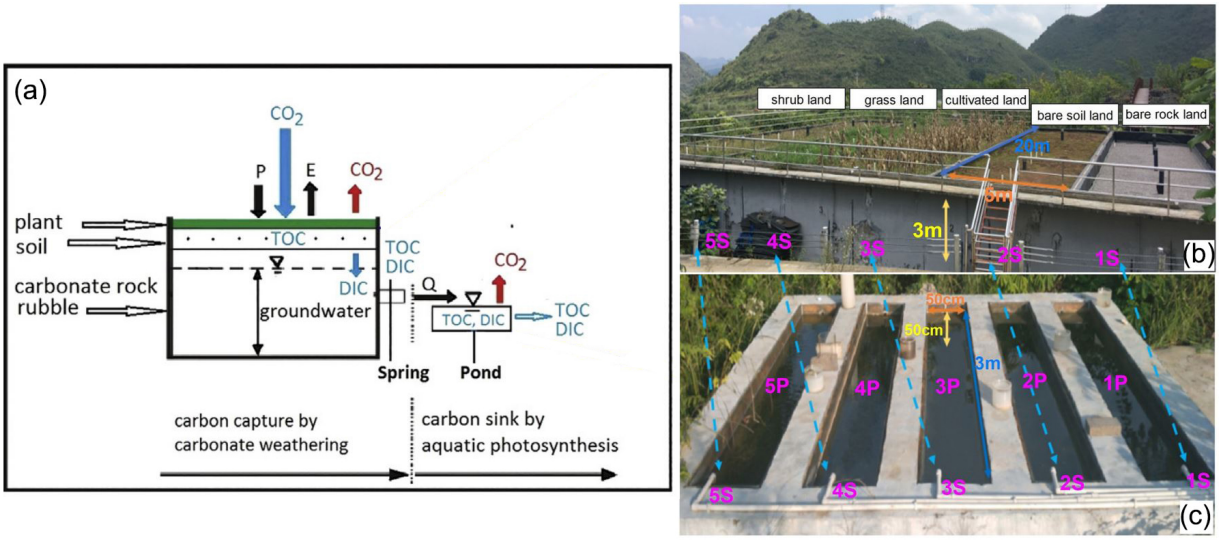

Fig 2.5: (a) *The structure of the spring-pond system in Shawan karst simulation test site. Where DIC is the dissolved inorganic carbon; Q is the runoff; TOC is the total organic carbon; P is the precipitation and E is the evapotranspiration.* ***(b)*** *The simulated catchments (tanks) of different land use. Five land-use include bare rock land, bail soil land, cultivated land, grassland and shrub land (T1-T5).* ***(c)*** *Five corresponding spring-fed ponds connect with the tanks(S-P(1) - S-P(5)).*

3. Comparisons of the effects of temperature, runoff, and land cover on carbonate weathering between different karst catchments: insight into the future global carbon cycle

Abstract:

This study compares and analyzes high-frequency hydrochemical data from three karst catchments in the mountainous Gadenalpe (GAC, Austrian Alps), Tsanfleuron-Sanetsch (TSC, Swiss Alps), and Banzhai (BZC, SW China) regions, to differentiate the effects of temperature, runoff, and land-cover on carbonate weathering. The results show that when bare rock dominates in the recharge area, as in the GAC and TSC, the seasonal discharge variations account for the most significant change in HCO_3^- concentration. In these two alpine catchments, maximum HCO_3^- concentrations occurred in the cold season when the areas were covered by snow and discharge was low, whereas minimum HCO_3^- concentrations occurred in the warm season, when snowmelt and/or glacier melt caused higher discharge and dilution. In contrast, control by the strong seasonal variation in soil respiration in the subtropical catchment (BZC), caused by the well-developed forest cover, exceeded the negative impact of temperature on carbonate weathering. This led to higher HCO_3^- concentration s during the summer growing season than in the winter dormant season. This study demonstrates that the occurrence of different soils/vegetation has a profound impact on the behavior of carbonate weathering on land, from negative temperature- and discharge-driven correlations in alpine catchments to positive soil CO_2-driven correlation in subtropical catchments.
Based on the equilibrium modeling of HCO_3^- concentration for a global temperature range, it is predicted that under future global warming, karst regions in cold climates with vegetation cover will have increasingCO_2 consumption potential, whereas karst regions in warm climates will have decreasing CO_2 consumption potential.

Published as:

Zeng, S., Liu, Z., Goldscheider, N., Frank, S., Goeppert, N., Kaufmann, G., Zeng, G., Zeng. Q., Sun, H. (2021). Comparisons of the effects of temperature, runoff, and land cover on carbonate weathering between different karst catchments: insight into the future global carbon cycle. *Hydrogeology Journal*, 29, 331-345,

DOI: https://doi.org/10.1007/s10040-020-02252-5

Contribution of Sibo Zeng to article

- Part of field investigation team in Gadenalpe catchment and spring water sample collection
- Physicochemical data collection and preparation
- Visualization, interpretation, and discussion of results
- Writing all the sections of the article

4. Natural and anthropogenic driving forces of carbonate weathering carbon sink flux: a model comparison study at global scale

Abstract:

Continental weathering is a carbon-dioxide (CO_2) sink in the global carbon cycle. The weathering process is driven by environmental factors such as changes in temperature, moisture, CO_2 concentration, which can have natural (climate) or anthropogenic (land use) origins. In this paper, we attempt to evaluate the global applicability of different environmental drivers, which can be used to estimate the global carbonate dissolution intensity (bicarbonate concentration, HCO_3^-, as a proxy) and carbon sink flux (*CCSF*). We use three ecological models and satellite-based databases, which provide estimates on soil CO_2-concentrations (pCO_2), temperature (T) and runoff (N). For all three models, we obtain similar global average HCO_3^- concentrations and *CCSF*, ranging from 2.73-2.81 mmol L^{-1} and 4.52-5.36 t C km^{-2} yr^{-1}. However, their spatial patterns differ significantly, depending on the database used.
We compare our calculated HCO_3^- concentrations to observed carbonate spring records, and we compare the contributions from both natural and anthropogenic driving forces on the global scale: Natural drivers dominate the carbonate weathering intensity (HCO_3^-), where the ecosystem is dominated by a single land cover type. Antropogenically induced global land-use changes, however, alter the global HCO_3^- distribution significantly. Furthermore, our simulation results indicate that the different water yield caused by land-use changes could be more significant for the total carbon-sink budget than dissolution intensity. The HCO_3^- flux is statistically more dependent on the changes of water flow instead of solutes concentration. Accordingly, we stress that anthropogenic factors are as significant as natural climatic changes for the carbonate weathering process.

Submitted as:

Zeng, S. & Kaufmann, G. & Liu, Z. (2021). Natural and anthropogenic driving forces of carbonate weathering carbon sink flux: a model comparison study at global scale. *Global Biogeochemical Cycles*.

DOI:

Contribution of Sibo Zeng to article:

- Global soil pCO_2 model selection and operation
- Remote sensing data collection and preparation
- Visualization, interpretation, and discussion of results
- Writing all the sections of the article

5. Sensitivity of the global carbonate weathering-related carbon sink flux to future climate and land-use changes

Abstract:

The response of carbonate weathering carbon-sink flux (CCSF) to its environmental drivers is still not well understood on the global scale. This hinders understanding of the terrestrial carbon cycle. Here, we show that there is likely to be a widespread and consistent increase in the global CCSF (ranging from + 9.8% (RCP4.5) to + 17.1% (RCP8.5)) over the period 1950–2100. In the coming years the increasing temperature might be expected to have a negative impact on carbonate weathering. However, the increasing rainfall and anticipated land-use changes will counteract this, leading to a greater CCSF. This finding has been obtained by using long-term historical (1950–2005) and modeled future (2006–2100) data for two scenarios (RCP4.5 and RCP8.5) for climate and land-use change in our CCSF equilibrium model. This study stresses the potential role that carbonate weathering may play in the evolution of the global carbon cycle over this century.

Published as:

Zeng, S. & Liu, Z. & Kaufmann, G. (2019). Sensitivity of the global carbonate weathering-related carbon sink flux to future climate and land-use changes. *Nature Communications*, 10, 5749.

DOI: https://doi.org/10.1038/s41467-019-13772-4

Contribution of Sibo Zeng to article

- Data collection and preparation
- Visualization, interpretation, and discussion of results
- Writing all the sections of article

6. Seasonal and diurnal variations in DIC, NO_3^- and TOC concentration in spring-pond ecosystem under different land-uses: Carbon limitation of aquatic photosynthesis

Abstract:

Human activities have altered terrestrial carbon (C) and nitrogen (N) dynamics via changes to land cover and use such as deforestation, agriculture, application of fertilizers, etc. and have influenced the patterns of organic C input and eutrophication in downstream freshwater ecosystems. Biogeochemical cycling of C and N and the related organic carbon (OC) production may display correlated diurnal and seasonal variations due to photosynthesis and respiration in these ecosystems, whose underlying mechanisms still need to be resolved. In this study, we document the diurnal and seasonal variations measured in DIC (dissolved inorganic carbon), NO3−, TOC (total organic carbon) and other related hydrochemical parameters (pH and DO-dissolved oxygen) in five artificial spring-pond ecosystems with differing land-uses in tanks draining into springs and corresponding ponds, constructed at the Shawan Karst Test Site, SW China. It was found that diurnal changes in DIC, NO3− and TOC in all ponds were dominated by aquatic ecosystem metabolism (i.e., photosynthesis and respiration), as evidenced by the pertinent variations in DO and pH. Daily DIC and NO3− uptake and OC production were higher in October (growing period) and lower in January (dormant period), indicating seasonal differences in assimilation that were determined by both changes in weather (temperature and light) and nutrient inputs. Under conditions of bare rock or bare soil, there was very low DIC and NO3− additions to the spring-pond ecosystems, resulting in lower OC productivity in the ponds. Cropped land yielded higher DIC and NO3− to the pond, due to growth of corn and use of fertilizers that enhanced OC production. Highest productivity and densest vegetation cover on tanks with grassland or shrubs (with higher N retention in soils) resulted in higher DIC but limited NO3− addition to the ecosystems downstream. The highest DIC concentration (in the grassland) resulted in maximum OC production in the pond. These results indicate that OC production in the ponds with elevated pH was limited by DIC fertilization. In general, the supply of DIC is not considered to limit aquatic primary productivity because its concentration exceeds that of other plant macronutrients such as NO3 and PO43− by two or three orders of magnitude. Therefore, the carbon limitation detected here may indicate that photoautotrophs in karst dominated aquatic terrains (dominated by Charophyta and Spirogyra) cannot use the total DIC for photo-synthesis but only the dissolved CO2, which comprises < 1% of total DIC at pH > 8.2 that is characteristic in these environments. This may have implications for control of eutrophication in such alkaline aquatic ecosystems, i.e., rates of eutrophication in freshwater ecosystems may be regulated not only by N and/or P but also by C. It is also projected that there will be an increase in OC sequestration with the current land-use and global climate change-driven increases in DIC, due to carbon limitation of aquatic primary production.

Published as:

Zeng, S., Liu, H., Liu Z., Kaufmann, G., Zeng, Q., Chen, B. (2019). Seasonal and diurnal variations in DIC, NO3- and TOC concentrations in spring-pond ecosystems under different land-uses at the Shawan Karst Test Site, SW China: Carbon limitation of aquatic photosynthesis. *Journal of Hydrology*, 574, 811-821.

DOI: https://doi.org/10.1016/j.jhydrol.2019.04.090

Contribution of Sibo Zeng to article

- Field investigation in Shawan test site and laboratory experiments
- Diurnal and seasonal data collection
- Visualization, interpretation, and discussion of results
- Writing all the sections of article

7. Conclusions and Outlook

The main focus of this thesis is a characterization of the behavior and the variation of carbonate-weathering carbon-sinks under global natural and anthropogenic perturbations, based on field observations and model simulations. We have achieved this task with four steps:

1. We have conducted a comparison study among three different typical karst catchments to discuss the behavior of carbonate-weathering carbon-sink flux under different climatic and land-cover conditions.
2. We used three ecologically-based soil pCO_2 models and a potential maximum carbonate dissolution equation to detect the optimal environmental parameter for estimating global HCO_3^- and the related carbon sink flux.
3. After comparing the accuracy of different pCO_2 models, a new mixed-effect model which combined both climatic and anthropogenic drivers is constructed to simulate the historical and future change of carbonate-weathering carbon-sink flux.
4. The impact of human land-use strategies on terrestrial aquatic carbon-pump effect coupled by carbonate weathering is quantified based on the evidence from an artificial karst simulation test site.

High-resolution field measurements, simulation test experiments, meteorological interpolation data and satellite-based land surface data are the main data source throughout the four studies. By using these data, four consecutive studies systematically describe how carbonate-weathering carbon-sink flux evolves in a dynamic earth system and how this carbon removal mechanism impacts on the present and future global carbon cycle.

In the introduction, we derived four questions, which this thesis attempts to answer:

- **Question 1: How do temperature, runoff and land cover control the carbonate weathering behaviour and related carbon sink flux?**

In order to answer the first question, the first article compares a two-year high-resolution hydro-chemical measurement from three typical carbonate-dominant catchments, which have distinctive environmental backgrounds. By comparing their long-term hydro-chemical measurements, the impacts of temperature, runoff and land-cover on carbonate-weathering carbon-sink flux are well quantified and discussed. The results of this study show that in two alpine carbonate catchments with a low proportion of vegetation and seasonal snow cover, the

variation of HCO_3^- concentrations are mainly controlled by air temperature and water flow. The HCO_3^- concentrations in two high-alpine catchments are higher in drier freezing season. As the glaciers thaw in the warm season, the increasing water flow decreases the concentration of HCO_3^-, yet this amplified discharge increases the total alkalinity flux. Hourly temperature fluctuation rules the diurnal variation of HCO_3^- in high alpine catchments (mostly dominated by bare rock), showing a primary control of temperature when vegetation is missing.

By contrast, a different seasonal HCO_3^- pattern is found in a forest-dominant subtropical catchment. Due to the active relation between temperature and forest ecosystem respiration, the HCO_3^- variation then presents an inverse seasonal pattern, when compared to alpine catchments. The HCO_3^- is higher in the wet season and lower in the dry season. The strong soil pCO_2 produced by forest in the wet season (summer and autumn) promotes the carbonate dissolution, counteracting the negative impact caused by higher temperatures. The carbonate weathering intensity (HCO_3^-) in the forest-dominant subtropical catchment is 40%~60 higher than that of alpine catchments owing to the vegetation cover. Yet, after summing up the influence of total runoff, the two alpine catchments show a higher carbon-sink flux in comparison to the subtropical catchment, which is a result of the ice/snow water and the chemo-statistic behavior of weathering loads. The findings in these three catchments stress that the environmental background may strongly alter the carbonate weathering behavior and related carbon sink flux.

- **Question 2: Which models or parameter values can be better applied to estimate the carbonate-weathering intensity on a global scale?**

In the second study, three ecologically-based soil pCO_2 models and a series of satellite-based products are applied to investigate the parameter space for the environmental drivers controlling HCO_3^- and carbonate-weathering carbon-sink at the global scale. The results of the three models show similar global mean HCO_3^- and CCSF, ranging from 2.73~2.81 mmol L^{-1} and 4.52~5.36 t C km^{-2} yr^{-1}. However, their spatial patterns differ significantly, depending on the database used (net primary production NPP, evapotranspiration ET and soil volumetric-water content SWC). The results for the net primary production based soil pCO_2 model (*NPP-*pCO_2) matches well with most globally observed carbonate-spring HCO_3^- records. The general applicability of *NPP-*pCO_2 can be attributed to the crucial role of land cover in controlling soil respiration in this model. Moreover, according to our model results, we find that natural drivers dominate the carbonate-weathering intensity (HCO_3^-), where the ecosystem is dominated by a single land cover type. Antropogenically induced land-use changes, however, also alter the global HCO_3^- distribution significantly. More importantly, the HCO_3^- flux is statistically more dependent on

the changes of water flow instead of solute's concentration due to the competing process between thermodynamics and soil respiration. Thus, this study suggests that anthropogenic factors are as significant as natural climatic changes for the carbonate weathering process.

- **Question 3: How does the carbonate-weathering related carbon sink response to future global changes?**

The results of our first two studies detect the behavior of HCO_3^- and carbonate-weathering carbon-sink under different environmental conditions, but it still cannot answer the question of how this carbon-removal mechanism responds to future global change. Hence, in our third study, we constructed a new mixed-effects model to simulate the historical and future change of carbonate weathering carbon sink. This model adopts the optimal parameter *NPP* (which has been identified in our second study) to estimate soil pCO_2, but using a modified version of the original *NPP*-based pCO_2 model. We utilize the CMIP5 future projected meteorological data and land-use data to calculate *NPP*, pCO_2 and runoff. This is the first attempt to simulate the long-term temporal and spatial variation of carbonate-weathering carbon-sink flux, which extends the study period to 150 years (1950-2100). The results show that there is likely to be a widespread and consistent increase in global carbonate-weathering carbon-sink flux (ranging from +9.8 % to +17.1 %) from 1950 to the end of this century. The greatest HCO_3^- enhancement will occur in high latitudes, yet the carbon sink flux will increase the most in low latitudes. Generally, future warming climate will lead a HCO_3^- decline globally. However, the increasing rainfall and anticipated land-use changes will counteract this, leading a greater carbon sink flux. The model simulations indicate that carbonate-weathering carbon-sink flux may response sensitively to global change. Therefore, we stress that this carbon sink should be considered into the future global carbon cycle model. This finding answers the third question in section 1.3.

- **Question 4: What is the influence of different human land-use strategies on the terrestrial BCP effect in surface water system?**

The carbonate-weathering process captures atmospheric CO_2 and transforms it to dissolved inorganic carbon (mostly HCO_3^-), transported to inland waters. The aquatic phototrophs can utilize the weathering products for primary production via CCMs, thus forming a geological long-term carbon sink. Human activities are strongly involved in this aquatic biotic process by altering the nutrient inputs by different land-uses. The fourth study investigates the relation between DIC and NO_3^- input with aquatic OC production (mainly TOC) in a karst simulation

test site in Southwest China. The results show that the diurnal and seasonal variations of aquatic DIC, NO_3^- and TOC are controlled by the aquatic photosynthesis and respiration as evidenced by the pertinent variations in DO and pH. The total TOC exports are varying widely among spring-pond systems with different land uses, which can be related to different DIC and NO_3^- input caused by different land-use scenarios. We found that the high DIC produced by grassland promotes the aquatic organic production, leading a high TOC export than bare rock land or bare soil land, although the NO_3^- input is highly limited. This finding indicates that the BCP effect in elevated pH environment is limited by HCO_3^- input. The rising DIC supply by carbonate-weathering counters the aquatic ecosystem carbon limitation. In karst terrains, carbon may become a limited nutrient if the aquatic photoautotrophs cannot efficiently utilize the total DIC. Thus, human land-use strategies could have a great potential for regulating the BCP effect in carbonate terrain.

The four consecutive studies presented in this thesis provide a general overview on how carbonate-weathering carbon-sinks evolve and their responses to global change. According to our findings, we suggest that the carbon-dioxide removal mechanism could be a new direction for future carbon-cycle studies due to its great sensitivity to environmental perturbations. The evidence from field sites and the findings from models indicate that carbonate-weathering carbon-sink flux will experience a great enhancement in the future, especially in the areas with intense human impacts, although the weathering intensity may be constrained by the global warming trend. Future human land-use strategies could be applied to promote the HCO_3^- flux through karst terrain, promoting the CO_2 sequestration. This thesis is not only important to fully characterize the behavior and variations of carbonate-weathering carbon-sink under global change, but also provides the perspective of further research in this field. We suggest that improvements can be made regarding following aspects:

- First, when estimating the carbon sink from cropland, the impacts from nitric acid and sulfuric acid need to be excluded, because the carbonate weathering caused by these acids generate no carbon sink. Instead, these two acids could lead to CO_2 emission.
- Second, the CCMs efficiency vary widely among different aquatic phototrophs species. To improve the BCP in karst aquatic water systems, the impacts of DIC fertilization for different species need be further detected in future study.
- Third, we suggest that different CO_2 emissions will determine future warming trends and the environmental perturbations they induce, so the responses of carbonate weathering may also vary widely. However, CO_2 removal by deliberate land-use

practices may make it easier to understand and account for these uncertainties. Therefore, we stress that carbonate weathering enhancement by land-use changes is applicable which can potentially help mitigate the current climate trends.

8. References

Abell, J.M., Ozkundakci, D., Hamilton, D.P., 2010. Nitrogen and phosphorus limitation of phytoplankton growth in New Zealand lakes: Implications for eutrophication control. *Ecosystems*, 13, 966–977.

Adams J. M., Post W. M., 1999. A preliminary estimate of changing calcrete carbon storage on land since the Last Glacial Maximum. *Global Planetary Change*, 20, 243–256.

Amiotte-Suchet, P., Probst, J.-L., 1995. A global model for present-day atmospheric/soil CO_2 consumption by chemical erosion of continental rocks (GEM-CO_2). Tellus, B. 47 (1–2), 273–280.

Andrews, J. A., Schlesinger, W. H., 2001. Soil CO_2 dynamics, acidification, and chemical weathering in a temperate forest with experimental CO_2 enrichment. *Global Biogeochemical Cycle*, 15, 149-162.

Arvidson, R.S., Mackenzie, F.T., Guidry, M., 2006. MAGic: a Phanerozoic model for the geochemical cycling of major rock-forming components. *American Journal of Science*, 306 (3), 135–190.

Arora, V. K., Boer, G. J., 2010. Uncertainties in the 20th century carbon budget associate with land use change. *Global Change Biology*, 16, 3327-3348.

Balmer, M.B., Downing, J.A., 2011. Carbon dioxide concentrations in eutrophic lakes: undersaturation implies atmospheric uptake. *Inland Waters*, 1(2), 125–132.

Beaulieu, E., Goddéris, Y., Donnadieu, Y., Labat, D., Roelandt, C., 2012. High sensitivity of the continental-weathering carbon dioxide sink to future climate change. *Nature Climate Change*, 5, 46-349.

Berner, R.A., Lasaga, A.C., Garrels, R.M., 1983. The carbonate-silicate geochemical cycle and its effect on atmospheric carbon-dioxide over the past 100 million years. *America journal of Science,* 283, 641-683.

Berner, R.A., 1997. The rise of plants and their effect on weathering and atmospheric CO_2. *Science*, 276, 544- 546.

Bluth, G.J., Kump, L.R., 1994. Lithologic and climatologic controls of river chemistry. *Geochimica et Cosmochimica Acta*, 58 (10), 2341–2359

Bond-Lamberty, B., Thomson, A., 2010. Temperature-associated increases in the global soil respiration record. *Nature*, 464, 579-582.

Brook G. A., Folkoffff M. E., Box E. O., 1983. A world model of soil carbon dioxide. *Earth Surface Processes and Landforms*, 8, 79–88.

Calmels, D., Gaillardet, J., François, L., 2014. Sensitivity of carbonate weathering to soil CO2 production by biological activity along a temperate climate transect. *Chemical Geology*, 390, 74–86.

Chen, B., Yang, R., Liu, Z., Sun, H., Yan, H., Zeng, Q., Zeng, S., Zeng, C., Zhao, M., 2017. Coupled control of land uses and aquatic biological processes on the diurnal hydrochemical variations in the five ponds at the Shawan Karst Test Site, China: Implications for the carbonate weathering-related carbon sink. *Chemical Geology*, 456, 58-71.

Chen, C.Y., Durbin, E.G., 1994. Effect of pH on the growth and carbon uptake of marine phytoplankton. *Marine Ecology-Progress Series*, 109, 83-94.

Chen, S., Huang, Y., Zou, J., Shen, Q., Hu, Z., Qin, Y., Chen, H., Pan, G., 2010. Modeling interannual variability of global soil respiration from climate and soil properties. *Agricultural. Forest Meteorology*, 150, 590–605.

Chen, Z., Auler, A.S.., Bakalowicz, M., 2017. The World Karst Aquifer Mapping project: concept, mapping procedure and map of Europe. *Hydrogeology Journal*, 25, 771-785.

Cicerone, D.S., Stewart, A.J., Roh, Y., 1999. Diurnal cycles in calcite production and dissolution in a eutrophic basin. *Environmental Toxicology and Chemistry*, 18, 2169–2177.

Clarke, S.J., 2002. Vegetation growth in rivers: influences upon sediment and nutrient dynamics. *Progress in Physical Geography*, 26, 159–172.

Cochran M.F., Berner R.A., 1996. Promotion of chemical weathering by higher plants: field observations on Hawaiian basalts. *Chemical Geoology*,132, 71-77.

Conley, D.J., Paerl, H.W., Howarth, R.W., Boesch, D.F., Seitzinger S.P., Havens, K.E., Lancelot, C., Likens, G.E., 2009. Controlling eutrophication: nitrogen and phosphorus. *Science*, 323, 1014-1015

Del Grosso S., Parton W., Stohlgren T., Zheng D. L., Bachelet D., Prince S., Hibbard K., Olson. R., 2008. Global potential net p9rimary production predicted from vegetation class, precipitation, and temperature. *Ecology,* 89, 2117–2126.

DeFries R.S., Rudel, T., Uriarte, M., Hansen, M., 2010. Deforestation driven by urban population growth and agricultural trade in the twenty-first century. *Nature Geoscience*, 3, 178–181

Deines, P., Langmuir, D., Harmon, R.S., 1974. Stable carbon isotope ratios and the existence of a gas phase in the evolution of carbonate ground waters. *Geochimica et Cosmochimica Acta*. 38, 1147-1164.

Dinnes, D.L., Karlen, D.L., Jaynes, D.B., 2002. Nitrogen management strategies to reduce nitrate leaching in tile-drained Midwest soils. *Agronomy Journal*, 94, 153-171.

Drake, T.W., Tank, S.E., Zhulidov, A.V., Holmes, RM., Gurtovaya, T., Spencer RGM., 2018. Increasing alkalinity export from large Russian arctic river. *Environmental Science & Technology*. 52, 8302–8308.

Dreybrodt, W., 1988 Processes in Karst Systems. Springer, Heidelberg.

Dreybrodt. W., Lauckner, J., Liu, Z.H., 1996. The kinetics of the reaction $CO_2+H_2O \rightarrow H^++HCO_3^-$ as one of the rate limiting steps for the dissolution of calcite in the system H_2O-CO_2-$CaCO_3$. *Geochimica et Cosmochimiac Acta*, 60, 3375–3381.

Faust, K., 2017. Dynamik hydrochemischer Parameter von Karstquellen und Gewässern im Gadental (Österreich) unter besonderer Berücksichtigung von Wasserhaushaltsprozessen. Master Thesis.

Ford, D.C., 1971. Characteristics of limestone solution in the Southern Rocky Mountains and Selkink Mountains.*Canadian Journal of Earth Science*. 8, 585-609.

Ford, D.C., Williams, P.W., 2007. *Karst Hydrogeology and Geomorphology*. Wiley, London.

Forkel, M., Carvalhais, N., Rödenbeck, C., Keeling, R., Heimann, M., Thonicke, K., Zaehle, S., Reichstein, M., 2016. Enhanced seasonal CO_2 exchange caused by amplified plant productivity in northern ecosystems. *Science*, 351, 696–699.

Fekete, B. M., Vörösmarty, C., Grabs, W., 2002. High-resolution fields of global runoff combining observed river discharge and simulated water balances. *Global Biogeochemical Cycles*, 16, 15–1.

Ferguson, P. R., Dubois, K. D., Veizer, J., 2011. Fluvial carbon fluxes under extreme rainfall conditions: inferences from the Fly River, Papua New Guinea. *Chemical Geology*, 281 (3), 283–292.

Frank, S., Goeppert, N., Goldscheider, N., 2020. Dynamic water and mass budget of an alpine karst catchment. *Hydrogeology Journal*, submitted.

Elser, J.J., Bracken, M.E.S., Cleland, E.E., Gruner, D.S., Harpole, W.S., Hillebrand, H., Ngai, J.T., Seabloom, E.W., Shurin, J.B., Smith, J.E., 2007. Global analysis of nitrogen and phosphorus limitation of primary producers in freshwater, marine and terrestrial ecosystems. *Ecology Letters*, 10, 1135–1142.

Gabrovsek F., 2009. On concepts and methods for the estimation of dissolutional denudation

rates in karst areas. *Geomorphology*, 106:9–14.

Gaillardet, J., Dupré, B., Louvat, P., Allegre, C., 1999. Global silicate weathering and CO_2 consumption rates deduced from the chemistry of large rivers. *Chemical Geology*. 159 (1), 3–30.

Gaillardet, J., Calmels, D., Romero-Mujalli, G.Z., Zakharova, E., Hartmann, J., 2019. Global climate control on carbonate weathering intensity. *Chemical Geology*, 527, UNSP 118762.

Gislason, S.R., Oelkers, E.H., Eiriksdottir, E.S., Kardjilov, M.I., Gisladottir, G. Sigfusson, B., 2009. Direct evidence of the feedback between climate and weathering. *Earth Planetary Science Letters*. 277, 213-222.

Giusti, E.V., 1978. Hydrogeology of the Karst of Puerto Rico. vol. 1012 *US Govt. Print. Off.*

Goddéris, Y., Williams, J.Z., Schott, J., Pollard, D., Brantley, S.L., 2010. Time evolution of the mineralogical composition of Mississippi Valley loess over the last 10kyr: Climate and geochemical modelling. *Geochimica et Cosmochimica Acta*, 74, 6357-6374.

Godsey, S.E., Kirchner, J.W., Clow, D.W., 2009. Concentration-discharge relationships reflect chemostatic characteristics of US catchments. *Hydrology Process*, 23, 1844–1864.

Goldscheider, N., 2019. A holistic approach to groundwater protection and ecosystem services in karst terrains. *Carbonates and Evaporites*, 34(4): 1241-1249.

Goldscheider, N., Chen, Z., Broda, S., Auler, A.S., Bakalowicz, M., Drew, D., Hartmann, J., Jiang, G., Moosdorf, N., Stevanovic, Z. Veni, G., 2020. Global distribution of carbonate rocks and karst water resources. *Hydrogeology Journal*, 28, 1661-1677.

Gombert, P., 2002. Role of karstic dissolution in global carbon cycle. *Global and Planetary Change*, 33, 177–184.

Gremaud, V., Goldscheider, N., Savoy, L., Favre, G., Masson, H., 2009. Geological structure, recharge processes and underground drainage of a glacierised karst aquifer system, Tsanfleuron-Sanetsch, Swiss Alps. *Hydrogeology Journal.* 17, 1833–1848.

Gremaud, V., Goldscheider, N., 2010. Geometry and drainage of a retreating glacier overlying and recharging a karst aquifer, Tsanfleuron–Sanetsch, Swiss Alps. *Acta Carsologica*, 39, 289–300.

Gruber, N., Galloway, J.N., 2008. An Earth-system perspective of the global nitrogen cycle. *Nature*, 451, 293-296.

Gwiazda, R.H., Broecker, W.S., 1994. The separate and combined effects of temperature, soil pCO_2 and organic acidity on silicate weathering in the soil environment: Formulation of a model and results. *Global Biogeochemical Cycles*, 8, 141-155.

Haberl, H., Erb, K.H., Krausmann, F., Gaube, V., Bondeau, A., Plutzar, C., Gingrich, S., Lucht, W. Fischer-Kowalski, M.. 2007. Quantifying and mapping the human appropriation of net primary production in Earth's terrestrial ecosystems. *Proceedings of the National Academy of Sciences. USA*, 104, 12942-12947.

Hall, R.O., Tank, J.L., Sobota, D.J., Mulholland, P.J., O'Brien, J.M., Dodds, W.K., Webster, J.R., Valett, H.M., Poole, G.C., Peterson, B.J., Meyer, J.L., McDowell, W.H., Johnson, S.L., Hamilton, S.K., Grimm, N.B., Gregory, S.V., Dahm, C.N., Cooper, L.W., Ashkenas, L.R., Thomas, S.M., Sheibley, R.W., Potter, J.D., Niederlehner, B.R., Johnson, L.T., Helton, A.M., Crenshaw, C.M., Burgin, A.J., Bernot, M.J., Beaulieu, J.J., Arango, C.P., 2009. Nitrate removal in stream ecosystems measured by ^{15}N addition experiments: Total uptake. *Limnology Oceanography*, 54, 653–665.

Harrison, J.A., Matson, P.A., Fendorf, S.E., 2005. Effects of a diurnal oxygen cycle on nitrogen transformations and greenhouse gas emissions in a eutrophied subtropical stream. *Aquatic Sciences*, 67, 308–315.

Hartmann J., 2009. Bicarbonate-fluxes and CO_2-consumption by chemical weathering on the Japanese Archipelago - Application of a multi-lithological model framework. *Chemical Geology*, 265, 237-271.

Hartmann. J., West, J.A., Renforth, P., Köhler, P., De La Rocha, C.L, Wolf-Gladrow, D.A., et al., 2013. Enhanced chemical weathering as a geoengineering strategy to reduce atmospheric carbon dioxide, supply nutrients, and mitigate ocean acidification. *Review of Geophysics*, 51, 113–149.

Hartmann, J, West, J.A, Renforth, P., Köhler, P., De La Rocha, C.L., Wolf-Gladrow, D.A., Dürr, H.H., Scheffran, J., 2013. Enhanced chemical weathering as a geoengineering strategy to reduce atmospheric carbon dioxide, supply nutrients, and mitigate ocean acidification. *Reviews Geophysics*, 51, 113–149.

Hartmann, J., Moosdorf, N., Lauerwald, R., Hinderer, M., West, A.J., 2014b. Global chemical weathering and associated P-release-the role of lithology, temperature and soil properties. *Chemical Geology*, 363, 145–163.

Hattanji. T., Ueda. M., Song. W., 2014. Field and laboratory experiments on high dissolution rates of limestone in stream flow. *Geomorphology*, 204, 485-492.

Hecky, R.E., Kilham, P., 1988. Nutrient limitation of phytoplankton in fresh-water and marine environments: a review of recent evidence on the effects of enrichment. *Limnology Oceanography*. 33, 796–822.

Heffernan, J.B., Cohen, M.J., 2010. Direct and indirect coupling of primary production and

diurnal nitrate dynamics in a subtropical spring-fed river. *Limnology Oceanography*, 55, 677–688.

Hein, M., Sand-Jensen, K., 1997. CO_2 increases oceanic primary production. *Nature*, 388, 526–527.

Hein, M., 1997. Inorganic carbon limitation of photosynthesis in lake phytoplankton. *Freshwater Biology*, 37, 545–552.

Hessen, D.O., Henriksen, A., Smelhus, A.M., 1997. Seasonal fluctuations and diurnal oscillations in nitrate of a heathland brook. *Water Research*, 31, 1813–1817.

Hibbard, K.A., Law, B.E., Reichstein, M., Sulzman, J., 2005. An analysis of soil respiration across northern hemisphere temperate ecosystems. *Biogeochemistry*, 73, 29–70.

Howarth, R,W., Marino, R., 2006. Nitrogen as the limiting nutrient for eutrophication in coastal marine ecosystems: Evolving views over three decades. *Limnology Oceanography*, 51(1), 364-376.

Huang, F., Zhang, C., Xie, Y., Li, L., Cao, J., 2015. Inorganic carbon flux and its source in the karst catchment of Maocun, Guilin, China. *Environmental Earth Science*. 74(2), 1079-1089.

Huang, N., Wang, L., Song, X.P., Black, A., Jassal, R.S., Myneni, R.B., et al., 2020. Spatial and temporal variations in global soil respiration and their relationships with climate and land cover. *Science Advance*. 6,eabb8508.

Huang, C., Zhang, L., Li, Y., Lin, C., Huang, T., Zhang, M.L., Zhu, A.X., Yang, H., Wang, X.L., 2018. Carbon and nitrogen burial in a plateau lake during eutrophication and phytoplankton blooms. *Science of the Total Environment*, 616-617, 296-304.

Hubau, W., Lewis, S., Phillips, O., Affffum-Baffffoe, K., Beeckman, H., Cuní-Sanchez, A., Daniels, A., Ewango, C., Fauset, S., Mukinzi, J., 2020. Asynchronous Carbon Sink Saturation in African and Amazonian Tropical Forests. *Nature*, 579: 80–87.

Huh, Y., Tsoi, M. Y., Zaitsev, A. Edmond, J. M., 1998. The fluvial geochemistry of the rivers of Eastern Siberia: I. Tributaries of the Lena River draining the sedimentary platform of the Siberian Craton. *Geochimica et Cosmochimica Acta*, 62, 1657–1676.

Hurtt, G.C., et al., 2011. Harmonization of land-use scenarios for the period 1500–2100: 600 years of global gridded annual land-use transitions, wood harvest, and resulting secondary lands. *Climatic Change*, 109,117.

Iversen, L.L., Winkel. A., Baastrup-Spohr, L., Hinke, A.B., Alahuhta, J., Baattrup-Pedersen, A., et al., 2019. Catchment properties and the photosynthetic trait composition of freshwater plant communities. *Science*, 366, 878-881.

Jeelani, G., Bhat, N.A., Shivanna, K., Bhat, M.Y., 2011. Geochemical characterization of surface water and spring water in SE Kashmir Valley, western Himalaya: implications to water-rock interation. *Journal of Earth System Science*, 120, 921-932.

Jarvie, H.P., Douglas, R. Smith., Lisa, R.N, Edwards, F.K., Bowes, M.J., King, S.M., Scarlett, P., Davies, S., Dils, R.M., Bachiller-Jareno, N., 2018. Phosphorus and nitrogen limitation and impairment of headwater streams relative to rivers in Great Britain: A national perspective on eutrophication. *Science of the Total Environment*, 621, 849-862.

Jiang, Y.J., Hu, Y.J., Schirmer. M., 2013. Biogeochemical controls on daily cycling of hydrochemistry and $\delta^{13}C$ of dissolved inorganic carbon in a karst spring-fed pool. *Journal of Hydrology*. 478, 157-168.

Jiao, F., Wen, Z. M. An, S.S., 2011. Changes in soil properties across a chronosequence of vegetation restoration on Loess Plateau of China. *Catena*, 86, 100-166.

Jin, Y., & Jury, W. A., 1996. Characterizing the dependence of gas diffusion coefficient on soil properties. *Soil Science Society of America Journal*, 60, 66-71.

Kalantari, N., Alizadeh, B., Mohammadi, A.R., Keshavarzi, M.R., 2011. A hydrochemical and Dye- tracing investigation in the Posht-e-Naz Karstic Aquifer, Alburz Mountain, Northern Iran. *Journal of Mountain Sciences*, 8, 37-45.

Khaledian, Y., Kiana, F., Ebrahimi, S., Brevik, E., Aitkenhead-Peterson, J., 2016. Assessment and monitoring of soil degradation during land use change using multivariate analysis. *Land Degradation & Development*, 28, 128-141.

Lecomte, K.L.,Bicalho, C., Silva-Filho, E.V., 2016. Geochemical characterization in karst basin tributaries of the San Franciscan depression: The Corrente River, Western Bahia, NE-Brazil. *Journal of South America Earth Sciences*, 69, 119-130.

Lerman, A. L., Wu, L., Mackenzie, F. T., 2007. CO_2 and H_2SO_4 consumption in weathering and material transport to the ocean, and their role in the global carbon balance. *Marine Chemistry*, 106, 326–350.

Lieth, H. Modeling the primary productivity of the world, In *Primary Productivity of the Biosphere* (Springer, Berlin Heidelberg, 1975), pp. 237–263.

Liu, H., Liu, Z., Macpherson, G.L., Yang, R., Chen, B., Sun, H., 2015. Diurnal hydrochemical variations in a karst spring and two ponds, Maolan Karst Experimental Site, China: Biological pump effects. *Journal of Hydrology*, 522, 407-417.

Liu, Z., & Zhao, J., 2000. Contribution of carbonate rock weathering to the atmospheric CO_2 sink. *Environmental Geology*, 39, 1053-1058.

Liu, Z., Li, Q., Wang, J., 2007. Seasonal, diurnal and storm-scale hydrochemical variations of typical epikarst springs in subtropical karst areas of SW China: soil CO_2 and dilution effects. *Journal of Hydrology*, 337, 207–223.

Liu, Z., Liu, X., Liao, C., 2008. Daytime deposition and nighttime dissolution of calcium carbonate controlled by submerged plants in a karst spring-fed pool: insights from high time-resolution monitoring of physicochemistry of water. *Environmental Geology*, 55, 1159–1168.

Liu, Z., Dreybrodt, W., Wang, H., 2010. A new direction in effective accounting for the atmospheric CO_2 budget: Considering the combined action of carbonate dissolution, the global water cycle and photosynthetic uptake of DIC by aquatic organisms. *Earth-Science Reviews*, 99, 162-172.

Liu, Z., Dreybrodt, W., Liu, H., 2011. Atmospheric CO_2 sink: silicate weathering or carbonate weathering? *Applied Geochemistry*, 26, 292-294.

Liu, Z., Macpherson, G.L., Groves C., Martin, J.B., Yuan, D., Zeng, S., 2018. Large and active CO_2 uptake by coupled carbonate weathering. *Earth-Science Reviews*, 182, 42-49.

Low-Decarie, E., Fussmann, G.F., Bell, G., 2014. Aquatic primary production in a high-CO2 world. *Trends in Ecology & Evolution*, 29, 223-232 .

Long, X., Sun, Z., Zhou, A., Liu,D., 2015. Hydrogeochemical and isotopic evidence for flow paths of karst waters collected in the Heshang Cave, Central China. *Journal of Earth Sciences*. 26, 149-156.

López-Chicano, M., Bouamama, M., Vallejos, A., Pulido-Bosch, A., 2001. Factors which determine the hydrogeochemical behaviour of karst springs. A case study from the Betic Cordilleras, Spain. *Applied Geochemistry*. 16, 1179-1192.

Macpherson, G.L., Sullivan, P.L., Stotler, R.L., Norwood, B.S., 2019. Increasing groundwater CO_2 in a mid-continent tallgrass prairie: Controlling factors. *E3S Web of Conferences*, 98, 06008.

Mangan, N.M., A. Flamholz, R.D., Hood, R.M., Savage, D.F., 2016. pH determines the energetic efficiency of the cyanobacterial CO_2 concentrating mechanism. *Proceedings of the National Academy of Sciences*, *USA*, 113, E5354–E5362.

Martin, J. B., 2017. Carbonate minerals in the global carbon cycle. *Chemical Geology*, 449, 58-72.

Melnikov, N.B., O'Neill, B.C., 2006. Learning about the carbon cycle from global budget data. Geophysical Research Letters, 33, L02705.

Millot, R., Gaillardet, J., Dupré, B., Allègre, C. J., 2003. Northern latitude chemical weathering

rates: clues from the Mackenzie River Basin, Canada. *Geochimica et Cosmochimica Acta*, 67, 1305–1329.

Moore, P. J., Martin, J. B., Screaton, E. J., 2009. Geochemical and statistical evidence of recharge, mixing, and controls on spring discharge in an eogenetic karst aquifer. *Journal of Hydrology*, 376, 443-455.

Moosdorf, N., Hartmann, J., Lauerwald, R., Hagedorn, B., Kempe, S., 2011. Atmospheric CO_2 consumption by chemical weathering in North America. *Geochimica et Cosmochimica Acta*, 75, 7829-7854.

Morales-Williams, A.M., Wanamaker, A.D., Downing, J.A., 2017. Cyanobacterial carbon concentrating mechanisms facilitate sustained CO_2 depletion in eutrophic lakes. *Biogeosciences*, 14, 2865–2875.

Mulholland, P.J., Thomas, S.A., Valett, H.M., Webster, J.R., Beaulieu, J., 2006. Effects of light on NO_3^- uptake in small forested streams: diurnal and day-to-day variations. *Journal of the North American Benthological Society*, 25, 583–595.

Mulholland, P.J., Helton, A.M., Poole, G.C., Hall, R.O., Hamilton, S.K., Peterson, B.J., Tank, J.L., Ashkenas, L.R., Cooper, L.W., Dahm, C.N., Dodds, W.K., Findlay, S.E.G. Gregory, S.V., Grimm, N.B., Johnson, S.L., McDowell, W.H., Meyer, J.L., Valett, H.M., Webster, J.R., Arango, C.P., Beaulieu, J.J., Bernot, M.J., Burgin, A.J., Crenshaw, C.L., Johnson, L.T., Niederlehner, B.R., O'Brien, J.M., Potter, J.D., Sheibley, R.W., Sobota, D.J., Thomas, S.M., 2008. Stream denitrification across biomes and its response to anthropogenic nitrate loading. *Nature*, 452, 202-206.

Meybeck, M., 1987. Global chemical weathering of surfificial rocks estimated from river dissolved loads. *America Journal of Science*, 287, 401–428.

Norby, R. J., DeLucia, E. H., Gielen, B., 2005. Forest response to elevated CO_2 is conserved across a broad range of productivity. *Proceedings of the National Academy of Sciences. USA*, 102, 18052-18056.

Pan, Y., Birdsey, R.A., Fang, J., Houghton, R., Kauppi, P., Kurz, W.A., Phillips, OL., Shvidenko, A., Lewis, SL., Canadell, JG., Ciais, P., 2011. A large and persistent carbon sink in the world's forests. *Science*, 333, 988–993.

Parker, S.R., Gammons, C.H., Poulson, S.R., DeGrandpre, M.D., 2007. Diurnal variations in stream chemistry and isotopic composition of dissolved inorganic carbon, upper Clark Fork River, Montana, USA. *Applied Geochemistry*. 22, 1329–1343.

Parker, S.R., Gammons, C.H., Poulson, S.R., DeGrandpre, M.D., Weyer, C.L., Smith, M.G., Babcock, J.N., Oba, Y., 2010. Diurnal behavior of stable isotopes of dissolved oxygen

and dissolved inorganic carbon in rivers over a range of trophic conditions, and in a mesocosm experiment. *Chemical Geology*, 269, 22–32.

Parkhurst, D.L., Appelo, C.A.J., 1999. User's guide to PHREEQC (Version 2)—a computer program for speciation, reaction path, 1D-transport, and inverse geochemical calculations. United State Geological Survey — Water Resources Investigations Report 99–4259.

Perrin, A. S., Probst, A., Probst, J.L., 2008. Impact of nitrogenous fertilizer on carbonate dissolution in small agricultural catchment: implications for weathering CO_2 uptake at regional and global scales. *Geochimica et Cosmochimica Acta*, 72, 3015-3213.

Pentecost, A., 1992. Carbonate chemistry of surface waters in a temperate karst region: the southern Yorkshire Dales, UK. *Journal of Hydrology*. 139:211-232.

Piao, S., Friedlingstein, P., Ciais, P., de Noblet-Ducoudré, N., Labat, D., Zaehle, S., 2007. Changes in climate and land use have a larger direct impact than rising CO_2 on global river runoff trends. *Proceedings of the National Academy of Sciences. USA*, 104: 15242-15247.

Pitman, J.I., 1978. Carbonate chemistry of groundwater from tropical tower karst in south Thailand. *Water Resource Research*, 14, 961–967.

Plaza, C., Pegoraro, E., Bracho, R., Celis, G., Crummer, K.G., Hutchings, J.A., Pries, CEH., Mauritz, M., Natali, S.M., Salmon, V., 2019. Direct observation of permafrost degradation and rapid soil carbon loss in tundra. *Nature Geoscience*, 12, 627-631.

Plummer, L.N., Wigley, T.M.L., Parkhurst, D.L., 1978. Kinetics of calcite dissolution in CO_2-water systems at 5℃to 6℃and 0.0 to 1.0 atm CO_2. *America Journal of Science*, 278, 179-216.

Poulson, S.R., Sullivan, A.B., 2010. Assessment of diurnal chemical and isotopic techniques to investigate biogeochemical cycles in the upper Klamath River, Oregon, USA. *Chemical Geology*. 269, 3–11.

Price, G.D., Badger, M.R., Woodger, F.J., Long, B. M., 2008. Advances in understanding the cyanobacterial CO_2-concentrating-mechanism (CCM): Functional components, Ci transporters, diversity, genetic regulation and prospects for engineering into plants. *Journal of Experiment Botany*. 59, 1441–1461.

Price, G.D., 2011. Inorganic carbon transporters of the cyanobacterial CO_2 concentrating mechanism. *Photosynthesis Research*, 109, 47–57.

Raymond, P.A., Cole, J.J., 2003. Increase in the Export of Alkalinity from North America's Largest River. *Science*, 301, 88-91.

Raymond P. A., Oh N. H., Turner R. E., Broussard, W., 2008. Anthropogenically enhanced

fluxes of water and carbon from the Mississippi River. *Nature*, 451, 449–452.

Raymond, P. A., Hamilto, S. K., 2018. Anthropogenic influences on riverine fluxes of dissolved inorganic carbon to the oceans. *Limnology Oceanography Letters*, 3, 141-155.

Redfield, A.C., Ketchum, B.H., Richards F.A., 1963. The influence of organisms on the composition of seawater. *New York: Interscience*, 26-77.

Reddy, M.M., Plummer, L.N., Busenberg, E., 1981. Crystal growth of calcite from calcium bicarbonate solutions at constant pCO_2 and 25 °C: a test of a calcite dissolution model. *Geochimica et Cosmochimica Acta*. 45 (8), 1281–1289.

Riebesell, U., Wolf-Gladrow, D.A., Smetacek, V., 1993. Carbon-dioxide limitation of marine-phytoplankton growth-rates. *Nature*, 450, 545–549.

Riebesell, U., Schulz, K.G., Bellerby, R.G.J., Botros, M., Fritsche, P., Meyerhoefer, M., Neill, C., Nondal, G., Oschlies, A., Wohlers, J., Zoellner, E., 2007. Enhanced biological carbon consumption in a high CO_2 ocean. *Nature*, 450, 545–548.

Romero-Mujalli, G.J., Hartmann, B., Boerker, J., 2019a. Temperature and CO_2 dependency of global carbonate weathering fluxes - Implications for future carbonate weathering research. *Chemical Geology*. 527, UNSP 118874.

Romero-Mujalli, G., Hartmann, J., Borker, J., Gaillardet, J., Calmels, D., 2019b. Ecosystem controlled soil-rock pCO_2 and carbonate weathering - Constraints by temperature and soil water content. *Chemical Geology*. 527, 118634.

Rusjan, S., Mikoš, M., 2010. Seasonal variability of diurnal in-stream nitrate concentration oscillations under hydrologically stable conditions. *Biogeochemistry*, 97, 123–140.

Sarazin, G., Ciabrini, J.P., 1997. Water geochemistry of three mountain streams from carbonate watersheds in the Southern French Alps. *Aquatic Geochemistry*, 3, 233–265.

Schenk, H.J., Jackson, R.B., 2002. The global biogeography of roots. *Ecology Monographs*. **72**, 311-328.

Schimel, D.S., 1995. Terrestrial ecosystems and the carbon cycle. *Global Change Biology*, 1, 77–91.

Schindler, D.W., Hecky, R.E., Findlay, D.L., Stainton, M.P., Parker, B.R., Paterson, M.J., Beaty, K.G., Lyng, M., Kasian, S.E.M., 2008. Eutrophication of lakes cannot be controlled by reducing nitrogen input: Results of a 37-year whole-ecosystem experiment. *Proceedings of the National of Academy of Science. USA*, 105, 11254–11258.

Schindler, D.W., Carpenter, S.R., Chapra, S.C., Hecky, R.E, Orihel, D.M., 2016. Reducing phosphorus to curb lake eutrophication is a success. *Environmental Science & Technology*. 50(17), 8923-8929.

Schlesinger, W.H., 2009. On the fate of anthropogenic nitrogen. *Proceedings of the National of Academy of Science. USA*, 106, 192-196.

Schulte, P., Geldern, R.V., Freitag, H., Karim, A., Negrel, P., Petelet, G., 2011. Applications of stable water and carbon isotopes in watershed research: Weathering, carbon cycling, and water balances. *Earth-Science Reviews*. 109, 20-31

Schulze, E.-D., Mooney, H.A., Sala, O.E., Jobbagy, E., Buchmann, N., 1996. Rooting depth, water availability, and vegetation cover along an aridity gradient in Patagonia. *Oecologia*, 108, 503-511.

Sheng, H., Yang, Y., Yang, Z., Chen, G., Xie, J., Guo, J., Zou, S., 2010. The dynamic response of soil respiration to land use changes in subtropical China. *Global Change Biology*, 16, 1007–1121.

Simon, K.S., Townsend, C.R., Biggs B.J., Bowden, W.B., 2005. Temporal variation of N and P uptake in 2 New Zealand streams. *Journal of the North American Benthological Society*, 24, 1-18.

Spencer, R.G.M., Pellerin, B.A., Bergamaschi, B.A., 2007. Diurnal variability in riverine dissolved organic matter composition determined by in situ optical measurements in the San Joaquin River (California, USA). *Hydrological Processes*, 21, 3181–3189.

Strickland, J. D. H., 1965. Production of organic matter in the primary stages of the marine food chain. Chemical Oceanography Vol. 1. pp. 477–610 (eds Riley, J. P. and G., Skirrow) London: Academic Press.

Szramek, K. *et al*., 2007. Weathering intensity of calcite versus dolomite in carbonate-bearing temperate zone watersheds: carbonate geochemistry and fluxes from catchments within the St. Lawrence and Danube river basins. *Geochemistry, Geophysics, Geosystems*, 8, Q04002.

Talling, J.F., 1976. The depletion of carbon dioxide from lake water by phytoplankton. *The Journal of Ecology*. 64, 79–121.

Tang, X., Fan, S., Du, M., Zhang, W., Gao, S., Liu, S., Chen, G., Yu, Z., Yang, W., 2020. Spatial and temporal patterns of global soil heterotrophic respiration in terrestrial ecosystems. *Earth System Science Data*, 12, 1037-1051.

Taylor, P.G., Townsend, A.R., 2010. Stoichiometric control of organic carbon-nitrate relationships from soils to the sea. *Nature*, 464, 1178-1181.

Thomey, M.L., Collins, S.L., Vargas, R., Johnson J.E., Brown, R.F., Natvig, D.O. Friggens, M.T., 2011. Effect of precipitation variability on net primary production and soil respiration in a Chihuahuan Desert grassland. *Global Change Biology*, 17, 1505– 1515.

Thrasher, B., *et al.* 2013. Downscaled climate projections suitable for resource management. *Eos Transactions American Geophysical Union*, 94, 321-321.

Tortell, P.D., 2000. Evolutionary and ecological perspectives on carbon acquisition in phytoplankton. *Limnology Oceanography*. 45, 744–750.

Trimmer, M., Grey, J., Heppell, C.M., Hildrew, A.G., Lansdown, K., Stahl, H., Yvon-Durocher, G., 2012. River bed carbon and nitrogen cycling: State of play and some new directions. *Science of the Total Environment*. 434, 143-158.

Wigley, T. M. L., 1997. WATSPEC: A computer program for determining equilibrium speciation of aqueous solutions. British Geomorphological Research Group, London, 1-48.

Van Dam, B.R., Tobias, C., Holbach, A., Paerl, H.W., Zhu, G., 2018. CO_2 limited conditions favor cyanobacteria in a hypereutrophic lake: An empirical and theoretical stable isotope study. *Limonology Oceanography*. 63, 1643-1659.

Verspagen, J.M.H., Van de Waal, D.B., Finke, J.F., Visser, P.M., Van Donk, E., Huisman, J., 2014. Rising CO_2 levels will intensify phytoplankton blooms in eutrophic and hypertrophic lakes. *PloS One*, 9 (8), e104325.

Verschoor, A.M., Van Dijk, M.A., Huisman, J., Van Donk, E., 2013. Elevated CO_2 concentrations affect the elemental stoichiometry and species composition of an experimental phytoplankton community. *Freshwater Biology*. 58, 597–611.

Visser, P., Verspagen, J.M.H, Sandrini. G., Stal, L.J., Matthijs, H.C.P, Davis, T. W., Paerl, H.W., Huisman, J., 2016. How rising CO_2 and global warming may stimulate harmful cyanobacterial blooms. *Harmful Algae*, 54, 145-159.

Xu, Z., Liu, C., 2007. Chemical weathering in the upper reaches of Xijiang River draining the Yunnan-Guizhou Plateau, Southwest China. *Chemical Geology*, 239, 83-95.

Yang, M., Liu, Z., Sun, H., Yang, R., Chen, B., 2016. Organic carbon source tracing and DIC fertilization effect in the Pearl River: insights from lipid biomarker and geochemical analysis. *Applied Geochemistry*. 73, 132-141.

Yang, R., Liu, Z., Zeng, C., Zhao, M., 2012. Response of epikarst hydrochemical changes to soil CO_2 and weather conditions at Chenqi, Puding, SW China. *Journal of Hydrology*. 468-469, 151–158.

Yang, R., Chen, B., Liu, H., Yan, H., 2015. Carbon sequestration and decreased CO_2 emission caused by terrestrial aquatic photosynthesis: insights from diurnal hydrochemical variations in an epikarst spring and two spring-fed ponds in different seasons. *Applied Geochemistry*, 63, 248–260.

Young, C.S., Gobler, C., 2017. The organizing effects of elevated CO_2 on competition among estuarine primary producers. *Scientific Report*, 7, 7667.

Zeebe, R.E, Wolf-Gladrow, D.A., 2001. *CO_2 in seawater: equilibrium, kinetics, isotopes.* Amsterdam: Elsevier, 346 pp.

Zeng , C., Gremaud, V., Zeng, H., Liu, Z., Goldscheider N., 2012. Temperature-driven meltwater production and hydrochemical variations at a glaciated alpine karst aquifer: implication for the atmospheric CO_2 sink under global warming. *Environmental Earth Sciences*, 65, 2285-2297.

Zeng, C., Liu, Z., Yang, J., Yang, R., 2015a. A groundwater conceptual model and karst-related carbon sink for a glacierized alpine karst aquifer, Southwestern China. *Journal of Hydrology*, 529, 120-133.

Zeng C., Liu Z., Zhao M., Yang R., 2016. Hydrologically-driven variations in the karst-related carbon sink fluxes: Insights from high-resolution monitoring of three karst catchments in Southwest China. *Journal of Hydrology*, 533, 74-90.

Zeng, Q., Liu, Z., Chen, B., Hu, Y., Zeng, S., Zeng, C., Yang, R., He, H., Zhu, H., Cai, X., Chen, J., Ou, Y., 2017. Carbonate weathering-related carbon sink fluxes under different land uses: A case study from the Shawan Simulation Test Site, Puding, Southwest China. *Chemical Geology*, 474, 58-71.

Zeng, S., Jiang, Y., Liu, Z., 2016. Assessment of climate impacts on the karst-related carbon sink in SW China using MPD and GIS. *Global Planetary Change*, 144,171–181.

Zeng, S., Liu, Z., Kaufmann, G., 2019. Sensitivity of the global carbonate weathering carbon-sink flux to climate and land-use changes. *Nature Communications*, 10, 5749.

Zeng, S., Liu, Z., Goldscheide,r N., Frank, S., Goeppert, N., Kaufmann, G., Zeng, H., Zeng, C., Zeng, Q., Sun, H., 2020. Comparisons on the effects of temperature, runoff, and land-cover on carbonate weathering between different karst catchments: insights into the future global carbon cycle. *Hydrogeology Journal*, 29, 331-345.

Zhang, L., Dawes, W. R., Walker, G.R., 2001. Response of mean annual evapotranspiration to vegetation changes at catchment scale. *Water Resource Research*, 37, 701-708.

Zhao, M., Liu, Z., Li H.C., Li, H.C., Zeng, C., Rui, Y., Chen, B., Yan, H., 2015. Response of dissolved inorganic carbon (DIC) and $\delta^{13}C_{DIC}$ to changes in climate and land cover in SW China karst catchments. *Geochimica et Cosmochimica Acta*, 165, 123-136.

9. Acknowledgements

Throughout the entire PhD project and the writing of this dissertation, I learned to look at with an open mind and grow up to an independent researcher. I have received a great deal of support and assistance from my supervisor, colleagues, family and friends. I want to take this opportunity to express my thanks to all of them.

First of all, I would like to express my sincere appreciation to my supervisor Prof. Dr. Georg Kaufmann. He gave me this great opportunity to pursue my PhD in the institute of Geological Sciences, FUB. During the past four years, he gave me constructive suggestions whenever I need and helped me to conquer many great scientific challenges. It's his great support and help that enables me to finish my PhD.

I am grateful to Dr. Douchko Romanov for his support during past four years and always giving me valuable feedback on my article manuscripts and presentations.

I greatly acknowledge Prof. Dr. Nico Goldscheider for offering me the opportunity to join his challenging project and field investigation in Austria. I sincerely appreciate Dr. Simon Frank and Dr. Nadine Goeppert for their help on my PhD research and their assistance in Austria.

I appreciate the China Scholarship Council (CSC) and FUB for providing me the financial support.

Finally, I want to thank my family for accompanying and supporting me through this challenging time. The support and encouragement from my mother Haitao Zeng, my father Zaihua Liu as always helped me to conquer all the difficulties I faced through this journey.

10. Appendix

Original papers:

1. Zeng, S., Liu, Z., Goldscheider, N., Frank, S., Goeppert, N., Kaufmann, G., Zeng, G., Zeng. Q., Sun, H. (2021). Comparisons of the effects of temperature, runoff, and land cover on carbonate weathering between different karst catchments: insight into the future global carbon cycle. *Hydrogeology Journal*, 29, 331-345, DOI: https://doi.org/10.1007/s10040-020-02252-5
2. Zeng, S. & Kaufmann, G. & Liu, Z. (2021). Natural and anthropogenic driving forces of carbonate weathering carbon sink flux: a model comparison study at global scale. *Global Biogeochemical Cycles,* submitted.
3. Zeng, S. & Liu, Z. & Kaufmann, G. (2019). Sensitivity of the global carbonate weathering-related carbon sink flux to future climate and land-use changes. *Nature Communications*, 10, 5749. DOI: https://doi.org/10.1038/s41467-019-13772-4
4. Zeng, S., Liu, H., Liu Z., Kaufmann, G., Zeng, Q., Chen, B. (2019). Seasonal and diurnal variations in DIC, NO3- and TOC concentrations in spring-pond ecosystems under different land-uses at the Shawan Karst Test Site, SW China: Carbon limitation of aquatic photosynthesis. *Journal of Hydrology*, 574, 811-821. DOI: https://doi.org/10.1016/j.jhydrol.2019.04.090

For copyright reasons, there are no pdf versions attached in the online thesis for paper 1 and paper 4.

Pages 331–345 of paper 1 are not included in the online version.

Natural and anthropogenic driving forces of carbonate weathering carbon sink flux: a model comparison study at global scale

Sibo Zeng [a*], Georg Kaufmann [a*], Zaihua Liu[b,c]

[a] *Institute of Geological Sciences, Geophysics Section, Freie Universität Berlin, 12249 Berlin, Malteserstr. 74-100, Haus D, 12249 Berlin, Germany*

[b]*State Key Laboratory of Environmental Geochemistry, Institute of Geochemistry, CAS, 550081 Guiyang, China.*

[c]*CAS Center for Excellence in Quaternary Science and Global Change, 710061 Xi'an, China*

***** Corresponding author.

E-mail address: sibozeng@zedat.fu-berlin.de (SZ); georg.kaufmann@fu-berlin.de (GK).

Abstract

Continental weathering is a carbon-dioxide (CO_2) sink in the global carbon cycle. The weathering process is driven by environmental factors such as changes in temperature, moisture, CO_2 concentration, which can have natural (climate) or anthropogenic (land use) origins. In this paper, we attempt to evaluate the global applicability of different environmental drivers, which can be used to estimate the global carbonate dissolution intensity (bicarbonate concentration, [HCO_3^-], as a proxy) and carbon sink flux (*CCSF*). We use three ecological models and satellite-based databases, which provide estimates on soil CO_2-concentrations (pCO_2). By using three different pCO_2 models, global temperature (T) and runoff (N), we obtain similar global average HCO_3^- concentrations and *CCSF*, ranging from 2.73-2.81 mmol L^{-1} and 4.52-5.36 t C km^{-2} yr^{-1}. However, their spatial patterns differ significantly, depending on the database used.

We compare our calculated HCO_3^- concentrations to observed carbonate spring records, and we compare the contributions from both natural and anthropogenic driving forces on the global scale: Natural drivers dominate the carbonate weathering intensity (HCO_3^-), where the ecosystem is dominated by a single land cover type. Antropogenically induced global land-use changes, however, alter the global HCO_3^- distribution significantly. Furthermore, our simulation results indicate that the different water yield caused by land-use changes could be more significant for the total carbon-sink budget than dissolution intensity. The HCO_3^- flux is statistically more dependent on the changes of water flow instead of solute's concentration due to the competing process between thermodynamics and soil respiration. Accordingly, we stress that anthropogenic factors are as significant as natural climatic changes for the carbonate weathering process.

Key words: Carbonate weathering; Climate change; Land use; Soil pCO_2, Carbon cycle

1. Introduction

The responses of continental weathering processes to natural changes in the climate-system and anthropogenic activities are highly uncertain, impeding the scientific community to evaluate the global carbon budget correctly. Carbonate rock is the largest carbon reservoir on the Earth's surface and covers nearly 15.2% of the global ice-free continental surface, according to latest global classification by Goldscheider et al. (2020). In addition, carbonate minerals are also frequently found in the soil on non-karst terrains (Adams and Post. 1999; Ford and Williams. 2007). On a global scale, carbonate weathering contributes 50-60% of dissolved loads in terrestrial waters (Gaillardet et al., 1999). The HCO_3^- flux produced by this weathering process is an important component of the terrestrial carbon cycle (Gombert 2002; Liu et al 2010; Raymond and Hamilton., 2018; Gaillardet et al., 2019). The influx of HCO_3^- to inland waters can accelerate the aquatic photosynthesis (Liu et al., 2010; Yang et al., 2015; Chen et al., 2017), and the submerged plants and plankton can convert the carbonate weathering-formed dissolved inorganic carbon (*DIC*) to organic matters, thus resulting in a long-term carbon sink (Liu et al., 2011). Meanwhile, the changed HCO_3^- may alter the species composition of freshwater plant communities (Iversen et al, 2019). Moreover, the increasing bicarbonate flux (or alkalinity flux) to the oceans could buffer the pH, thus averting ocean acidification (Hartmann et al., 2013). Therefore, the abiotic or biotic processes involved in carbonate weathering may not only influence the global carbon cycle but also change the freshwater or marine environment.

The previous estimation of the global total carbon sink generated by carbonate weathering is nearly 0.7 Gt C yr^{-1}, accounting for nearly 25% of the terrestrial carbon sink (Liu et al., 2010, 2018). The amount of this carbon sink is robust, yet it has received little attention by

biogeochemists. In addition, the variation of carbonate weathering intensity is strongly affected by the environmental perturbations due to its rapid dissolution kinetics, which is 10-20 times faster than those of silicate (Meybeck 1986; Liu et al., 2011). Recently, a growing number of studies show that the carbonate weathering process is accelerating owing to contemporary climate and land-use change (Raymond et al., 2008; Drake et al., 2018; Macpherson et al., 2019). The fast responses and the strong environmental sensitivity of carbonate weathering to global change has been thought to have a great potential for mitigating global warming (Zeng et al., 2019).

We first introduce the carbon-sink flux CCSF [t/km^2/yr] as (e.g. Liu et al., 2010, 2018):

$$CCSF = n\, m_r N[HCO_3^-] \quad (1)$$

with N [m/yr] runoff, [HCO_3^-] [mmol/L] the bicarbonate concentration, m_r [g/mol] the molar mass of carbon. The partitioning factor n is 1 for silicate weathering, and 0.5 for limestone or dolomite weathering, as in the latter case one part of HCO_3^- is from atmospheric CO_2 and the other part from limestone ($CaCO_3$) or dolostone ($CaMg(CO_3)_2$). The total amount of CCSF is subsequently controlled by the runoff and the HCO_3^- concentration in (Eq.1).

Note that the bicarbonate concentration in (Eq.1) represents more than 90% of the dissolved inorganic carbon (DIC) for pH-values around 7-9, valid for the global budget.

From (Eq.1), it is clear that both the runoff N and the bicarbonate concentration [HCO_3^-] depend on climatic parameter values, and both natural and anthropogenic causes. Thus, we need to know more about these dependencies.

The chemical reaction of carbonate weathering can be expressed as follows:

$$Ca_xMa_{1-x}CO_3 + CO_2 + H_2O \Leftrightarrow xCa^{2+} + (1-x)Mg^{2+} + 2HCO_3^- \quad (2)$$

with $x \in [0,1]$ in (Eq.2) the partitioning coefficient between calcium (Ca^{2+}) and magnesium (Mg^{2+}), and the species carbon-dioxide CO_2, water H_2O, and carbonate and bicarbonate, CO_3^{2-} and HCO_3^-, respectively.

The equilibrium concentration of HCO_3^- in (Eq.1), driven by the reaction (Eq.2), is

97 controlled by the temperature-dependent reaction constants K_1, K_C, K_H, and K_2, with T [°C]
98 temperature, and the partial pressure of CO_2, pCO_2 [atm] at the water-rock interface
99 (atmosphere or soil) and the carbonate rock types (limestone or dolomite). For limestone, a
100 cubic relation (e.g. Dreybrodt, 1988)

$$[HCO_3^-]_{eq}^3 = \frac{2K_1(T)K_C(T)K_H(T)}{K_2(T)\gamma_{Ca^{2+}}\gamma_{HCO_3^-}^2} p_{CO_2} \quad (3)$$

101 for the equilibrium concentration of bicarbonate holds, and γCa^{2+} and γHCO_3^- are the activity
102 coefficients for calcium and bicarbonate, respectively.
103 We have seen that both temperature and carbon-dioxide concentration in the soil are
104 fundamental parameters for carbonate dissolution (Eq.3), and runoff is additionally needed to
105 calculate CCSF (Eq.1).
106 Global temperature variations have been well documented and quantified by the scientific
107 community in the past decades. Yet, the knowledge of the pCO_2 in global soils is less well
108 constrained so far. In order to estimate the soil pCO_2 at rock-soil interface, previous studies
109 included natural or anthropogenic factors into process-based or empirical models. These
110 models use parameters such as evapotranspiration *ET* (Brook et al., 1983), net primary
111 productivity *NPP* (Gwiazda and Broecker., 1994; Goddéris et al., 2010) and soil volumetric
112 water content (Romero-Mujalli et al., 2019) to estimate the soil pCO_2 and thus carbonate
113 dissolution intensity. However, there are still no comparative studies systematically to discuss
114 the applicability and accuracy of these models for evaluating the HCO_3^- concentration on the
115 global scale. More importantly, natural and anthropogenic climate drivers are coupled in
116 nature, altering the soil respiration as well as carbonate weathering intensity (Beaulieu et al.,
117 2012; Chen et al., 2016). Yet, some of previous models only consider natural climate drivers
118 but ignore the anthropogenic factors. Thus, a new comparison study is needed to evaluate the
119 importance of both natural and anthropogenic climate changes on the global carbonate
120 weathering process. Furthermore, the past studies are mainly focusing on how the bicarbonate

has been generated. However, to quantify the weathering related carbon-sink flux needs to synchronously account for changes of water flow (Eq.1). Water balance is also affected by both natural and anthropogenic factors. Therefore, in order to capture the fate of carbonate weathering related carbon-sink flux under different future global-change scenarios, the mechanisms of how carbon-sink formation and carbon transport needs to be further investigated.

In this paper, we use three soil pCO_2 models and the carbonate equilibrium equation to evaluate the HCO_3^- concentration and *CCSF* at global scale and compare these model results against actual HCO_3^- observations of global carbonate springs. In a previous study (Zeng et al., 2019), we constructed a mixed-effects model of natural and anthropogenic climatic changes, based on different land-use fractions and empirical models to simulate HCO_3^- and *CCSF* for a long-term period. In order to improve the result of our previous model, we use a series of satellite-based land-surface parameters, and maps of global temperature and runoff based on observed data. Our main aims are:

(1) **Detection** of optimal parameters for evaluating the carbonate dissolution intensity on the global scale.

(2) **Determination** of the role of natural and anthropogenic factors for carbonate weathering process.

(3) **Prediction** of the potential future hot-spot areas of *CCSF*.

We believe this work will help to better understand the fate of carbonate weathering in the global carbon cycle and judge future land-use policies.

2. Methods

In order to evaluate the global carbonate dissolution intensity and related carbon sink flux with a higher resolution and accuracy, we need improve estimates of bicarbonate concentration [HCO_3^-]. As the bicarbonate concentration depends on surface temperature T and carbon-dioxide concentration pCO_2, we need estimates for these two parameter values, too. The carbon-dioxide concentration is mainly controlled by soil respiration and soil properties, and we therefore use three different ecological models, based on net primary production *NPP* (Gaillardet et al., 2019), evapotranspiration *ET* (Brook et al., 1983) and soil-water content *SWC* (Romero-Mujalli et al., 2019).

We use remote-sensing products for *NPP*, *ET* and *SWC*, and improved runoff and temperature data based on global terrestrial observations. In addition, we use a new carbonate rocks map to better present the global distribution of HCO_3^- and *CCSF*. Finally, we use a global map of land-cover categories.

2. 1. New world karst aquifer map

In order to extract the carbonate weathering intensity in global carbonate rock area, we use the new world karst aquifer map (WOKAM, Fig. 1a). This map provides global coverage of carbonate rocks, but it does not include the covered carbonate rock types by other strata (Chen et al., 2017; Goldscheider et al., 2020). The major carbonate rock types in the natural environment consist chiefly of limestone ($CaCO_3$) and dolostone ($CaMg(CO_3)_2$). Due to the uncertainties of precisely distinguishing limestone from globally less common dolostone in the geological map, we calculated carbonate weathering intensity by assuming that all carbonates are mainly calcite.

All of the following data sets are mapped onto the karst outcrop map.

2.2. T, NPP, SWC, ET

The following databases were used to derive global parameter maps:

- **Temperature T (Fig. 1b)**

  Climatic Research Unit TS database (CRU TS) provided a globally land-only monthly time series of commonly used surface climate variables (https://crudata.uea.ac.uk/cru/data/hrg/cru_ts_4.02/). The temperature during 2000-2014 were used in this study for calculating soil pCO_2, HCO_3^-.

- **Net primary production NPP and evapo-transpiration ET (Figs. 1c and 1d)**

  The latest MODIS products provided the high-resolution *NPP and ET data.* The *NPP* and *ET* were calculated by the annual mean values of MOD16 and MOD17 data during the period 2000-2014 (the version edited by Numerical Terradynamic Simulation Group, University of Montana, https://www.ntsg.umt.edu/project/modis/). The original MODS *NPP* has been changed to the unit of amount of organic matter in g of dry matter/m^2. We use these satellite-based data resources to estimate the global soil pCO_2 by using *NPP*-pCO_2 and *ET*-pCO_2.

- **Soil-water content SWC (Fig. 1e)**

  The ESA soil moisture database (ESA CCI SM v04.2) provided high-resolution soil volumetric water content (*SWC*) data (https://esa-soilmoisture-cci.org/). The annually averaged *SWC* between 2000-2014 is used in (6).

- **Runoff N (Fig. 1f)**

  The Long-term (circa year 2000) Composite Runoff V1.0 database published by Fekete et al (2002) was used for global runoff maps.

2. 3. Carbonate weathering intensity

To estimate the bicarbonate concentration [HCO_3^-] produced by carbonate weathering, we assume that the actual bicarbonate concentration [HCO_3^-] is equal to the equilibrium bicarbonate concentration $[HCO_3^-]_{eq}$. Thus our estimate is an upper bound on the CCSF. We also assume that the global HCO_3^- signature is mostly generated by limestone dissolution, thus (3) holds.

2. 4. Soil pCO_2

Soil pCO_2 is a key parameter for carbonate dissolution. In previous studies, soil pCO_2 was estimated by abiotic or biotic changes, including temperature (*T*), evapotranspiration (*ET*), net primary production (*NPP*) and soil volumetric water content (*SWC*) (Gwiazada and Broecker et al., 1994; Goddéris et al., 2010; Brook et al., 1983; Romero-Mujalli et al., 2019; Gaillardet et al., 2019). In order to compare the differences in soil pCO_2 models, we calculate bicarbonate concentration and carbon-sink flux based on all three models on the global scale, and we compare our modelling results with global carbonate spring data. Their detailed methods were listed as follows:

(1) *NPP*-based soil pCO_2 (*NPP*-pCO_2) was first introduced by Gwiazda and Broecker (1993), and been simplified to a new form in Gaillardet et al. (2019). This is a semi-mechanistic model which calculates the pCO_2 profile across soil layers. The soil pCO_2 under the deepest roots [g C m^2 yr^{-1}] is set to 75% of the net primary production (*NPP*). Soil

217 pCO_2 can then be expressed as a function of atmospheric CO_2 concentration, temperature T,
218 and net primary production NPP:

$$pCO_{2(\mathrm{Soil})} = pCO_{2(atm)} + \frac{A \times 0.75 \times NPP}{T^2} \quad (4)$$

219 where $A = 1.03 \times 10^6$, a conversion unit constant, pCO_{2atm} is the atmospheric CO_2 pressure
220 [ppmv], NPP in grams of dry matter per square meter per year [g m^{-2} yr^{-1}], T the surface
221 temperature [K] and $pCO_{2(soil)}$ is the maximum CO_2 pressure reached below the root zone
222 [ppmv].

223 (2) ET-based pCO_2 (ET-pCO_2) was first introduced by Brook et al. (1983). This
224 model only depends on one parameter, the mean annual evapotranspiration ET [m/s]. This is
225 an empirical model constructed by the world soil pCO_2 data of different soil depth from 19
226 monitoring sites:

$$\log pCO_{2(Soil)} = \log pCO_{2(atm)} + 2.09(1 - e^{-0.00172\,ET}) \quad (5)$$

227 where $pCO_{2(atm)}$ is the atmospheric CO_2 concentration [ppmv].

228 (3) Soil-water content based pCO_2 model (SWC-pCO_2) was introduced by
229 Romero-Mujalli et al. (2019). This model was derived from global spring water pCO_2 data
230 from 26 publications. The Levenberg-Marquardt algorithm was applied to establish a relation
231 between soil-water pCO_2 and temperature T, while soil-water content was added as a fixed
232 level factor. The equation is shown as follow:

$$\log pCO_{2(Soil)} = \log pCO_{2(atm)} + \frac{e(-3\theta - \frac{0.25}{\theta})}{(0.09 + e^{-0.34T})} \quad (6)$$

233 where T is temperature [℃], and θ the soil volumetric water content [m^3m^{-3}]. The log
234 $pCO_{2(atm)}$ here is fixed to -3.4, close to the current atmospheric CO_2 concentration.

235

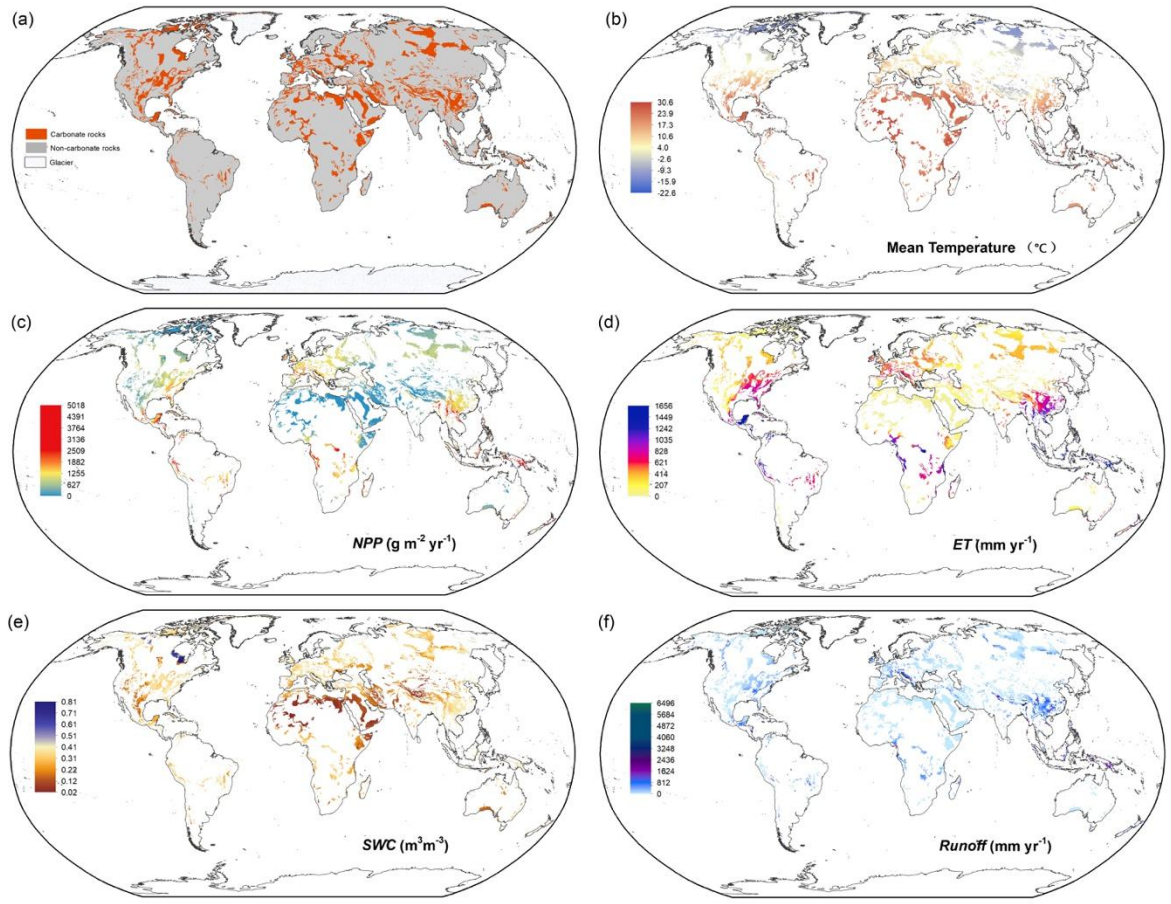

Fig. 1. Maps of input parameter values. **(a)** global carbonate rock outcrop map extracted from WOKAM , **(b)** CRU TS annual mean temperature (2000-2014), **(c)** MODIS MOD16 net primary production (2000-2014), **(d)** MODIS MOD17 evapotranspiration (2000-2014), **(e)** ESA CCI SM v04.2 soil volumetric water content (2000-2014), **(f)** global runoff driven from Composite Runoff V1.0 database. For details see text.

2. 5. IGBP Land cover categories

We finally introduce land-use categories to compare the performance of each model on different global biomes. We therefore reclassify the ISLSCP II MODIS (Collection 4) IGBP land cover database (https://daac.ornl.gov/cgi-bin/dsviewer.pl?ds_id=968) to three major land-use categories: forest, non-forest and bare land. The input parameters, calculated pCO_2, [HCO_3^-], and *CCSF* will be compared for each land-use category to discuss the role of anthropogenic forces for the carbonate weathering process.

3. Results

In this section, we derive results for the bicarbonate concentration and the carbon-sink flux from the data sets of the previous section.

3.1. Spatial variations of *soil* pCO_2, land use and soil-water content

We first start to calculate the soil pCO_2 variations, using eqs. 4, 5, and 6, and relate them to land-use categories and soil-water content. We emphasize the latitudinal variations here by averaging the globally calculated values over longitude.

In Fig. 2a, the results for the three soil pCO_2 models are shown, with mean values of these models ranging from 5834 to 8909 ppmv. The three models generated result in two distinct global pCO_2 patterns:

Results based on the *NPP*-pCO_2 and *ET*-pCO_2 model exhibit a similar latitudinal pCO_2 pattern, with three pCO_2 peaks occurring between 45°N~60°N, 0°~15°S, and 30°S~45°S, whereas the lowest soil pCO_2 for these two models occurs at around 75°N, 30°N, and 30°S. This spatial pCO_2 pattern is similar to the results shown in Zeng et al. (2019) (red pCO_2 curve in Fig. 2a), which is based on the same *NPP*-pCO_2 model, but a simpler parameterization of climatic and land-use database.

Results for the *SWC*-pCO_2 model exhibit a different spatial pattern, when compared to *ET*-pCO_2 and *NPP*-pCO_2 (grey line in Fig. 2a). The pCO_2 rises gradually to a maximum value close to the tropics. The higher soil pCO_2 values of *SWC*-pCO_2 are mostly occurring between 0°~15°S, higher than other model results. On the other hand, the *SWC*-pCO_2 model demonstrates an extremely low pCO_2 (close to atmospheric level) in the region higher than 60°N, where the average temperature is lower than 0 °C. Generally, the latitudinal variation

based on the *SWC*-pCO_2 model resembles as a single-peak curve, while the *NPP*-pCO_2 and *ET*-pCO_2 based models show two peaks.

In order to better understand the relationships between each soil pCO_2 model and its environmental drivers, Fig. 2b summarizes the reclassified IGBP land-cover categories (land cover is a key factor for MODIS *ET* and *NPP*) fractions and ESA soil volumetric water content data. The forest-cover fraction shows a similar latitudinal pattern as the *NPP*-pCO_2 and *ET*-pCO_2-based curves (compare to Fig. 2a). The soil volumetric water content (*SWC* in Fig. 2b) shares a similar spatial pattern with global forest fraction, but this cannot really match the *SWC*-pCO_2 result in Fig. 1a, especially the values in middle and high latitudes.

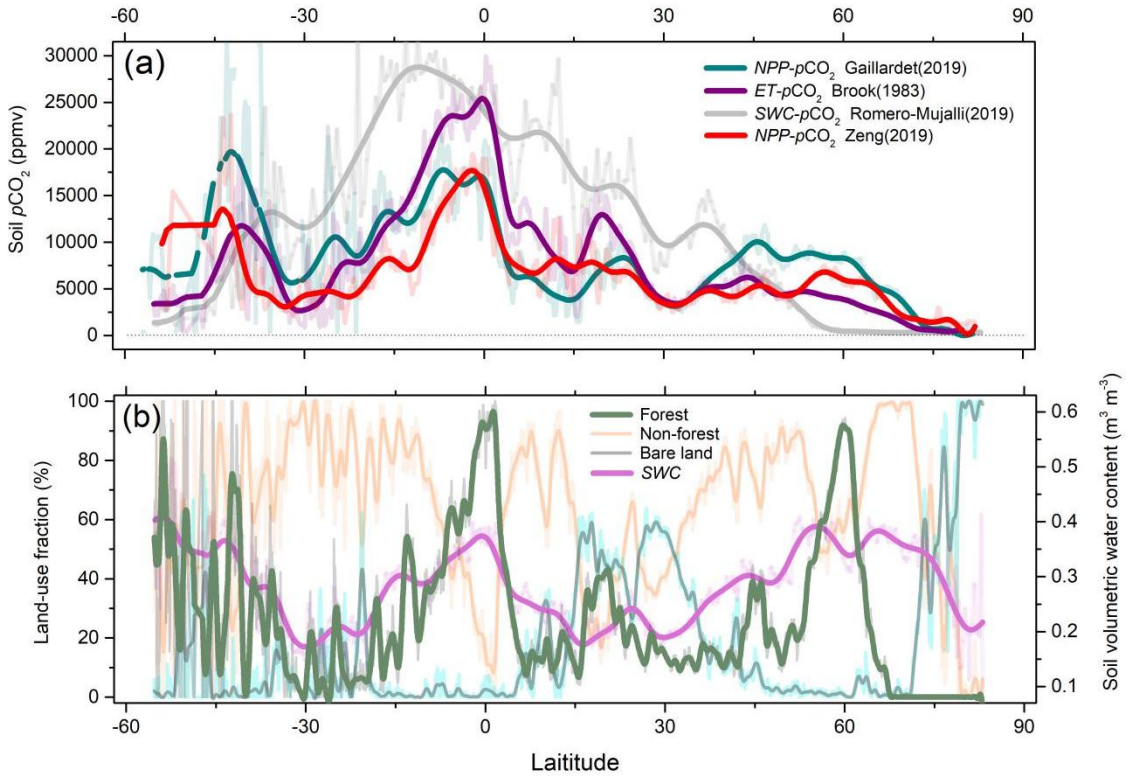

Fig. 2. Latitudinal soil pCO_2, land-use fraction and soil volumetric water content. **(a)** Latitudinal distributions of soil pCO_2. The methods are introduced by Brook et al. (1983), Gaillardet et al. (2019), Romero-Mujalli et al. (2019) and Zeng et al (2019). **(b)** Latitudinal distribution of forest, non-forest, bare-land fractions and soil volumetric water content (*SWC*). Original IGBP land cover categories were reclassified to three main land cover/

land use, forest (rainforest, broad-leaf forest, boreal forest, woody savanna), non-forest (grass, shrub, crop, savanna) and bare land (desert, bare rock, ice sheet). The transparent lines are the original model results and solid lines are smoothed data.

3.2. Spatial bicarbonate distribution

We continue to discuss the global bicarbonate concentrations based on the three soil pCO_2 models (Fig. 3), using eq. 3. Basically, eq. 3 rescales the pCO_2 concentrations non-linearly and adds a temperature dependency via the reaction-rate coefficients.

The calculated global [HCO_3^-] for the three pCO_2 models range from 2.73~2.81 mmol L^{-1}. The highest global mean HCO_3^- value occurs for the *NPP*-pCO_2 model, followed by the *SWC*-pCO_2 and *ET*-pCO_2 models. Globally, [HCO_3^-] for the *NPP*-pCO_2 and *ET*-pCO_2 models is lower than for the *SWC*-pCO_2 model in most tropical and subtropical regions, which is clear after our previous discussion (Fig. 2). In contrast, [HCO_3^-] for the *SWC*-pCO_2 model in northern high latitudes is significantly lower than for the other two models, especially the areas close to the Arctic. All three models generate the lowest [HCO_3^-] in the Middle East and North Africa, where *NPP*, *ET* and *SWC* are low.

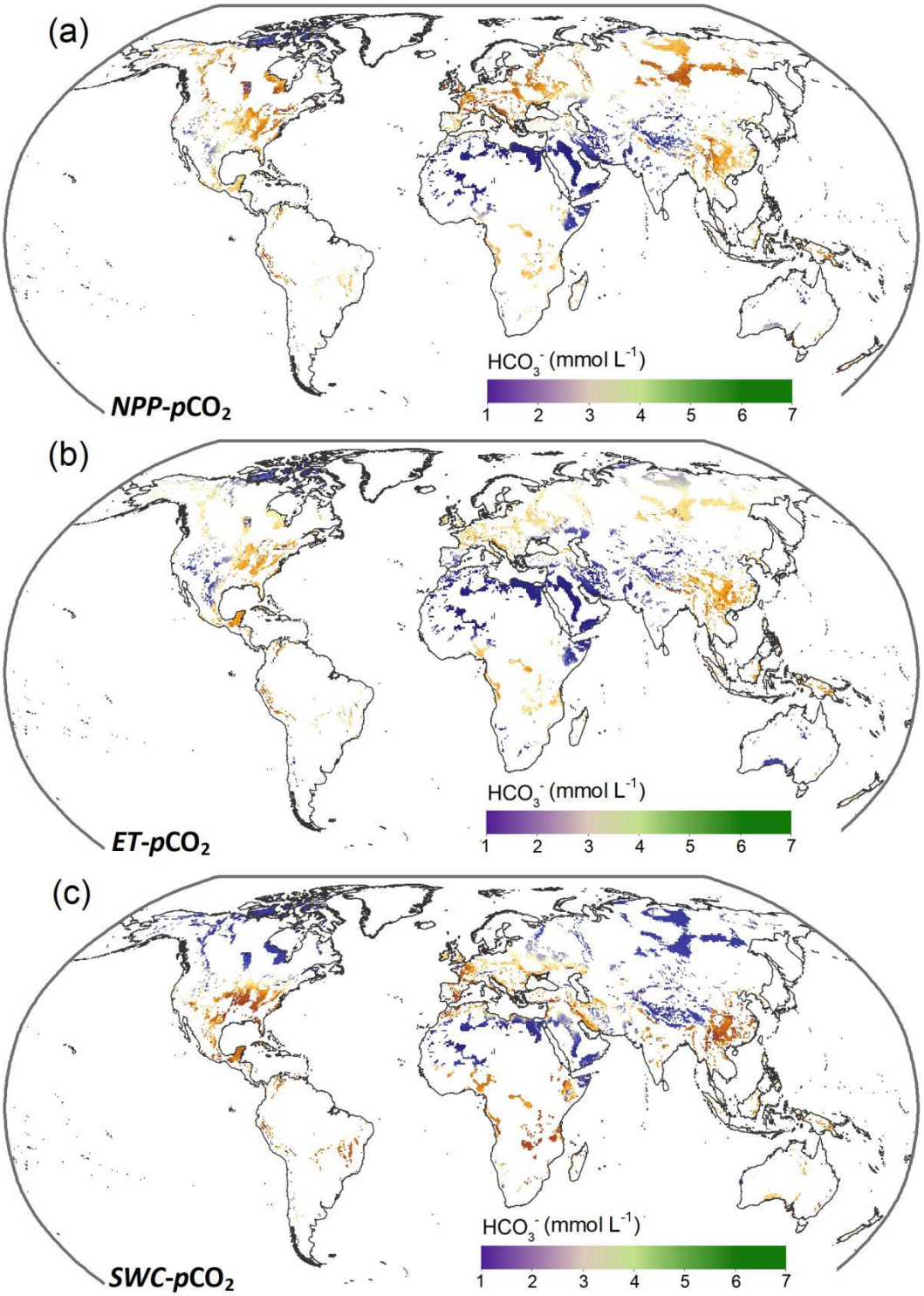

Fig. 3. Annual average HCO_3^- (DIC) concentrations in carbonate rock area. The soil pCO_2 for carbonate equilibrium function are calculated by *NPP*-pCO_2 **(a)**, *ET*-pCO_2 **(b)** and SWC-pCO_2 **(c)**.

We summarize the mapped [HCO_3^-] data by averaging along longitudes (Fig. 4a). For the *NPP-p*CO_2 and *ET-p*CO_2 models, the latitudinally-averaged curves peak at around 50°N~70°N, 0°~10°S and 40°S~50°S, whereas the lower [HCO_3^-] values occur at around 30°N and 30°S. This behavior is similar to our earlier findings (Zeng et al., 2019), red curve in Fig. 4a). In contrast, the *SWC-p*CO_2-based model results in a distinctly different spatial [HCO_3^-] pattern, with very low values between 60°N~90°N, while from the Arctic to the Tropics, the *SWC-p*CO_2-based model exhibits a sharp increase with two peaks at around 15°S and 40°N, but these high values could match the HCO_3^- curves of other two models.

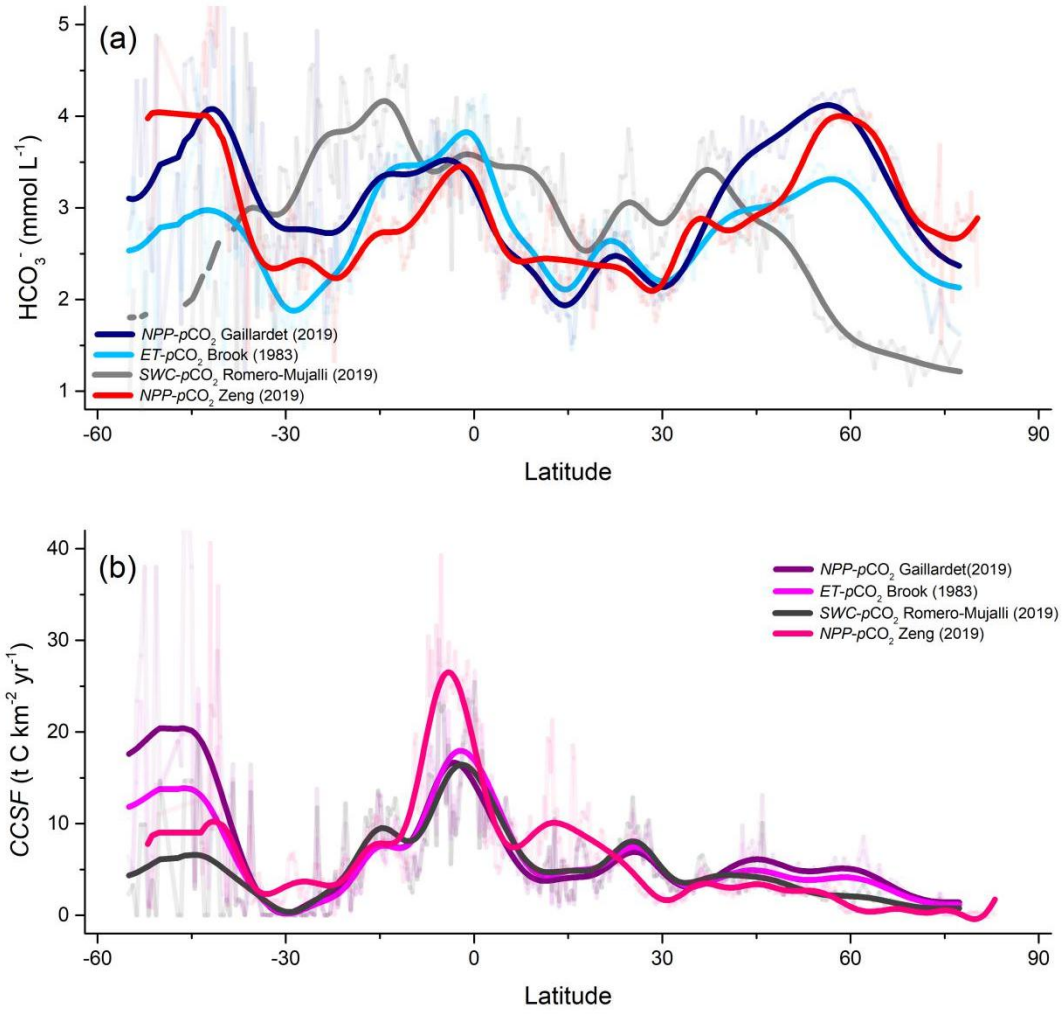

Fig. 4. Global [HCO_3^-] and *CCSF* patterns. **(a)** Latitudinal distributions of HCO_3^- based on three simulated soil *p*CO_2 in Figure.1(a). (b) Latitudinal distributions of *CCSF* calculated by eq.2. The runoff and temperature were

driven from Composite Runoff V1.0 database (Fekete et al., 2002) and CRU4.0 database. The transparent lines are the original model results and solid lines are the smoothed data.

3.3. Spatial variations of carbon-sink flux

We continue discussing the carbon-sink flux CCSF derived from eq. 1, which weights the bicarbonate concentration with runoff (Fig. 4b). The *CCSF* for all three pCO_2 models (and for comparison also the Zeng et al., 2019 model) shows a remarkable peak around the Equator, while another peak appears between 40°S~ 45°S (Fig. 4b). The global mean values of three simulated *CCSF* are similar, ranging from 4.52~5.36 t C km^{-2} yr^{-1}, and thus higher than our earlier estimation (4.15 C km^{-2} yr^{-1}, Zeng et al., 2019). The latitudinal *CCSF* is thus not really synchronous with the HCO_3^- concentration.

3.4. Statistics of soil pCO_2, [HCO_3^-], and *CCSF* for different land-use categories in different climatic regions

Table 1.1 summarizes the soil pCO_2, [HCO_3^-], *runoff and CCSF* of three land-cover categories in different climatic regions. Globally, the pCO_2 of *NPP*-pCO_2 and *ET*-pCO_2 show large differences between forest and non-forest (pCO_2 in forest is almost 2-fold higher than in non-forest and an order of magnitude higher than on bare land), which leads to a large difference of [HCO_3^-] (1 mmol/L) between these two land-cover types. Due to the highly limited *ET and NPP* over bare land, its pCO_2 and [HCO_3^-] are almost 80% and 36% lower than that of *SWC*-pCO_2. The [HCO_3^-] of *SWC*-pCO_2 in forest is close to the non-forest ecosystems (<0.1 mmol/L). These parameters also widely differ between different climatic regions within different cover types. *SWC*-pCO_2 has the highest pCO_2 in tropical forest,

non-forest and bare land. In the temperate zone, pCO_2 in non-forest is even higher than forest. Yet, the three land cover types reduce to a similarly low level in boreal areas. These spatial differences can also be found in [HCO_3^-] and *CCSF*. By contrast, *NPP*-pCO_2 and *ET*-pCO_2 have extreme low pCO_2 in tropical and temperate bare land (<800 ppmv), whereas *SWC*-pCO_2 generates 5-10 folds higher pCO_2 than the atmospheric level. Although, the pCO_2 and [HCO_3^-] of *NPP*-pCO_2 and *ET*-pCO_2 are lower in bare land, the two parameters for these two models in temperate and boreal forest could exceed *SWC*-pCO_2. The highest *CCSF* of all land-covers are found in *SWC*-pCO_2 result of tropics. However, *NPP*-pCO_2 and *ET*-pCO_2 have higher *CCSF* in whole global carbonate areas, owing to the extremely low boreal pCO_2 and [HCO_3^-] that calculate by *SWC*-pCO_2 (all simulations use a same runoff database).

373 **Table 1** The spatial statistics of Soil pCO_2, HCO_3^-, *Runoff* and *CCSF* of three parameterized pCO_2 based

374 simulations. (*NPP*-pCO_2, *ET*-pCO_2 and SWC-pCO_2). All values are means for each climatic region.

375

NPP-pCO_2	unit	Boreal			Temperate			Tropical			Global		
		Forest	NF	BL	Forest	NF	BL	Forest	NF	BL	Forest	NF	BL
pCO_2	ppmv	4674	3085	438	10298	6750	611	16305	8262	621	11645	6172	632
DIC	mmol L^{-1}	4.19	2.87	1.61	4.21	3.31	1.28	3.48	2.66	1.11	4.07	3.10	1.26
RF	mm yr^{-1}	58.6	109.4	50.1	374	189.1	51.9	697	192	0.09	463.2	181.6	39.5
CCSF	t C km^{-2} yr^{-1}	1.49	1.91	0.49	9.61	3.81	0.4	14.79	3.11	<0.01	11.49	3.44	0.30

ET-pCO_2	unit	Boreal			Temperate			Tropical			Global		
		Forest	NF	BL	Forest	NF	BL	Forest	NF	BL	Forest	NF	BL
pCO_2	ppmv	2109	1688	512	7229	4891	720	24614	10619	509	11027	5197	634
DIC	mmol L^{-1}	3.41	2.45	1.67	3.58	2.93	1.30	4.05	2.85	1.06	3.69	2.80	1.26
RF	mm yr^{-1}	58.6	109.4	50.1	374	189.1	51.9	697	192	0.09	463.2	181.6	39.5
CCSF	t C km^{-2} yr^{-1}	1.21	1.63	0.51	8.16	3.37	0.41	17.21	3.33	<0.01	10.42	3.10	0.30

SWC-pCO_2	unit	Boreal			Temperate			Tropical			Global		
		Forest	NF	BL	Forest	NF	BL	Forest	NF	BL	Forest	NF	BL
pCO_2	ppmv	380	380	380	6232	8964	3974	28123	23998	2025	11187	9707	3234
DIC	mmol L^{-1}	1.55	1.55	1.55	2.67	3.2	2.15	4.31	3.91	1.57	3.03	2.96	1.97
RF	mm yr^{-1}	58.6	109.4	50.1	374	189.1	51.9	697	192	0.09	463.2	181.6	39.5
CCSF	t C km^{-2} yr^{-1}	0.55	1.03	0.47	6.09	3.69	0.68	18.32	4.57	<0.01	8.56	3.27	0.47

376

377

378

4. Discussion

In this section, we discuss the results obtained in the last section and relate them to natural and anthropogenic changes in climate and land use.

4.1. Two different global soil pCO_2 and bicarbonate patterns

Our results have demonstrated that with the three pCO_2 models chosen we obtain two different global distributions (Fig. 2a). This discrepancy is of course related to the input parameters of the three models. The similar latitudinal soil pCO_2 calculated for *ET*-pCO_2 and *NPP*-pCO_2 can be attributed to the significant role of land cover in controlling either *NPP* or *ET* in these models. Land cover is a significant factor for soil respiration. Land-cover change therefore strongly alters the vegetation structure, plant species composition, local microclimate and the soil properties (Alekseev et al., 2018; Huang et al., 2020). As an example, forest requires more water and produces more organic matters than herbaceous plants. Bare land generates the lowest *NPP* and *ET* due to its sparse vegetation cover. Thus, the type of land use strongly influences soil respiration, if we follow the equations of *ET*-pCO_2 and *NPP*-pCO_2. A three-year experiment for a typical karst test site reported in Zeng et al. (2017) has verified this relation: Observed soil pCO_2 levels for five different land-cover types (bare rock, bare soil, shrubland, cropland, grassland) showed large differences, and this has been attributed to the different vegetation species, biomass and primary productivity of the five land-caver types. As a result, the five land-cover types also resulted in different *ET*, corresponding to their different soil pCO_2 levels. More importantly, Zeng et al. (2017) found that land cover eventually results a variation of [HCO_3^-] in the different compartments of the test site, corresponding to their different *ET* levels.

According to our global estimations reported here, the *ET*-pCO_2 and *NPP*-pCO_2 models present similar soil pCO_2 variations as reported in the experiments (Fig. 2a vs Fig. 2b). For example, an increasing fraction of forest leads to a higher soil pCO_2 and [HCO_3^-]. Based on these findings, we suggest that global land-use patterns are the reason that for the *ET*-pCO_2 and *NPP*-pCO_2 models we observe a similar latitudinal variation in [HCO_3^-]. Yet, using *NPP* and *ET* as a proxy for pCO_2 has limitations, because *ET* or *NPP* cannot fully reflect the total soil respiration. *NPP* could better reflect the respiration of roots but not for microbial respiration.

The *SWC*-pCO_2 model is characterized by a distinctly different pCO_2 pattern, when compared to the other two models. The soil pCO_2 of this model depends on climatic drivers only (soil-water volumetric content and temperature). Although global *SWC* variations seem to correlate to the forest fraction (Fig. 2b), the *SWC* curve (Fig. 2b) does not really match with its soil pCO_2 variation (Fig. 2a). The different latitudinal variations between two spatial soil pCO_2 patterns appear mostly in high latitudes, where the average temperature usually is below 0 °C. For the *SWC*-pCO_2 model, pCO_2 starts to increase later, when compared to the other two models in northern hemisphere (Gaillardet et al., 2019). Another discrepancy can be observed in tropics at around 5°S, with higher pCO_2 values for the *SWC*-pCO_2 model. This peak can be attributed to the "optimal" *SWC* value (~0.3 m^3/m^3), but not to land use. These two reported features are the reasons why the spatial pattern of *SWC*-pCO_2 is very distinct from other two patterns. The *SWC*-pCO_2 model may have uncertainties, when employed to the tropics or cold regions due to the limited range of original data which were used for constructing the model (the model has been constructed by using the global spring water pCO_2 and a polynomial fitting method calculated by Levenberg-Marquardt algorithm). In the original spring database, only few sites are located in extremely cold or hot regions (Romero-Mujalli et al., 2019). Thus, there is a temperature range (< 3℃ or > 19℃) and a *SWC* range (< 0.17 m^3/m^{-3} or >

429 0.37 m^3/m^{-3}), for which the *SWC-pCO₂* model is less robust. Yet, in order to compare the
430 *SWC-pCO₂* model to the other parameterized pCO_2 models at the global scale, the global-scale
431 simulation ignores the uncertainties in these regions. We note, however, that before applying
432 this global-scale model we need further evidence or calibration.

4.2. Bicarbonate concentration as a function of temperature

We continue discussing the differences of three soil pCO_2 models on the bicarbonate concentration by rearranging the calculated [HCO_3^-] as a function of temperature. We sample our global results in 0.5×0.5 degree bins, group them by land-use, and then sort them with respect to temperature. The resulting scatter plots for the three pCO_2 models are shown in Fig. 5. The bicarbonate concentration scatters widely. While for the forest regions we obtain the largest values (3-5 mmol/L), the bare rock surface exhibit the smallest concentrations (around 1.5 mmol/L). Non-forest regions are characterized by the largest spread in data, as here several land-use types are grouped.

We try to fit a polynomial through the scatter data for each land-use type and all three pCO_2 models. To identify the best fit, we start with linear polynomials, and then successively increase the degree, until the misfit is no longer improved significantly. In Fig. 5 we then see, that [HCO_3^-] modelled with the *NPP*- pCO_2 model can be predicted by a quadratic polynomial, for the *ET*- pCO_2 model by a linear polynomial, and for the *SWC*-pCO_2 model with a cubic polynomial. In *NPP*-pCO_2 and *ET*-pCO_2 results, there has a clear [HCO_3^-] differences between forest and non-forest. Meanwhile, their [HCO_3^-] in bare land all show a negative trend against temperature. By contrast, the [HCO_3^-] of all land cover types in *SWC*-pCO_2 are close to the same extreme low level under 0°C and with no variations associated with temperature and there is minor difference between forest and non-forest. Its [HCO_3^-] in bare land demonstrate a bell-shape relation vs temperature and this behavior cannot found in other two models.

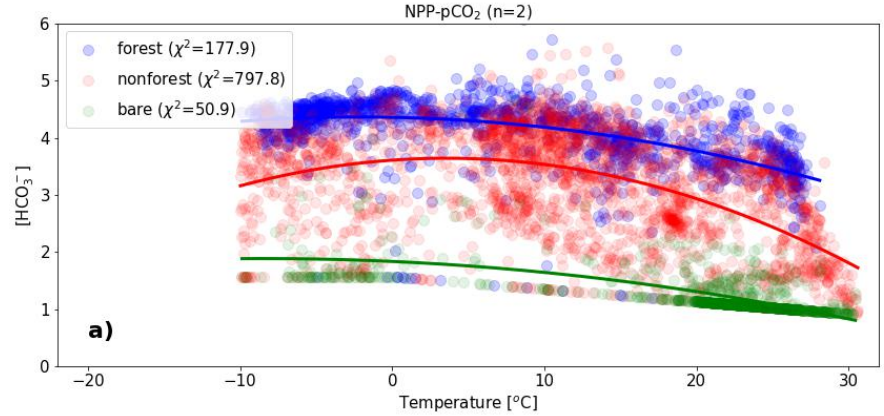

456

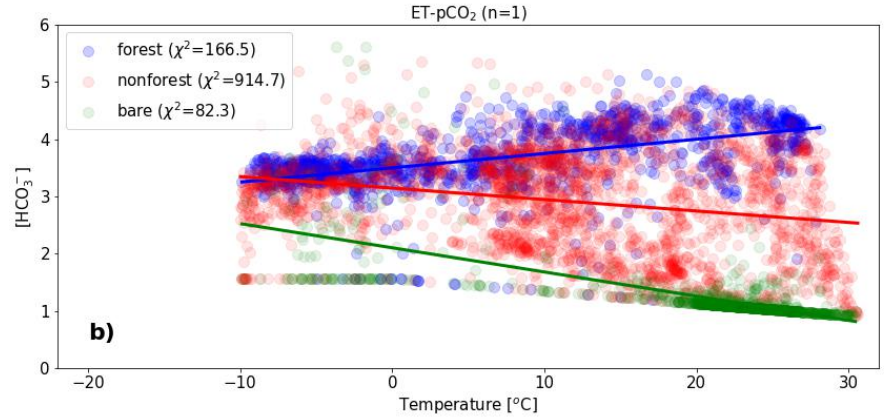

457

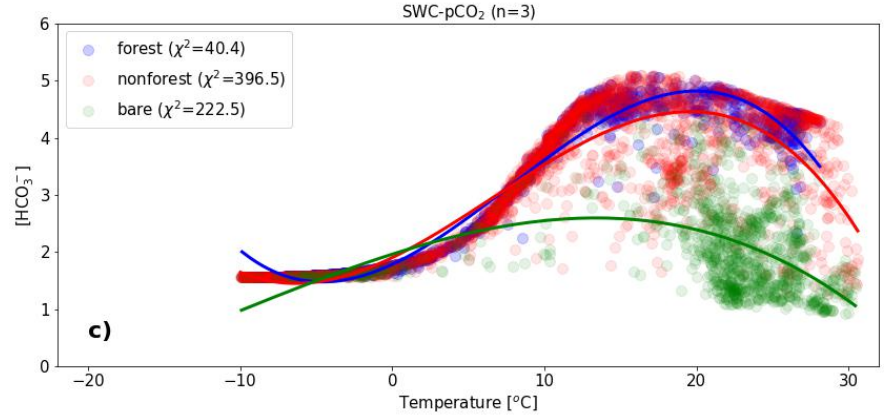

458

459

460 **Fig. 5.** Bicarbonate concentrations as a function of temperature for the three main land-cover types (forest,
461 non-forest, bare land) against temperature. The soil pCO_2 were separately calculated by **(a)** *NPP-*pCO_2, **(b)**
462 *ET-*pCO_2 and **(c)** SWC-pCO_2. The variable n in the title bar indicates the degree of the fitted polynomial, the
463 least-squares fit for each land-use type is given as χ^2-value.

4.3. The influence of climate on carbonate dissolution intensity

In the past decades, both natural and antropogenic changes in climate has changed the continental weathering processes (Raymond et al., 2008; Gislason et al., 2009). For carbonate minerals, warmer temperatures decrease the solubility of calcite (Dreybrodt, 1988). On the other hand, global warming will enhance soil respiration (Bond-Lamberty et al., 2010). Thus, for carbonate weathering, there is a counterbalancing effect between temperature and soil pCO_2 (Gaillardet et al., 2019). We will address this counter-balancing effect next.

We restrict our discussion to satellite-based *NPP*-CO_2. Fig. 6a shows the latitudinally-averaged variations in [HCO_3^-] for the three-single land-cover types (forest, non-forest, bare land), and the latitudinally-averaged global temperature. It is clear that for all land cover types in the southern hemisphere, [HCO_3^-] decreases towards the equator, while the [HCO_3^-] concentration follows a bell-shape curve occur in the north. For all land cover types, [HCO_3^-] in tropics is lowest, although the pCO_2 for some temperate regions peaks here (see Fig. 2a).

The HCO_3^- variations in non-forest areas present another mode of climate control, as here the [HCO_3^-] concentration is more variable than in forest and bare land areas. For example, between 0°~15°S and 15°N~30°N, in non-forest areas bicarbonate variability correlates with changes in precipitation (Fig. 6b). This variability can possibly be attributed to the strong relationship between herbaceous plant productivity (no clear relation with forest) and water availability (precipitation, soil water). Increasing water supply promotes the *NPP* in the non-forest regions, thus increasing the soil pCO_2. This trend also can be verified by the *SWC* trend in Fig. 2b: The *SWC* curve shows a similar variation as the bicarbonate concentration in non-forest areas for similar latitudinal zones. Thus, our models indicate that climate is the

fundamental driver for carbonate weathering intensity at global scale, especially for a single land-cover ecosystem.

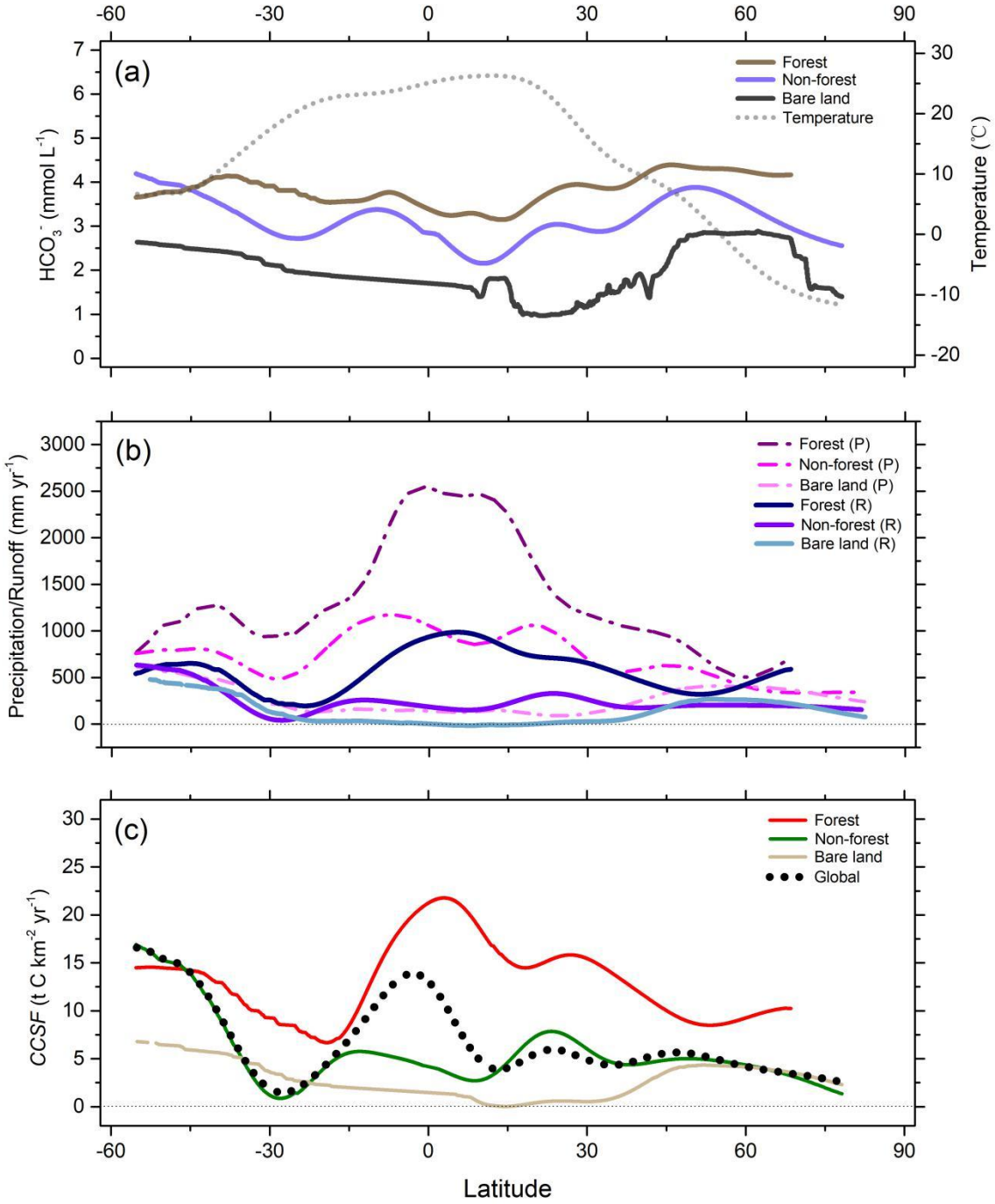

Fig. 6. Global [HCO_3^-], runoff, precipitation and *CCSF* patterns of three main land-cover types (forest, non-forest, bare land). **(a)** Latitudinal [HCO_3^-] of *NPP*-*p*CO_2 vs average surface temperature. **(b)** Latitudinal runoff and precipitation. **(c)** Latitudinal variations of *CCSF*.

4.4. The influence of land use on carbonate dissolution intensity

Naturally-induced climate changes have long been considered as main driver of carbonate weathering, while anthropogenic effects have received less attention. However, recent studies reveal that human activities such as different land-use strategies also have a considerable impact on carbonate weathering (Raymond et al., 2008; Zeng et al., 2017; Macpherson et al., 2019). According to our *NPP*-pCO_2 model results, the global [HCO_3^-] for forest is approximately 4.07 mmol L^{-1}. This value is 31 % higher than for non-forest regions, and almost two times higher than for bare land (Table.1). These differences in [HCO_3^-] are mostly occurring in low latitudes, especially between forest and bare land. The global land-use patterns essentially determine the global [HCO_3^-] concentration, when we consider the soil pCO_2 equations for *NPP*-pCO_2 or *ET*-pCO_2.

In order to further confirm this role and compare the performances of three pCO_2 models, we collect pure carbonate-spring data from 15 publications with different land-cover types across the globe (more details in Appendix Table S1). The land-use information at the different spring sites is either introduced in the publications or can be derived from high-resolution satellite images due to its sizes and boundaries. We restrict ourselves to spring data instead of rivers, because river bicarbonate may be strongly affected by in-stream biological or geochemical processes.

We define several criteria to avoid a contamination of the spring data by other non-carbonic acid and gypsum dissolution processes: (1) the carbonate springs with molar $(Ca^{2+}+Mg^{2+})/SO_4^{2-}$ ratio under 10 are not considered. This removes samples influenced by sulfuric acid and gypsum dissolution. (2) the carbonate springs with high NO_3^- concentration ($(Ca^{2+}+Mg^{2+})/NO_3^- < 5$) are excluded to avoid the impacts of nitric acid (N-fertilizers use). (3) the carbonate springs with higher Na^+ concentrations ($(Ca^{2+}+Mg^{2+})/Na^+ < 10$) are excluded to eliminate samples strongly influenced by silicate weathering.

The locations of the remaining carbonate springs are shown in Fig. 7a. The total carbonate dissolution intensity of these springs is presented as the sum of calcium and magnesium concentrations, [Ca^{2+}+Mg^{2+}] (mmol L^{-1}) to avoid the need to distinguish different carbonate lithologies (Fig. 6b). The [Ca^{2+}+Mg^{2+}] concentration as a function of temperature varies between 1-3 mmol/L, with cropland springs clustering along the lower temperature, and forest springs spreading from lower to higher temperatures. Generally, the carbonate dissolution intensity of forest springs are much higher than grassland, cropland and bare land dominant springs. Forest carbonate dissolution intensity is almost 2-fold higher than that of bare land.

Fitting a polynomial through the data, we obtain a bell-shaped relationship, when considering all land-use types. The peak in this fitted curve occurs at around 15°C, a temperature also found to describe peak carbonate dissolution (e.g. Gaillardet et al., 2019). Next, we compare our three calculated [HCO_3^-] concentrations for the three soil-pCO_2 models with the measured values (Fig. 7c). We relate the proportion of limestone and dolomite of each spring to the Ca^{2+}/Mg^{2+} ratio: For $Ca^{2+}/Mg^{2+} > 2$, we assume limestone dissolution, for $1 < Ca^{2+}/Mg^{2+} < 2$ we assume dolomite. Our results show that the *NPP*-pCO_2 model can better match the observed spring data (R^2=0.70), while the fit of the other two models is lower than expected (R^2<0.5). However, the bicarbonate concentration for some forest springs based on the *NPP*-pCO_2 model predict lower values in tropical areas, while soil SWC-pCO_2-based models perform better in those ecosystems. We speculate that the CO_2 production in the root zone in tropical forests may higher than 75% of the net primary production (the standard value for the NPP model in Gwiazada and Broecker (1993), because of the strong microbial respiration. In contrast, the *SWC*-pCO_2 model prediction performs better than *NPP*-pCO_2 for tropical springs, although the global total correlation is lower. This is consistent with the findings that soil respiration (especially heterotrophic respiration) has a better relationship

with *SWC* than *NPP* in tropical ecosystem (Tang et al., 2020). Yet, for a global scale estimation, the *NPP*-pCO_2 results are more accurate for other regions and ecosystems.

Indeed, previous studies employed temperature, soil moisture and plants productivity as main parameter values to predict global soil respiration. The choice of these parameter values has advantages for certain areas, yet it is suggested that no single parameter can fully explain the global soil respiration individually (Hursh et al., 2017; Warner et al., 2019). At global scale, *NPP* is a great positive predictor of soil respiration, with significant control of the respiration rates within most biomes, except some forested biomes. In contrast, soil moisture is much more important in regulating soil respiration in forest, because soil moisture may help to better reflect the heterotrophic component of soil respiration (Hursh et al., 2017). Thus, the combination of climate, vegetation types, and soil property will ultimately influence the rates of soil respiration. However, soil respiration itself also can not directly be used to calculate [HCO_3^-], because carbonate weathering intensity is controlled by the pCO_2 at the carbonate bedrock surface. Compared with microbial production, the deeper roots of plants are more important for carbonate weathering, because they determine how much CO_2 is transported vertical downwards to the deeper carbonate-rich zone and regulates the recharge and CO_2-carbonate contact at bedrock surface (Wen et al., 2021). The weathering rates without deep roots may be more than an order of magnitude lower than for forest or non-forest land. Thus neglecting this crucial role of plant roots for carbonate weathering will result in soil pCO_2 models overestimating the values for bare land. According to our investigations in the European Alps (Zeng et al., 2021) and in simulation tests in SW China (Zeng et al., 2017), the deep soil pCO_2 values in bare lands (bare rock or bare soil) are very low, which cannot be explained by the respiration rates that are calculated for these models. We speculate that the low values are a result of the absence of deepening roots and the diffusion of soil CO_2.

The [HCO_3^-] of an aquifer is thus determined by the soil pCO_2 at the soil-rock interface, but not the value in the upper soil. Bare land has only few plants with short roots, and its pCO_2 values will decline sharply in deep soils thus weakening the dissolution intensity. Therefore, we suggest the *NPP*-pCO_2 model is more feasible to calculate [HCO_3^-] at global scale, especially for bare lands. Accordingly, we stress that the human land-use/land-cover may play a significant role in controlling global carbonate dissolution intensity and could not be neglected in modelling approach. But we still suggest the future soil pCO_2 models need to synthesize the effects of different environmental drivers (temperature, plants productivity, soil moisture) on climate and land cover.

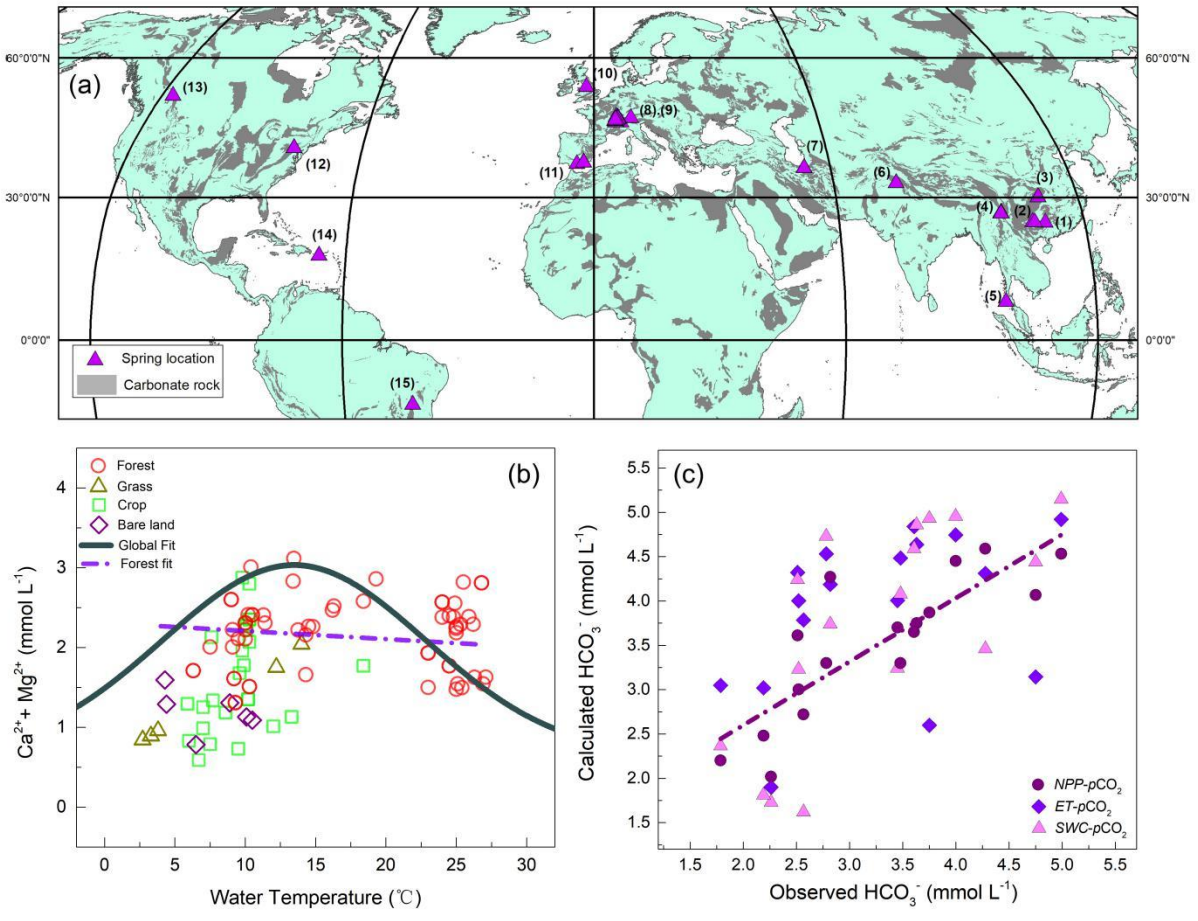

Fig. 7. The comparison between simulated carbonate dissolution intensity (The sum of Ca^{2+} and Mg^{2+} as a proxy) with the global carbonate spring geochemistry records. **(a)** The locations of carbonate rock dominant springs were derived from 15 publications worldwide. (1) Huang et al., 2015. (2) Zeng et al., 2016. (3) Long et al., 2015.

(4) Zeng et al., 2015. (5) Pitman, 1978. (6) Jeelani et al., 2001. (7) Kalantari et al., 2011. (8) Zeng et al., 2020. (9) Calmels et al., 2014. (10) Pentecost, 1992. (11) López-Chicano et al., 2001. (12) Deines and Langmuir, 1975. (13) Ford, 1971. (14) Giusti et al., 1978. (15) Lecomte et al., 2016. **(b)** The $[Ca^{2+}+Mg^{2+}]$ of different land-use dominant carbonate springs against water temperature. The grey fitting curve of global water samples was used the Levenberg-Marquardt algorithm for extreme peak function, and the violet line was the linear regression of all water samples that characterized by forest control. **(c)** The comparison between three simulated HCO_3^- vs the actual observed HCO_3^-.

4.5. The influence of land-use changes and global warming on carbonate dissolution intensity

From our previous work both on field sites and from simulations (e.g. Zeng et al., 2017; Zeng et al., 2020), we found that land-use changes will affect bicarbonate concentration as well as discharge.

We therefore consider a future warming scenario of 5°C, which is accompanied by a change in land use, either from forest to cropland, or from forest to bare land (representing urban sprawl). We calculate the change in carbonate carbon-sink flux (ΔCCSF) from eq. 1, with a constant runoff of N=600 mm/yr, and the bicarbonate concentration [HCO_3^-] derived from eq. 3. As for [HCO_3^-] we need both temperature T and soil-CO_2 pressure, we calculate the latter from eqs. 4, 5, and 6 for the NPP, ET, and SWC models, and assign a temperature change of ΔT=5°C for (a) cold climates (starting with T=5°C), and (b) tropical climates (starting from 20°C). Note that we use a value of 50% of the soil-CO_2 concentration for the cropland scenarios, warranted by our results (see Table 1).

In Fig. 8a, the projected change in carbonate carbon-sink flux is shown for the cold-climate scenario (a) and the tropical-climate scenario (b).

We first focus on the warming effect alone, increasing the temperature by 5°C and keeping the land-use to forest only (solid lines). For the cold climate, ΔCCSF will increase (up to 0.4 t C/yr/km^2), and the increase significantly differs for the three different soil-pCO_2 models. For the tropical scenario, ΔCCSF will decrease slightly.

This warming-only effect, however, is outpaced by a deforestation, creating agricultural expanses instead (cropland, dashed lines). Here, for all soil-pCO_2 models and both cold and tropical regimes, ΔCCSF increases, up to 0.8 t C/yr/km^2 for cold climates, and 0.2 t C/yr/km^2 in tropical regions.

If, instead we promote urban sprawl by the deforestation (dotted lines), the ΔCCSF is decreasing, substantially in the tropics (-0.5 t C/yr/km^2), and less pronounced in cold climates (-0.2 t C/yr/km^2), with the exception of the SWC-soil-pCO_2 model.

The above model experiments confirm our results from the field test site in southwest China (Zeng et al., 2017). Compared with natural land cover, bare rock generates the lowest *CCSF* while cropland produces the highest.

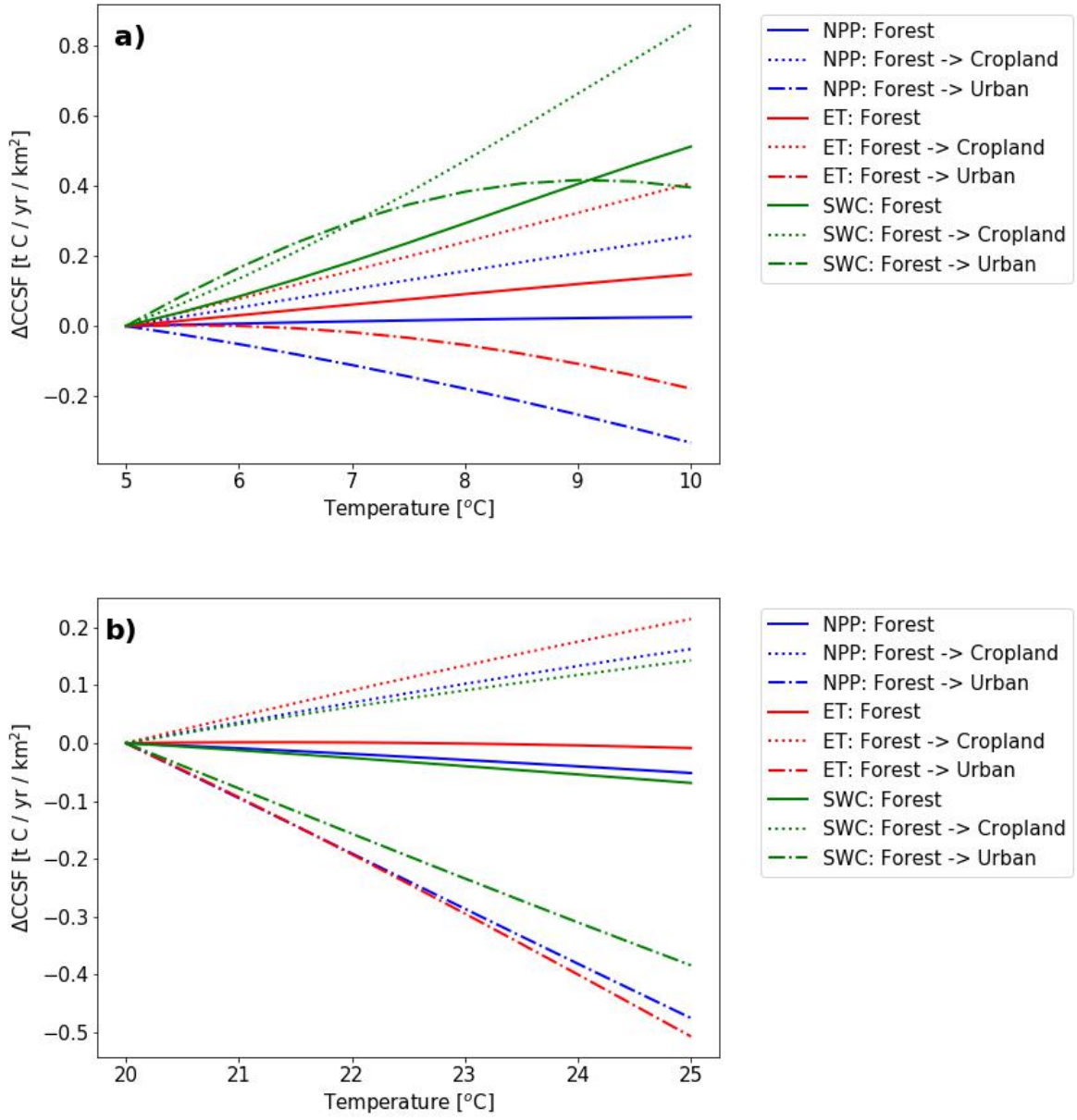

Fig. 8. Change in carbonate weathering carbon sink intensity (Δ*CCSF*) variations under warming conditions (from 5°C to 10°C for cold and 20°C to 25°C for tropical climates) and land-use changes (from forest to either

cropland or urban areas). We assume that each degree of temperature increase will accompany with 20% of forest loss due to human urbanization (forest→ urban) or agricultural expansion (forest→cropland) activities. The scenario with no land-cover change are also presented (forest). The infiltration rate of forest, cropland, bare rock are fixed to 0.35, 0.55 and 0.8 respectively. Precipitation is set to a constant value 600 mm yr^{-1} . Soil volumetric water content for SWC-pCO_2 model is set to 0.17 m^3m^{-3}. The pCO_2 of atmosphere is fixed to 400 ppmv, and the soil pCO_2 of cropland is set to 50% of the forest. Three parameterized soil pCO_2 are calculated by the simplified algorithm introduced by Gaillardet (2019) which depends on temperature only. **(a)** *CCSF* variations under a temperate temperature background. **(b)** *CCSF* variations under a tropical temperature background.

Note that we use saturated carbonate dissolution chemistry, which has been shown to be achieved in different land-use regimes (e.g. Zeng et al., 2017; Zeng et al., 2021). Although during some storm or melting events, HCO_3^- may be highly unsaturated, for a long-term period, however, we find annual [HCO_3^-] of a giving catchment is almost close to the equilibrium value due to the chemo-statistic behavior (Godsey et al., 2009; Zeng et al., 2016; Zeng et al., 2021). Therefore, on account of the significant role of land use in water yield, a better understanding the water balance during land-use conversion is crucial to estimate the *CCSF* variations.

5. Future perspectives of carbonate carbon sinks

On the basis of our global *CCSF* distribution modelling and its relation to environmental drivers, we believe that some regions will have potentially higher dissolution intensity and carbon-sink flux under the impact of global change. The first likely hot-spot is the tropical region. Tropical forests contribute a large proportion of terrestrial carbon storage. These ecosystems were seen as a great potential carbon sink for future global warming mitigation. However, recent studies demonstrate that the future CO_2 removal ability or the so-called CO_2 fertilization effect (Pan et al., 2011) of two largest tropical rainforest regions (Amazon and Africa) have already reached their maximum (Hubau et al., 2020). The carbonate areas in the tropics are mostly covered by forest. Therefore, an accelerating carbonate dissolution rate is unlikely to happen. Yet the plant productivity cannot fully represent the total respiration. Tropical forest ecosystems store a large amount of soil organic carbon. As temperature rises, the microbial respiration may considerably depend on soil water availability. Thus, the variation of HCO_3^- in tropical forest still need further investigation. Besides, some tropical forests are disappearing in recent decades due to the drastic population growth and agricultural expansion (DeFries et al., 2010). We believe that [HCO_3^-] will decline in these areas due to the deforestation. However, the future *CCSF* in the tropics may likely rely on the increasing runoff rather than the decline [HCO_3^-] during the deforestation. The drastic land-use change in low latitudes will lead to a stronger water yield (Piao et al., 2007), and this will overwhelm the declining HCO_3^- trends, amplifying the *CCSF* in tropical cropland (Zeng et al., 2019).

Another hot-spot of this terrestrial carbon sink is likely to occur in the northern ecosystems. Compared to the tropical ecosystems, the soil pCO_2 and HCO_3^- concentration in north high latitudes will likely exhibit a rapid increase due to the global warming and rising

atmospheric CO_2 concentration. The increasing temperature and CO_2 fertilization effect in northern ecosystems will obviously increase the ecosystem productivity, soil respiration and old carbon release (Forkel et al., 2015; Plaza et al., 2019; Tang et al., 2020), thereby enhancing soil pCO_2. Northern ecosystems respiration is more sensitive to temperature increase instead of precipitation or soil-water content (Lamberty et al., 2008; Tang et al., 2020). In the boreal ecosystems, temperature increase will promote the carbonate dissolution. In addition, the melting of glaciers may generate more river discharge, thus amplifying the bicarbonate flux. Recently, the rising continental weathering trends in northern rivers have been already recorded by many studies (e.g. Drake et al., 2018; Gislason et al., 2009). Finally, in order to better predict the carbonate dissolution intensity and related carbon sink flux in the future, we believe that a better understanding of vegetation-soil-water-rock interaction under global change is necessary. Both climatic and anthropogenic factors are intertwined and equally important for the carbonate weathering process and therefore should be considered in the global carbon cycle model.

6. Conclusions

In this paper, we have discussed the results of three soil-pCO_2 models derived from a series of satellite-based databases on carbonate carbon-sink flux. We derived a plausible range for the controlling parameter values for estimating both global carbonate dissolution intensity (HCO_3^- concentration as a proxy) and related carbon sink flux (*CCSF*). Our models reveal two different global carbonate dissolution intensity patterns but obtain similar global mean HCO_3^- concentrations and *CCSF,* ranging from 2.73~2.81 mmol L^{-1} and 4.52~5.36 t C km^{-2} yr^{-1}, respectively. The comparative results indicate that climatic parameters are the fundamental drivers for carbonate weathering, controlling the variation of the HCO_3^- concentration for single-vegetation ecosystems. However, global land-use changes will shape the global HCO_3^- concentration pattern due to the strong coupling between climatic signals and different use scenarios.

We compared selected global carbonate spring records, and we suggest models considering land use/land cover are better suited for a global-scale estimation. More importantly, we suggest that land-use changes are a multi-step controlling factor which may further change the *CCSF* by altering water flux. Due to the influences of runoff and HCO_3^- concentration on *CCSF,* we suggest the global *CCSF* patterns are mainly depending on runoff but not HCO_3^-. This dependency highlights the significant role of land use. We believe that future land-use change may strongly disturb the carbonate weathering and related carbon sink. Finally, we stress that climatic and anthropogenic factors are equally important in carbonate weathering process and therefore need be considered in predicting the global carbon-cycle model.

715
716 **References**

717 Adams J. M. and Post W. M. (1999). A preliminary estimate of changing calcrete carbon
718 storage on land since the Last Glacial Maximum. *Glob Planet. Chang.* **20**, 243–256.

719 Alekseev A., Alekseeva P., Kalinin P. and Hajnos M. (2018). Soils response to the land use
720 and soil climatic gradients at ecosystem scale: Mineralogical and geochemical data. *Soil*
721 *Tillage Res.* **180**, 38-47.

722 Beaulieu E., Goddéris Y., Donnadieu Y., Labat D. and Roelandt, C. (2012). High sensitivity
723 of the continental-weathering carbon dioxide sink to future climate change. *Nat. Clim.*
724 *Change* **5**, 46-349.

725 Bond-Lamberty B. and Thomson, A. (2010). Temperature-associated increases in the global
726 soil respiration record. *Nature* **464**, 579-582.

727 Brook G. A., Folkoff M. E. and Box E. O. (1983). A world model of soil carbon dioxide.
728 *Earth Surf. Process Landf.* **8**, 79–88.

729 Calmels D., Gaillardet J., and Françoise L. (2014). Sensitivity of carbonate weathering to soil
730 CO_2 production by biological activity along a temperate climate transect. *Chem. Geol.*
731 **390**, 74-86.

732 Chen Z., Auler A. S., and Bakalowicz M. (2017). The World Karst Aquifer Mapping project:
733 concept, mapping procedure and map of Europe. *Hydrogeol J.* **25**, 771-785.

734 DeFries R. S., Rudel T., Uriarte M. and Hansen, M. (2010). Deforestation driven by urban
735 population growth and agricultural trade in the twenty-first century. *Nat. Geosci.* **3**,
736 178–181.

737 Deines P., Langmuir D. and Harmon R. S. (1974). Stable carbon isotope ratios and the
738 existence of a gas phase in the evolution of carbonate ground waters. *Geochim.*
739 *Cosmochim. Acta.* **38**, 1147-1164.

Drake T. W., Tank S. E., Zhulidov A. V., Holmes R. M., Gurtovaya T. and Spencer, R. G. M. (2018). Increasing alkalinity export from large Russian arctic river. *Environ. Sci. Tech.* **52**, 8302–8308.

Dreybrodt W. (1988). Processes in Karst Systems: Physics. Chemistry, and Geology. Springer, Berlin.

Ford D. C. (1971). Characteristics of limestone solution in the Southern Rocky Mountains and Selkink Mountains.*Can. J. Earth Sci.* **8**, 585-609.

Fekete B. M., Vörösmarty C. J. and Grabs W. (2002). High-resolution fields of global runoff combining observed river discharge and simulated water balances. *Global. Biogeochem. Cycles* **16** (15-1-15-10).

Ford D. C. and Williams P. W. (2007). Karst Hydrogeology and Geomorphology. Wiley, London.

Forkel M., Carvalhais N., Rödenbeck C., Keeling R., Heimann M., Thonicke K., Zaehle S. and Reichstein M. (2016). Enhanced seasonal CO_2 exchange caused by amplified plant productivity in northern ecosystems. *Science* **351**, 696–699.

Gaillardet J., Dupré B., Louvat P. and Allegre C. (1999). Global silicate weathering and CO_2 consumption rates deduced from the chemistry of large rivers. *Chem. Geol.* **159**, 3–30.

Gaillardet J., Calmels D., Romero-Mujalli G., Sakarova E. and Hartmann J. (2019). Global climate control on carbonate weathering intensity. *Chem. Geol.* **527**, UNSP 118762.

Giusti E. V. (1978). Hydrogeology of the Karst of Puerto Rico. Washington, DC: U.S Geological Survey.

Gombert P. (2002). Role of karstic dissolution in global carbon cycle. *Glob. Planet. Chang.* **33**, 177–184.

763 Gislason S. R., Oelkers E. H., Eiriksdottir E. S., Kardjilov M. I., Gisladottir G., Sigfusson, B.,
764 Hardardottir J., Torssander P. and Oskarsson N. (2009). Direct evidence of the feedback
765 between climate and weathering. *Earth Planet. Sci. Lett.* **277**, 213-222.
766 Goddéris Y., Williams J. Z., Schott J., Pollard D. and Brantley S.L. (2010). Time evolution of
767 the mineralogical composition of Mississippi Valley loess over the last 10kyr: Climate
768 and geochemical modelling. *Geochim. Cosmochim. Acta* **74**, 6357-6374.
769 Godsey S. E., Kirchner J. W. and Clow, D. W. (2009). Concentration-discharge relationships
770 reflect chemostatic characteristics of US catchments. *Hydrol. Proc.* **23**, 1844–1864.
771 Gwiazda R. H. and Broecker W.S. (1994). The separate and combined effects of temperature,
772 soil pCO_2 and organic acidity on silicate weathering in the soil environment:
773 Formulation of a model and results. *Global Biogeochem. Cycles* **8**,141-155.
774 Hartmann J., West J. A., Renforth P., Köhler P., De La Rocha C. L, Wolf-Gladrow D. A.,
775 Dürr H. H. and Scheffran H. (2013). Enhanced chemical weathering as a geoengineering
776 strategy to reduce atmospheric carbon dioxide, supply nutrients, and mitigate ocean
777 acidification. *Rev. Geophys.* **51**, 113–149.
778 Huang F., Zhang C., Xie Y., Li L. and Cao J. (2015). Inorganic carbon flux and its source in
779 the karst catchment of Maocun, Guilin, China. *Environ. Earth Sci*. **74**, 1079-1089.
780 Huang N., Wang L., Song X. P., Black A., Jassal R.S., Myneni R. B., Wu C., Wang L., Song
781 W., Ji D., Yu S. and Niu Z. (2020). Spatial and temporal variations in global soil
782 respiration and their relationships with climate and land cover. *Sci. Adv.* **6**, eabb8508.
783 Hubau W., Lewis S., Phillips O., Affffum-Baffffoe K., Beeckman H., Cuní-Sanchez A.,
784 Daniels A., Ewango C., Fauset S. and Mukinzi J. (2020). Asynchronous Carbon Sink
785 Saturation in African and Amazonian Tropical Forests. *Nature* **579**, 80–87.

786 Hursh A., Ballantyne A., Cooper L., Maneta M., Kimball J. and Watts J. (2017). The
787 sensitivity of soil respiration to soil temperature, moisture, and carbon supply at the
788 global scale. *Glob. Change Biol.* **23**, 2090-2103.
789 Iversen L. L., Winkel A., Baastrup-Spohr L., Hinke A. B., Alahuhta J., Baattrup-Pedersen A.,
790 Birk S., Brodersen P., Chambers P. A., Ecke F., Feldmann T., Gebler D., Heino J.,
791 Jespersen T. S., Moe S. J., Riis T., Sass L., Vestergaard O., Maberly S. C., Sand-Jensen
792 K. and Pedersen O. (2019). Catchment properties and the photosynthetic trait
793 composition of freshwater plant communities. *Science* **366**, 878-881.
794 Jeelani G., Bhat N. A., Shivanna K. and Bhat M. Y. (2011). Geochemical characterization of
795 surface water and spring water in SE Kashmir Valley, western Himalaya: implications to
796 water-rock interation. *J. Earth Syst. Sci.* **120**, 921-932.
797 Kalantari N., Alizadeh B., Mohammadi A. R., Keshavarzi M. R. (2011). A hydrochemical
798 and Dye- tracing investigation in the Posht-e-Naz Karstic Aquifer, Alburz Mountain,
799 Northern Iran. *J. Mt. Sci.* **8**, 37-45.
800 Lecomte K. L., Bicalho C. and Silva-Filho E. V. (2016). Geochemical characterization in
801 karst basin tributaries of the San Franciscan depression: The Corrente River, Western
802 Bahia, NE-Brazil. *J. S. Am. Earth Sci.* **69**, 119-130.
803 Liu Z., Dreybrodt W. and Wang H. (2010). A new direction in effective accounting for the
804 atmospheric CO_2 budget: Considering the combined action of carbonate dissolution, the
805 global water cycle and photosynthetic uptake of DIC by aquatic organisms.
806 *Earth-science Rev.* **99**,162-172.
807 Long X., Sun Z., Zhou A. and Liu D. (2015). Hydrogeochemical and isotopic evidence for
808 flow paths of karst waters collected in the Heshang Cave, Central China. *J. Earth Sci.* **26**,
809 149-156.

López-Chicano M., Bouamama M., Vallejos A. and Pulido-Bosch A. (2001). Factors which determine the hydrogeochemical behaviour of karst springs. A case study from the Betic Cordilleras, Spain. *Appl. Geochem.* **16**, 1179-1192.

Macpherson G. L., Sullivan P. L., Stotler R. L. and Norwood B. S. (2019). Increasing groundwater CO_2 in a mid-continent tall grass prairie: Controlling factors. *E3S Web of Conferences* 98, 06008.

Pan Y., Birdsey R. A., Fang J., Houghton R., Kauppi P., Kurz W. A. Phillips O. L., Shvidenko A., Lewis S. L., Canadell J. G., Ciais P., Jackson R. B., Pacala S. W., McGuire A. D., Piao S., Rautianinen A., Sitch S. and Hayes D. (2011). A large and persistent carbon sink in the world's forests. *Science* **333**, 988–993

Pentecost A. (1992). Carbonate chemistry of surface waters in a temperate karst region: the southern Yorkshire Dales, UK. *J.Hydrol.* **139**, 211-232.

Piao S., Friedlingstein P., Ciais P., de Noblet-Ducoudré N., Labat D. and Zaehle S. (2007). Changes in climate and land use have a larger direct impact than rising CO_2 on global river runoff trends. *Proc Natl Acad Sci USA* **104**, 15242-15247.

Pitman J. (1978).Carbonate chemistry of groundwater from chalk, Givendale, East Yorkshire. *Geochim. Cosmochim. Acta* **42**, 1885-1897.

Plaza C., Pegoraro E., Bracho R., Celis G., Crummer K.G., Hutchings J.A. Hicks Pries C.E., Mauritz M., Natali S. M., Salmon V. G., Schädel C., Webb E. E and Schuur E. A. G. (2019). Direct observation of permafrost degradation and rapid soil carbon loss in tundra. *Nat. Geosci.* **12**, 627-631.

Raymond P. A., Oh N. H., Turner R. E. and Broussard W. (2008). Anthropogenically enhanced fluxes of water and carbon from the Mississippi River. *Nature* **451**, 449–452.

Raymond P. A. and Hamilto, S. K. (2018). Anthropogenic influences on riverine fluxes of dissolved inorganic carbon to the oceans. *Limnol. Oceanogr.* **3**, 141-155.

Romero-Mujalli G., Hartmann J., Borker J., Gaillardet J. and Calmels D. (2019). Ecosystem controlled soil-rock pCO_2 and carbonate weathering - Constraints by temperature and soil water content. *Chem. Geol.* **527**, 118634.

Tang X., Fan S., Du M., Zhang W., Gao S., Liu, S., Chen G., Yu Z. and Yang W. (2020). Spatial and temporal patterns of global soil heterotrophic respiration in terrestrial ecosystems. *Earth Syst. Sci. Data* **12**, 1037-1051.

Warner D. L., Bond-Lamberty B., Jian J., Stell E. and Vargas R. (2019). Spatial predictions and associated uncertainty of annual soil respiration at the global scale. *Glob. Biogeochem. Cycles* **33**, 1733-1745.

Wen H., Sullivan P. L. Macpherson G. L. Billings S. A. and Li L. (2021). Deepening roots can enhance carbonate weathering by amplifying CO_2-rich recharge. *Biogeosciences* **18**, 55-75.

Yang R., Chen B., Liu H. and Yan H. (2015). Carbon sequestration and decreased CO_2 emission caused by terrestrial aquatic photosynthesis: insights from diurnal hydrochemical variations in an epikarst spring and two spring-fed ponds in different seasons. *Appl. Geochem.* **63**, 248–260.

Zeng C., Liu Z., Yang J. and Yang R. (2015a). A groundwater conceptual model and karst-related carbon sink for a glacierized alpine karst aquifer, Southwestern China. *J. Hydrol.* **529**, 120-133.

Zeng C., Liu Z., Zhao M. and Yang R. (2016). Hydrologically-driven variations in the karst-related carbon sink fluxes: Insights from high-resolution monitoring of three karst catchments in Southwest China. *J. Hydrol.* **533**, 74-90.

Zeng Q., Liu Z., Chen B., Hu Y., Zeng S., Zeng C. Yang R., He H., Zhu H., Cao X., Chen J. and Qu Y. (2017). Carbonate weathering-related carbon sink fluxes under different land

859 uses: A case study from the Shawan Simulation Test Site, Puding, Southwest China.
860 *Chem. Geol.* **474**, 58-71.
861 Zeng S., Liu Z. and Kaufmann G. (2019). Sensitivity of the global carbonate weathering
862 carbon-sink flux to climate and land-use changes. *Nat. Commun*. **10**, 5749.
863 Zeng S., Liu Z., Goldscheider N., Frank S., Goeppert N., Kaufmann G. Zeng C., Zeng Q. and
864 Sun H. (2020). Comparisons on the effects of temperature, runoff, and land-cover on
865 carbonate weathering between different karst catchments: insights into the future global
866 carbon cycle. *Hydrogeol J* **29**, 331-345.

nature COMMUNICATIONS

ARTICLE

https://doi.org/10.1038/s41467-019-13772-4 OPEN

Sensitivity of the global carbonate weathering carbon-sink flux to climate and land-use changes

Sibo Zeng [1], Zaihua Liu [2,3*] & Georg Kaufmann [1*]

The response of carbonate weathering carbon-sink flux (CCSF) to its environmental drivers is still not well understood on the global scale. This hinders understanding of the terrestrial carbon cycle. Here, we show that there is likely to be a widespread and consistent increase in the global CCSF (ranging from + 9.8% (RCP4.5) to + 17.1% (RCP8.5)) over the period 1950–2100. In the coming years the increasing temperature might be expected to have a negative impact on carbonate weathering. However, the increasing rainfall and anticipated land-use changes will counteract this, leading to a greater CCSF. This finding has been obtained by using long-term historical (1950–2005) and modeled future (2006–2100) data for two scenarios (RCP4.5 and RCP8.5) for climate and land-use change in our CCSF equilibrium model. This study stresses the potential role that carbonate weathering may play in the evolution of the global carbon cycle over this century.

[1] Institute of Geological Sciences, Geophysics Section, Freie Universität Berlin, 12249 Berlin, Germany. [2] State Key Laboratory of Environmental Geochemistry, Institute of Geochemistry, CAS, 550081 Guiyang, China. [3] CAS Center for Excellence in Quaternary Science and Global Change, 710061 Xi'an, China. *email: liuzaihua@vip.gyig.ac.cn; georg.kaufmann@fu-berlin.de

There are huge uncertainties in the response of the terrestrial carbon cycle to changing environmental conditions, such as global warming and human intervention[1,2]. A growing body of evidence indicates that contemporary continental weathering processes are sensitively responding to climate change and human activities[3–6]. The carbonate weathering carbon sink, about 0.2–0.7 Gt C yr^{-1}, is an important component of the global carbon budget, accounting for ~7–25% of the estimated terrestrial carbon sink[5,7,8]. The rapid kinetics driving carbonate weathering (reaching equilibrium in three hours under experimental conditions[9]) results in dissolution rates nearly 15 times faster than those of silicate rocks[10], thereby responding quickly to environmental fluctuations. The chemical weathering of carbonate rocks is a complex terrestrial process that is controlled by numerous natural and anthropogenic drivers[5–9]. To summarize and simplify the mixed impacts of all drivers, a generic equation for the carbon-sink flux produced by carbonate weathering can be expressed as[11]:

$$\mathrm{CCSF} = 0.5 \times 12 \times R \times \mathrm{DIC} \quad (1)$$

where CCSF (t C km^{-2} yr^{-1}) is the carbonate weathering carbon-sink flux, R is runoff in m yr^{-1}, and DIC (mmol L^{-1}) is the concentration of dissolved inorganic carbon produced by carbonate weathering; 12 is the molar atomic weight of carbon, and the ratio 0.5 indicates that only one half of the HCO_3^- generated by carbonate weathering is of atmospheric origin[5].

Previous work has highlighted the diverse geochemical, climatic and ecological factors that influence both R and DIC, and thus the CCSF variations, including (amongst others) surface temperature[6], precipitation and runoff[11,12], net primary production of ecosystem and soil CO_2[6,13], carbonate lithologies[12], atmospheric CO_2 concentration[14], soil water content[15] and land-use patterns, and practices[4,16,17]. In natural environments, these factors are tightly interwoven and controlled by climate and land cover[17,18]. Recently, studies on different spatial scales have reported that climate perturbations and human interventions have dramatically changed CCSF over the past few decades. For example, in the Mississippi River basin the increased rainfall, high proportion of cultivated area, water management, and use of lime for fertilization have remarkably enhanced the HCO_3^- export flux, with a nearly +50% increase in the recent decades[4]. In addition, the N-fertilizer uses for agriculture also produced nitric acid which enhanced HCO_3^- flux as a CO_2 source[19]. The HCO_3^- and ground water CO_2 storage of a karst aquifer in Konza Prairie (central USA) displayed synchronous increases during the past 26.5 years, which was attributed to the long-term changes of temperature and land use[16]. In northern high latitudes, two large Russian arctic rivers have experienced major increases (135–180%) in alkalinity due to climate change and anthropogenic impacts during the past 40 years[20]. However, there are also reports of a decline of CCSF in some other regions. For instance, in the typical monsoon region of Southwest China, a model study found that climate change (especially, reduced rainfall) caused a 19% decrease in CCSF during the past 40 years[12]. In sum, although these individual studies have detected regional CCSF perturbations attributed to one or a few environmental drivers, a comprehensive analysis of the overall global CCSF fluctuation in response to all driving factors is still lacking. In particular, to our knowledge no studies have considered the impacts of long-term land-use change on CCSF fluctuations at the global scale. In many areas with intensive human intervention, land-use changes have altered the CCSF by changing the runoff patterns and affecting the soil pCO_2 through changing, amongst others, the productivity and soil properties[17], etc.

Here, we explore the spatiotemporal CCSF variations on global carbonate rock outcrops by constructing a mixed-effect model that considers the interrelated impacts of climate and land-use dynamics. We provide a comprehensive interpretation of environmental impacts on CCSF fluctuations by analyzing the spatialtemporal relationship over a lengthy historical period, 1950–2005. We further predict the response of CCSF to the changes in temperature, precipitation, and land use that are presented in the Coupled Model Intercomparison Project Phase 5 (CMIP5) climate projection, adopting two of its representative scenarios, RCP4.5 and RCP8.5. CMIP5 is trying to predict future climate by estimating the amounts of atmospheric carbon dioxide that will be produced in the future. Different RCPs predicting the radiative forcing achieved by the year 2100 AD range from 2.6 to 8.5 (RCP2.6–2RCP8.5) watts per square meter (Wm^{-2}). Here, RCP4.5 is selected to be representative of the moderate-stabilized emission scenarios (medium CO_2 increase), whereas RCP8.5 represents the more aggressive scenarios (large CO_2 increases). Based on these choices, we attempt to predict the coupled effects of current major shifts in climate and land use on the CCSF fluctuations in the future. We reveal the sensitivity of the CCSF response to the above-mentioned drivers in different latitudinal regions and estimate the role played by carbonate rock weathering in the global carbon cycle over the remainder of this century.

Results

General overview. In this section, we show the results of our CCSF model first at a global scale and then focus on drivers that will vary at broad regional scales. As a first step, soil CO_2 pressure ($pCO_{2(soil)}$) is derived from (3) and ET (evapotranspiration) is based on Eq. (6) (see Methods). Accordingly, we can calculate the calcium equilibrium concentration $[Ca^{2+}]_{eq}$ from Eq. (2) (see Methods), and the R from the difference between precipitation (P) and ET. Next, we extract the $[HCO_3^-]$ and P-ET for each grid cell located on a carbonate outcrop to obtain the CCSF by Eqs. (1) or (7) (see Methods), then sum to obtain the total carbon sink (TCS) budget using Eq. (8) (see Methods). We consider that these results can help us to estimate the feedback of CCSF response to climate and land-use change under the different future scenarios envisioned by CMIP5, thereby evaluating the role that carbonate weathering will play in the global carbon cycle in the future.

Overall fluctuation in $[HCO_3^-]_{eq}$, R, and CCSF. In Fig. 1a, b, we present the overall changes of the two fundamental CCSF drivers, $[HCO_3^-]_{eq}$, and runoff (R), over the full model period. $[HCO_3^-]_{eq}$ displays steadily increasing trends of +2.1–+2.6% from 1950 to 2100. The larger $[HCO_3^-]_{eq}$ increase is found in scenario RCP8.5, with about +0.0006 mmol L^{-1} yr^{-1} (Fig. 1a). The amplitude of global runoff variations, by contrast, is 5.7–8.0 times larger than the $[HCO_3^-]_{eq}$ in the same period (Fig. 1b), with runoff increasing at around +0.18 mm yr^{-2} for the historical period, a finding that is close to other published results[21,22]. For the full period, runoff from carbonate rocks increases around +12.0% (RCP4.5) or +20.9% (RCP8.5). After summing these two drivers by using Eq. (8) (see Methods), we found a widespread and consistent increase in global CCSF, with values around +9.8% (RCP4.5) or +17.1% (RCP8.5) at the end of this century (Fig. 1c). As with runoff, the CCSF increase under RCP8.5 (0.0068 t C km^{-2} yr^{-2}) is higher than under RCP4.5 (0.0043 t C km^{-2} yr^{-2}).

Spatial differences in CCSF and its long-term trend. To determine which areas have experienced significant CCSF changes, particularly the areas that are mainly responsible for the calculated increases, we now consider the different geographical regions. Figure 2a summarizes the spatial annual mean CCSF at the global scale for the historic period. Mean annual CCSF ranges from 0.06 t C km^{-2} yr^{-1} in the arctic regions to

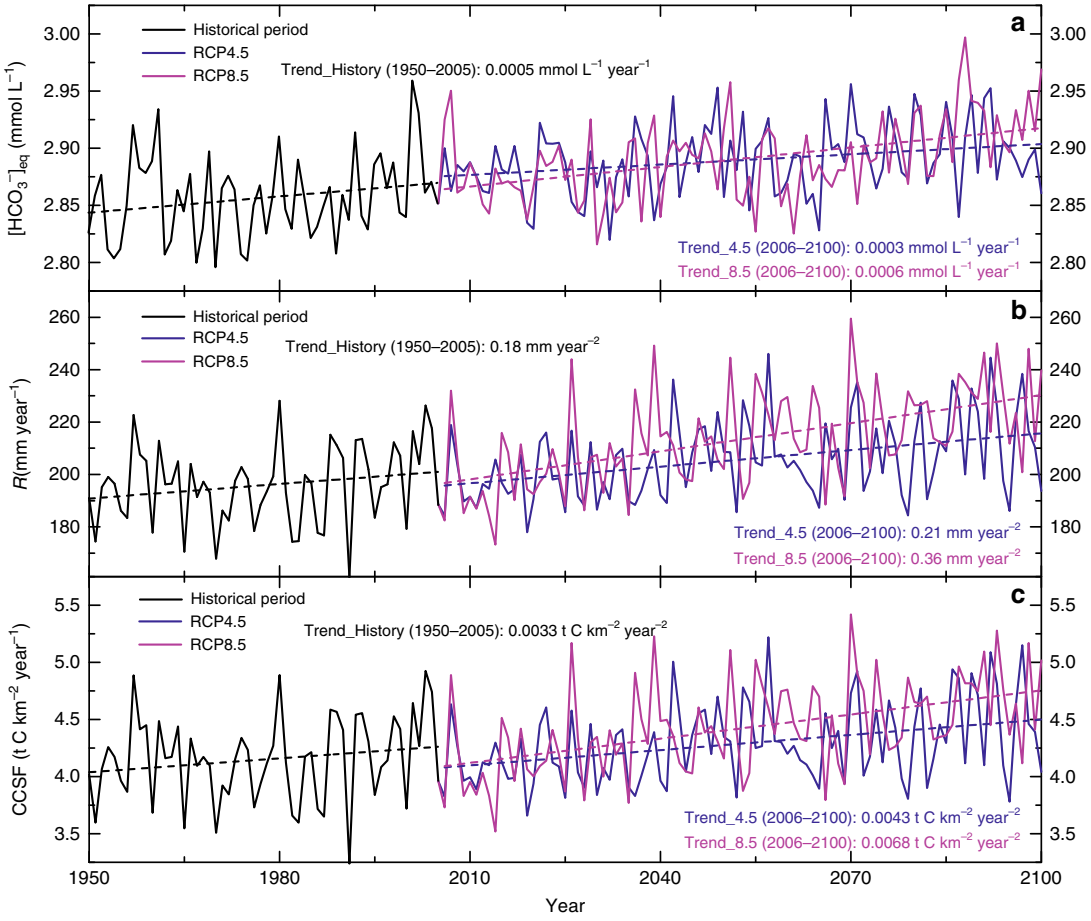

Fig. 1 Interannual changes in relevant variables. a $[HCO_3^-]_{eq}$, **b** *R* (runoff), and **c** CCSF (carbonate weathering carbon-sink flux) on global carbonate rock outcrops during the historical period (1950–2005) and the two future (2006–2100) scenarios (RCP4.5 and RCP8.5). All the variables display increasing trends. The historical period (black line) has the lowest CCSF variation and RCP8.5 (purple line) has the highest, indicating the substantial response of CCSF to dramatic climate change and land-use conversion.

46.42 t C km^{-2} yr^{-1} in and near the equatorial regions. We observe prominent spatial differences, with the highest CCSF occurring in tropical areas and temperate to subtropical humid areas, such as Southwest China, North America, and West Europe, whereas the lowest CCSF occurs mostly in the arctic regions and arid areas, e.g., Central Asia and Saharan Africa. We use spatial linear regression analysis to extend the spatialtemporal CCSF trends of 1950–2005 to 2006–2100. The two RCP scenarios show similar spatial CCSF trends. The strongest CCSF increases occur in most tropical regions and also in North America, West Europe, and Tibet (Fig. 2b, c). The CCSF under RCP8.5 displays similar but stronger increases in most of the areas than does RCP4.5. There are negative effects in the Middle East and North Africa, as these regions experience CCSF decrease due to a drier climate.

Latitudinal change of CCSF, *R*, and $[HCO_3^-]_{eq}$ trends. Next, we consider spatial CCSF changes by summarizing the latitudinal variation trends of soil pCO_2, CCSF, *R*, and $[HCO_3^-]_{eq}$ (Fig. 3). This approach can help us to get a better understanding of how the regional CCSF responses to climate and land-use change may differ during the two periods (historical, and future under RCP4.5 and RCP8.5). As shown in Fig. 3a, the soil pCO_2 increasing trends in high latitudes are generally higher than those in the low latitudes. RCP8.5 scenarios show a larger pCO_2 increase. Figure 3b demonstrates the modelled $[HCO_3^-]_{eq}$, which shows consistent increasing trends in cool and humid regions, such as the mid and high latitudes, but decreasing trends in lower latitudes. The more dramatic climate and land-use change scenario of the future (RCP8.5) results in a stronger negative $[HCO_3^-]_{eq}$ trend in low latitudes, and a more positive trend in high latitudes (−0.0005 mmol L^{-1} yr^{-1} versus 0.0025 mmol L^{-1} yr^{-1}). In contrast, runoff shows rising trends generally, especially at low latitudes under the two RCP scenarios (Fig. 3c), where there is a high proportion of land-use change from forest to crop. The latitudinal CCSF variation as shown in Fig. 3d behaves like the runoff changes, showing an increase in low latitudes and being 2.85–6.25 times greater than in high latitudes. Although $[HCO_3^-]_{eq}$ concentrations in high latitudes will experience dramatic increases, the CCSF variations in these regions are less significant when compared to their values in low latitudes. The southern mid latitudes are interesting regions, as here the changes are considerable. However, due to the small proportion of carbonate rock outcrops there (1.6%), those changes are less important for the global carbon-sink budget.

Discussion

From the Results section above, we have found that the coupling between natural and anthropogenic factors in different latitudinal zones results in large differences in the regional CCSF response. Thus, a better understanding of the sensitivity of carbonate weathering carbon flux to its different environmental drivers is crucial for estimating the role of CCSF in the global carbon cycle in the future. Therefore, the causes of CCSF variations under the climate and land-use change in different areas will be explored next.

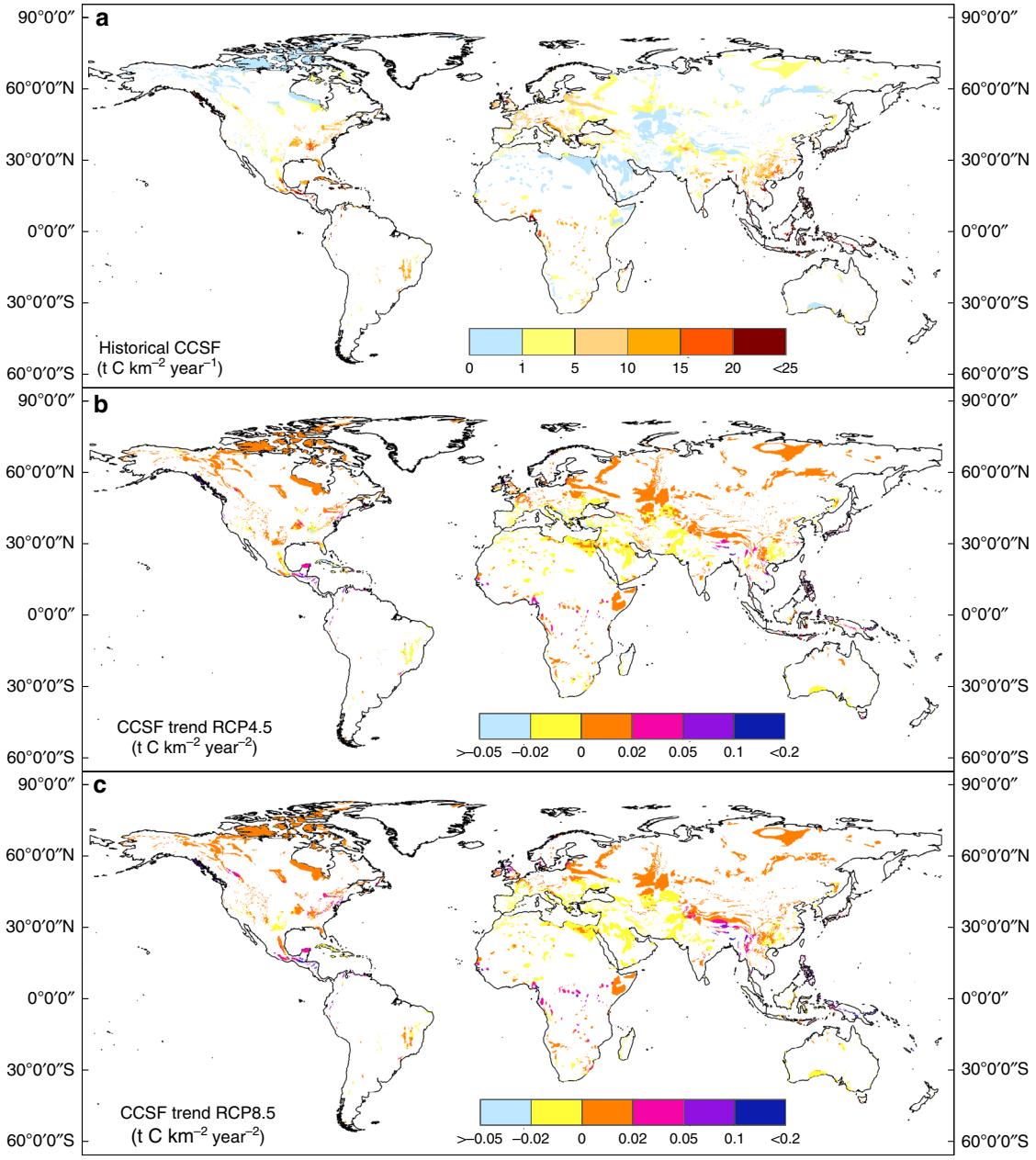

Fig. 2 Spatial distribution of CCSF and its changes. a Annual average CCSF (carbonate weathering carbon-sink flux) in carbonate rock outcrops for the historical period (1950–2005) and its changes for the two differing climate and land-use change scenarios, **b** RCP4.5, and **c** RCP8.5. Note: nearly 72% of carbonate rock outcrop is distributed in the mid and high latitudes (30°–90°) and less in the low latitudes (0°–30°).

First, we made a comparison of modelled CCSFs with observed global data. The aim here is to test the accuracy of our model estimates of CCSF changes in the different climatic and land-use patterns around the world. Table 1 compares our results to other studies to check reliability. Our modelled CCSF variations are in good agreement with a variety of independent carbonate weathering carbon-flux estimates around the world, including those from the full range of latitudinal zones and with distinct climate and land-use conditions: the difference (error) is generally <10%. Accordingly, we judge that our model reliably predicts spatial CCSF differences and can be used for future estimation.

If our global mean CCSF (4.3 t C km^{-2} yr^{-1}) is applied to the global carbonate area (i.e., ~50% of the continent surface[5]), we obtain a total annual global carbon sink of 0.32 Gt C yr^{-1}.

Temperature is a fundamental controlling factor in carbonate weathering as demonstrated by many studies[6,9,15]. Generally, it is found that [HCO_3^-] variation is highly sensitivity to temperature, reaching maximum values in the temperature range (10–15 °C), i.e., both very low and high temperatures will limit carbonate weathering[6,15]. This behavior is a result of competition between thermodynamic control of the weathering and the variability of soil CO_2 production by soil biota[6,15]. [HCO_3^-]$_{eq}$ will be positively correlated to temperature below 15 °C (Fig. 4a). In the inter-tropical zone, the warm temperatures may considerably decrease the [HCO_3^-]$_{eq}$. This is confirmed by inspecting the latitudinal trends of [HCO_3^-]$_{eq}$. For instance, the strongest warming trends (+0.015 °C yr^{-1} to +0.023 °C yr^{-1}) in high latitudes will significantly increase the [HCO_3^-]$_{eq}$ there. In contrast, rising temperatures in low latitudes will limit the carbonate dissolution, which results in a negative [HCO_3^-]$_{eq}$ trend (Fig. 3b). However, according to our results, latitudinal [HCO_3^-]$_{eq}$ variations do not always follow temperature variations alone. The impacts of

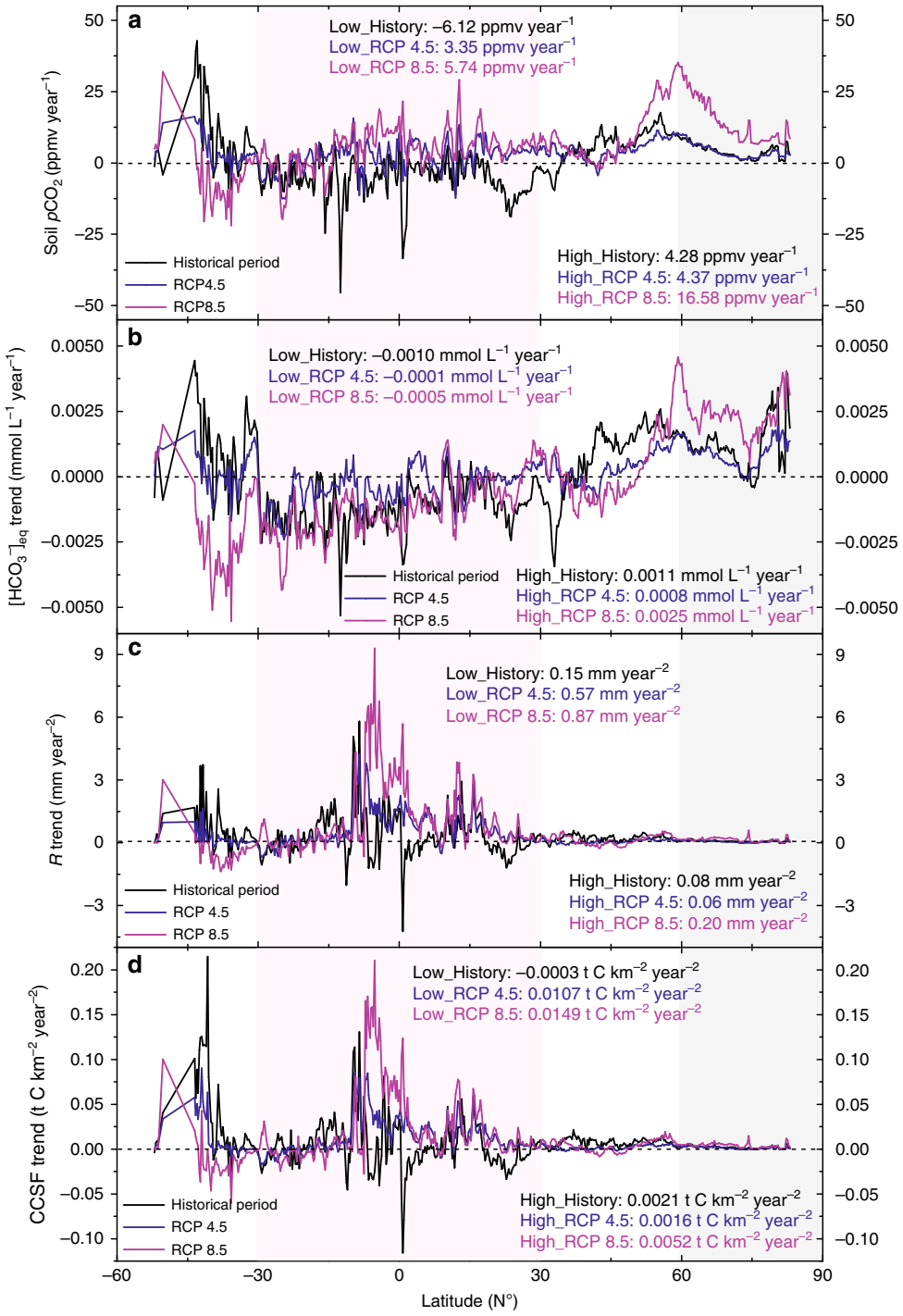

Fig. 3 Latitudinal distribution of relevant variable trends. a Soil pCO_2, **b** $[HCO_3^-]_{eq}$, **c** R (runoff), and **d** CCSF trends for three cases (the historical period, and the future period for RCP4.5 and RCP8.5). The shaded areas are the northern high latitudes (60°N–90°N, light gray) and the low latitudes (30°S–30°N, light pink).

changing precipitation and land use control soil pCO_2 distribution (Fig. 4d). Discussed together with temperature, these factors are also equally significant and therefore control the actual global $[HCO_3^-]_{eq}$ distribution (Fig. 4b, c). For example, we observe three $[HCO_3^-]_{eq}$ peaks on the global graph (Fig. 4a). Two of them are not located in the theoretical region of maximum dissolution (10–15 °C), a feature that has not received much attention. We argue that the higher $[HCO_3^-]_{eq}$ in these regions is mainly caused by changes in land-use patterns (Fig. 4c), soil pCO_2 (Fig. 4d), and increased precipitation (Fig. 4b).

According to our analysis, the CCSF fluctuations are strongly depending on the runoff, rather than on $[HCO_3^-]_{eq}$ or temperature (Figs. 1–3) alone. Precipitation, temperature, and vegetation cover are key factors that control runoff in many models (Fig. 4) and thus also CCSF variations.

We employ long-term spatial regression analysis to detect relationships between CCSF and the variables, runoff, and equilibrium HCO_3^- concentration. Figure 5 compares the individual impacts of $[HCO_3^-]_{eq}$, and R on the annual CCSF fluctuations. The results show that the regional variations of CCSF were

Table 1 Comparison of CCSF between our modelled results and other studies in different latitudinal zones with different climate and land-use conditions.

Location	Latitudinal zone (low/mid/high)	T (°C)	P (mm yr^{-1})	Main land-use type	CCSF (t C km^{-2} yr^{-1}) in other study	This study
Guizhou	Low	15	1225–1425	Forest/crop/grass	7.86–10.90(1)	7.63–11.16
Xijiang	Low	14–22	800–1200	Forest/crop/grass	7.31(2)	7.30
Kikori	Low	21	4330	Forest	29.36(3)	29.19
Thailand	Low	26	3168	Forest	42.30(4)	40.60
Puerto Rico	Low	24	2100	Forest/grass/crop	19.77(5)	28.24
Florida	Low	21.1	1336	Forest	9.49–10.05(6)	11.04
Slovenia	Mid	6–11	800–3000	Forest/grass/crop	15.16–32.89(7)	16.49–26.76
Southern Alps	Mid	9	1300	Forest	11.91(8)	11.58
Siberia	High	−7 to −14	250–400	Forest/non forest	1.52–2.15(9)	1.49–3.30
Mackenzie	High	−1	250–1500	Forest/non forest	4.94(10)	3.44

References: (1) Zeng et al.[11]; (2) Xu and Liu[38]; (3) Ferguson et al.[39]; (4) Pitman[40]; (5) Giusti[41]; (6) Moore et al.[42]; (7) Szramek et al.[43]; (8) Sarazin & Ciabrini[44]; (9) Huh et al.[45]; and (10) Millot et al.[46]. Note: the higher CCSF cited for the Mackenzie River basin in northern Canada may be due to sulfide oxidative weathering[46] contributing to the carbonate weathering, which does not contribute to the carbon sink but is possibly a CO_2 source

typically driven by trends in runoff (global mean $R^2 > 0.95$, $P < 0.001$) but not $[HCO_3^-]_{eq}$. The substantial variability of CCSF is responding to differing runoff, as noted also in other studies[11,12]. The reason why CCSF is more sensitive to runoff than to $[HCO_3^-]$ has been attributed chiefly to the chemostatic behavior of the latter[11].

To better explain the dominant control of this behavior, we divide global CCSF variations into three latitudinal zones (0°–30°, 30°–60°, and 60°–90°) with different mean temperatures, as shown in Fig. 6. $[HCO_3^-]$ shows a significant positive relationship with CCSF only for the high latitudes (60°–90°), while the correlation declines towards the equator (Fig. 6a). Runoff, however, shows a significant ($R^2 > 0.96$, $P < 0.001$) positive relationship with CCSF across all latitudinal zones (Fig. 6b). More importantly, it is noticed that when the $[HCO_3^-]_{eq}$ decreases in low latitudes due to global warming, the accompanying increase in runoff overwhelms the temperature effect, leading to net increases in CCSF. Therefore, based on the results of our model, we suggest that global CCSF variations are highly dynamic and mainly determined by the hydrological cycle (runoff).

For a long time human activities were not considered in global carbonate weathering models. However, recent studies[4,11,17] have found that land use does play a significant role in CCSF control and should be considered in carbon-sink models. On the one hand, consideration of land use can help us to explain why similar climate conditions present highly scattered $[HCO_3^-]_{eq}$ distributions in different datasets[6,15]. As indicated in Fig. 4, the latitudinal $[HCO_3^-]_{eq}$ curves should show similarities to temperature and/or precipitation trends if climatic factors are considered alone. However, we find that the three $[HCO_3^-]_{eq}$ peaks occur in three latitudinal zones (50–70°N, 0–10°S, and 40–50 S°) that have a high proportion of forest cover. Globally, as the proportion of forested areas increase, soil pCO_2 and $[HCO_3^-]_{eq}$ increases. In contrast, when grass and crop cover increase, soil pCO_2 and $[HCO_3^-]_{eq}$ decreases (Fig. 4c, d). Land-use change can also dramatically alter water balances. In northern high latitudes where precipitation is low and forest cover is high, runoff (R) decreases sharply (Fig. 4e–g). In contrast, the increasing cropland area in low latitudes drastically increases net runoff. Based on our simulation, the role of land-use change will be even more important in the future. From 2006 to 2100, cropland proportion in low latitudes will increase by a factor of two (from 8% to 16%), resulting in decreased $[HCO_3^-]_{eq}$ and increased runoff. In the historical period (1950–2005), mid and high latitudes dominated the increase of the annual TCS (100%, 7.7×10^4 t C yr^{-1}). During the continuing climate and land-use changes expected in the future (2006–2100), this situation will reverse. Although the carbonate rock outcrops in low latitudes constitute only 28% of the terrestrial carbonate area, the higher sensitivity of CCSF to climatic and anthropogenic changes in these areas in the future will contribute 61-68% of the TCS increase (5.6×10^4 t C yr^{-1} to 8.1×10^4 t C yr^{-1}). More importantly, the drastic land-use transition (mainly to agricultural land use following deforestation) will contribute 42–50% of total TCS increase in spite of the $[HCO_3^-]_{eq}$ decline. Therefore, we stress that the CCSF shows great sensitivity to anthropogenic impacts. Human land-use activities will significantly alter the CCSF and are as important as climatic drivers in certain areas.

The global annual average temperature in carbonate regions in the historical period (1950–2005) was 17 °C, which already exceeded the temperature range for maximum carbonate dissolution (Fig. 4a). If global warming continues in the future, the higher global mean temperatures will constrain carbonate weathering. In low latitudes, although the climate change will promote the soil CO_2, land-use transitions to agriculture after deforestation in this warming background will decrease $[HCO_3^-]_{eq}$ in the future. Carbonate weathering will show less sensitivity to the overheated environment in these regions. Our results find that increasing precipitation will offset the negative impacts of temperature and deforestation there. In the future, we believe that the CCSF fluctuations will become larger, sensitively responding to climate and land-use changes, and the increasing carbonate weathering flux from terrestrial waters to oceans may promote the biological carbon consumption by organisms in these systems[5,23]. Therefore, this increasing flux can be a considerable carbon sink that against the rising atmospheric CO_2 concentration in the future, potentially become a negative feedback to global warming.

Our model still needs some improvements for future studies. For example, a growing body of evidence finds that the elevated CO_2 in the atmosphere (CO_{2atm}) will affect the primary productivity of ecosystems by the so-called CO_2 fertilization effect[24]. Rising CO_{2atm} will also alter the soil CO_2 and water balances, and thus impact CCSF: it must be considered in global carbon-sink modeling. In addition, land-use change can prompt changes in subsurface flow paths and mineral water interaction, thus the resultant fluxes of solutes from landscapes. Given thermodynamic controls on carbonate weathering, water fluxes through the landscape will have the biggest control on $[HCO_3^-]_{eq}$, which need to be accounted for in land-use change dynamics. Meanwhile, anthropogenic N and S inputs from use of fertilizers[19] or

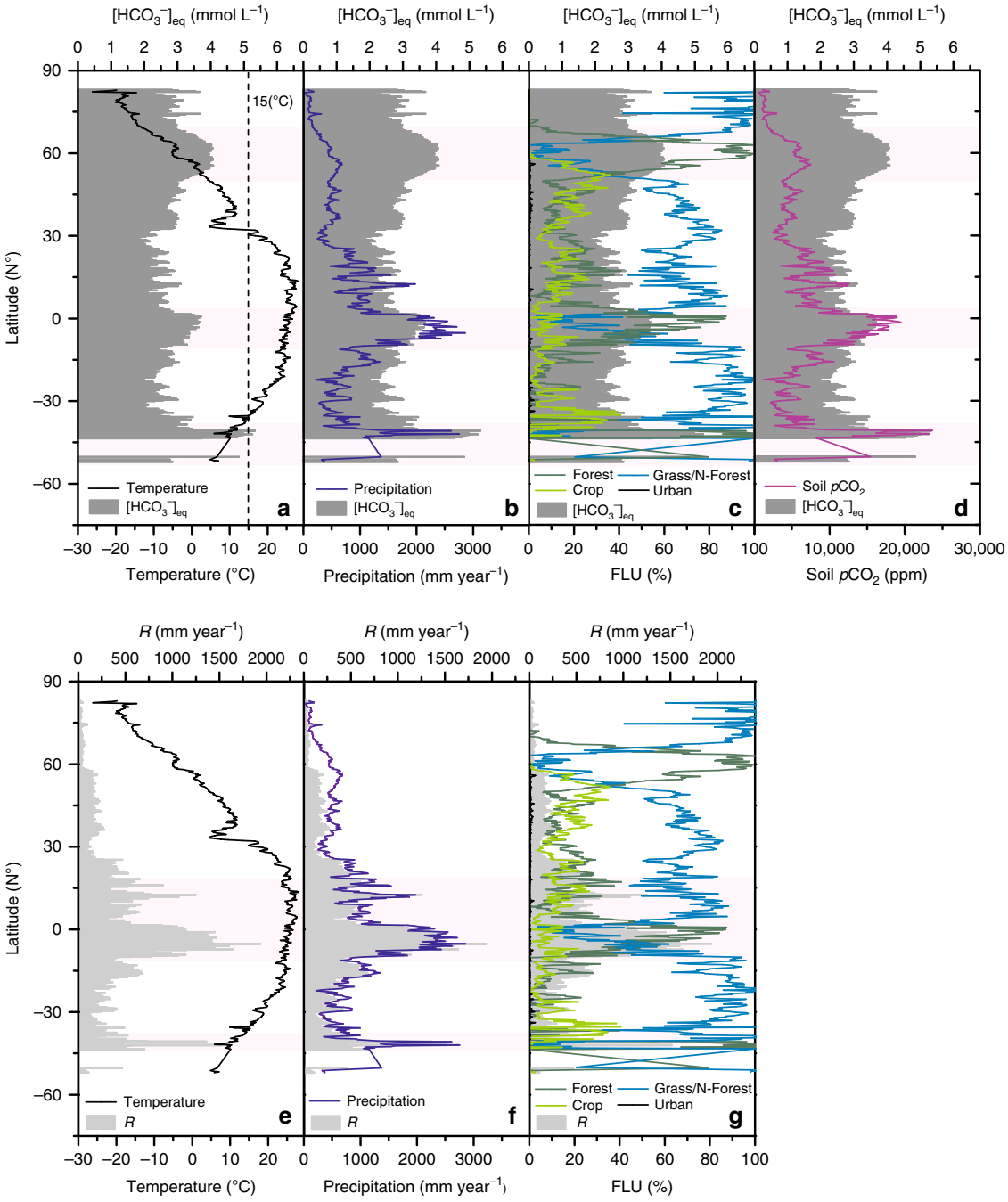

Fig. 4 Latitudinal variations of relevant variables. $[HCO_3^-]_{eq}$ (dark-shaded area in **a**–**d**) and *R* (runoff, light-shaded area in **e**–**g**) in relation with mean temperature (black line in **a** and **e**), mean precipitation (blue line in **b** and **f**), land-use type (multicolor lines in **c** and **g**), and soil pCO_2 (purple lines in **d**) in the historical period (1950–2005). Three $[HCO_3^-]_{eq}$ peaks occur in three latitudinal zones (50–70 °N, 0–10 °S, and 40–50 S°). The dashed line in **a** is the upper temperature limit (15 °C) for maximum carbonate dissolution. The highest runoff (*R*) can be found in the tropical zone and the area close to 40 °S.

coal combustion[25] have become additional drivers of carbonate weathering. The carbonate dissolution produced by nitrate or sulfuric acids will lead to increased $[HCO_3^-]_{eq}$ as a CO_2 source. For example, Perrin et al.[19] found this CO_2 source by nitric acid due to agriculture contribution is not negligible, since it could reach 6–15% of CO_2 uptake by natural silicate weathering and could consequently partly counterbalance this natural CO_2 sink. However, to give an estimate of this flux in the future may be difficult, which is out of the focus of this contribution.

In this study, we have assembled a new model to explore spatialtemporal global CCSF fluctuations over the historical period, 1950–2005, and extended it to the end of this century 2100 AD. Besides natural fluctuations in temperature and carbondioxide concentration, anthropogenic land-use changes have been considered. The results show that there will be widespread and consistent increases in global CCSF, ranging from +9.8% (RCP4.5) to +17.1% (RCP8.5), that are chiefly due to increasing runoff (+12% to +20.9%) and $[HCO_3^-]_{eq}$ (+2.1% to +2.6%). For the full period, 1950–2100, due to the increased runoff caused by both land-use transition and increasing rainfall, CCSF variations in low latitudes are expected to become the largest. Although the low latitudes contain only 28% of terrestrial

carbonate rock outcrops, the CCSF increase here accounts for 61–68% of the TCS in the future. The warming trend in mid and high latitudes will accelerate the carbonate dissolution but the total impact is less important. In future, the increase of runoff will dominate CCSF increases, due to the chemostatic behavior of HCO_3^-. Global warming, by contrast, will lead to lower $[HCO_3^-]_{eq}$ in tropical regions due to the warmer temperatures. However, land-use changes and the accompanying rise in water flux could well counteract this impact, leading a higher net CCSF. Our study highlights the significant role of land-use change in global CCSF variation, which needs to be considered in future global CCSF models.

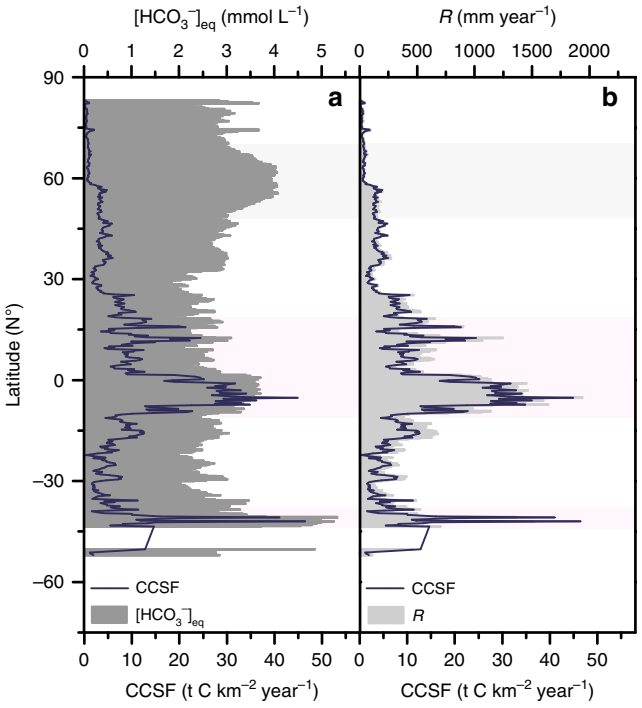

Fig. 5 Latitudinal CCSF variation with relevant variables. CCSF (carbonate weathering carbon-sink flux, blue line in **a** and **b**) in relation to **a** $[HCO_3^-]_{eq}$ (dark grey-shaded area) and **b** *R* (runoff, light-gray shaded area) in the historical period (1950–2005). CCSF shows a significant positive relationship to runoff (*R*) across all latitudes.

Methods

Selection of database. To simulate the CCSF fluctuations from the historical period to the end of this century, we use a long-term statistical climate dataset from the NASA Earth Exchange Global Daily Downscaled Projections (NEX-GDDP) CMIP5 archive (Coupled Model Intercomparison Project Phase 5). This estimates spatiotemporal variations in climate change[26], including a global dataset of reconstructed (1950–2005) historical precipitation, maximum and minimum near-surface temperatures, and future predictions (along the concentration pathways, RCP4.5 and RCP8.5, from 2006 to 2100). We calculate the mean temperature by using the average value of daily maximum and minimum temperatures. From the NEX-GDDP model suite, we select the Earth System Model of the Geophysical Fluid Dynamics Laboratory (GFDL-ESM2M), National Oceanic and Atmospheric Administration (NOAA), which is one of the most robust models considering interactions between each sphere.

Land-use harmonization products provided by the IPCC Fifth Assessment Report give opportunities for estimating the impacts of a wide range of land-use trends on long-term terrestrial ecosystem processes[27]. The land-use harmonization dataset (LUH; http://luh.umd.edu/data.shtml) provides the annual land-use grid dataset from a long-term historical period and also provides the future land-use predictions under the different RCP scenarios (CMIP5). The fraction of each land-use type is described on a 0.25° grid in the LUH report, with the historical reconstruction period and four land-use change scenarios for future predictions. We choose the two representative concentration pathways, RCP4.5 and RCP8.5, which correspond to the NEX-GDDP climate data. LUH provides seven land-use types (primary forest, secondary forest, pasture, crop, primary non forest, secondary non forest, and urban) and we reclassified each LUH land-use report into five different broad land cover types (forest, grass, non forest, crop, and urban) in each pixel.

For the spatial distribution of global carbonate rock, we use the v3.0 version world map of carbonate rock outcrops provided by the Geography and Environmental Science Department, University of Auckland (http//:www.sges.aukland.ac.nz/sges_research/karst.shtm). This map only displays the outcrop of karstic solid rocks. It does not include carbonate rock types that are covered by later consolidated strata. The carbonate rock types in the natural environment consist chiefly of limestone ($CaCO_3$) and dolostone ($Ca(Mg)CO_3$). Due to the uncertainties of precisely distinguishing limestone from globally less common dolostone in the geological maps, we calculated CCSF by assuming that all carbonate outcrops are calcite in this study.

Atmospheric CO_2 (CO_{2atm}) is also an important factor in the air–water–rock system. We added CO_{2atm} as an additional parameter for both historical and future emissions following the two pathways (RCP4.5 and RCP8.5). The historical CO_{2atm} trends and different future emission prediction data (til 2100) were obtained from Potsdam Institute for climate impact research (http://www.pik-potsdam.de/~mmalte/rcps/index).

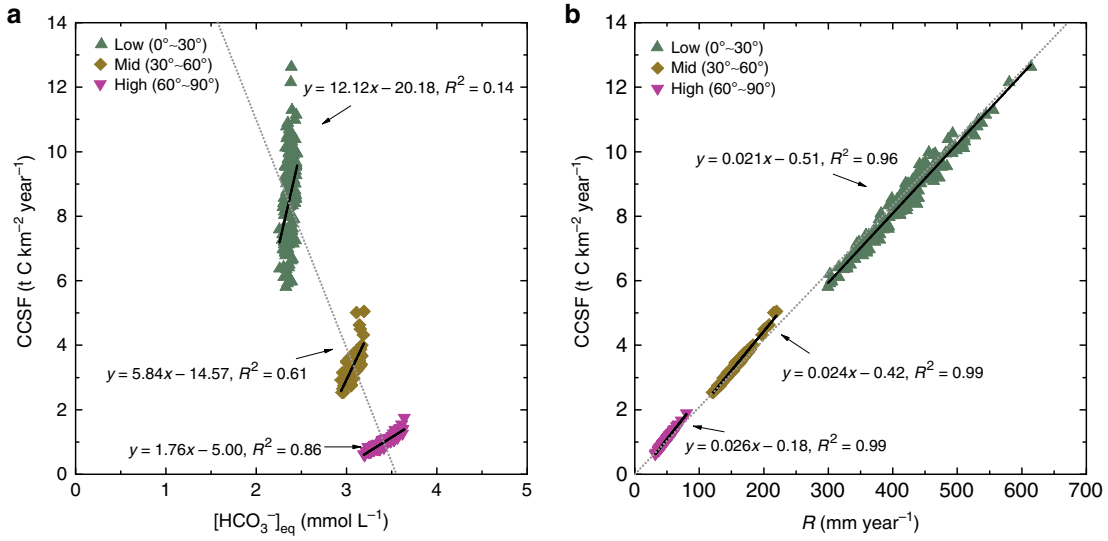

Fig. 6 Relationship between CCSF and relevant variables. a CCSF (carbonate weathering carbon-sink flux) and $[HCO_3^-]_{eq}$, and **b** CCSF and *R* (runoff) in the historical period (1950–2005), normalized into three global latitudinal zones. Runoff dominates the CCSF variation across different latitudinal zones. $[HCO_3^-]_{eq}$ shows a high ($R^2 = 0.86$) positive relation with CCSF only in high latitudes (60°–90°), where runoff is low.

Calculating equilibrium [Ca^{2+}] in a karst system. The calcium equilibrium concentration $[Ca^{2+}]_{eq}$ [mol m^{-3}] for a solution saturated with respect to calcite can be derived to very high accuracy from the analytical expression[9]:

$$[Ca^{2+}]_{eq}^3 = \frac{K_1 K_C K_H}{4K_2 \gamma_{Ca^{2+}} \gamma_{HCO_3^-}^2} pCO_2 \quad (2)$$

where K_1, K_2, K_c, and K_H are the temperature-dependent equilibrium constants for the chemical reactions, γ_{Ca2+} and $\gamma_{HCO3}{}^-$ are the activity coefficients for calcium and bicarbonate, respectively, and pCO_2 (in atm) is the carbondioxide partial pressure[9].

Calculation of pCO_2 for carbonate weathering. CO_2 is a key driving factor for carbonate dissolution. It is present in the atmosphere and will be enhanced by soil respiration. The pCO_2 along the soil–rock or atmosphere–rock interface controls the saturation state of carbonate chemistry for ground water, thereby determining the amount of carbonate that can be dissolved in a karst aquifer[6,9]. In this study, soil pCO_2 is calculated by the method given by the Gwiazada and Broecker[28] and more recently modified by Gaillardet et al.[6], who conclude that CO_2 production by respiration in the root zone (CO_2^{pr} in g C m^2 yr^{-1}) can be assumed to be 75% of the ecosystem net primary production (NPP). Meanwhile, a power function is used to define the pCO_2 profile by solving the complete CO_2 diffusion equation in soil. It is assumed at the basis of the root production zone, the soil CO_2 reaches maximum and becomes constant below this horizon: soil pCO_2 can thus be expressed as a function of atmospheric CO_2 concentration, temperature, and NPP, shown as below[6]:

$$pCO_{2(Soil)} = pCO_{2(atm)} + \frac{A \times 0.75 \times NPP}{T^2} \quad (3)$$

where $A = 1.03 \times 10^6$, a conversion unit constant, pCO_{2atm} is the atmospheric CO_2 pressure in ppmv. NPP is net primary productivity in grams of dry matter per meter square per year (g m^{-2} yr^{-1}), T is the surface temperature expressed in K and $pCO_{2(soil)}$ is the maximum CO_2 pressure reached below the root zone in ppmv. In the original version of Eq. (3), the soil pCO_2 also depends on the mean root depth, soil porosity, and tortuosity[13,28]. However, the rooting depths of global vegetations vary in different plants species. According to the data from 475 soil profiles around the world, the majority of rooting depths among different vegetation types are similar in most regions[29]. As suggested by Schenk and Jackson[29], for predictions on a global scale, it may be undesirable to assign fixed rooting depths to different vegetation types. Moreover, it has been found that the forest, scrub, and grass have a similar soil horizon 50–80 cm that contain 90% of the root biomass[30], and this horizon is matching well with the mean root depth in the soil pCO_2 model, we mentioned above[28]. On the other hand, recent studies show that different land use may have similar soil porosity (forest, cultivated land, and grassland), even after revegetation or deforestation for agriculture activities[31,32]. Human activities may impact the soil porosity at the surface soil layers[31], but may not alter the subsurface soil layers where the soil pCO_2 reaching maximum. Soil tortuosity depends on porosity as found by Jin and Jury[33]. Due to these evidences, we think the recommended soil porosity and tortuosity by Goddéris et al.[13] and Gaillardet et al.[6] are feasible in present research. Here, by using Eq. (3) we estimate the soil pCO_2 differences by NPP. We used the Miami model to calculate NPP in forest ecosystems[34]. The model assumes that the climate limits the vegetation primary production and that NPP increases with both increasing temperature and increasing precipitation:

$$NPP_{(T,P)} = \min\left\{\begin{matrix}\frac{3000}{1+e^{1.315-0.119\times T}} \\ 3000\times\left(e^{-0.000664\times P}\right)\end{matrix}\right\} \quad (4)$$

where NPP is net primary production for ecosystem (NPP is the amount of organic matter in g of dry matter m^{-2}), T [C] is the annual mean surface temperature, and P [m s^{-1}] is the annual mean precipitation. Though recent studies found that the response of NPP to changes in precipitation and temperature varies between ecosystems, the Miami model results are used to obtain a close approximation of NPP values in forest ecosystems, and probably overestimates NPP in non-tree-dominated (grass, shrub, and crop) ecosystems that are largely controlled by precipitation variation and soil water content. In order to quantify the soil pCO_2 differences between different land use/land cover, we employed another model which includes the NPP estimation in ecosystems without trees. This NCEAS model[35] is as follows:

$$NPP_{(non-tree)} = 6116\times\left[1-\exp(-6.05\times10^{-5}\times P)\right] \quad (5)$$

where $NPP_{(non\text{-}tree)}$ is net primary production (g C m^2 yr^{-1}) in non-tree-dominated ecosystems, and P the annual mean precipitation. Due to land-use reclassification in the LUH dataset, we used the NCEAS model to calculate the NPP for grass, non forest, and crop.

The pCO_2 in urban areas is set equal to the atmospheric level due to the absence of soil. In addition, the pCO_{2atm} trends under different RCP scenarios (1950–2100) given by the Potsdam Institute for climate impact research http://www.pik-potsdam.de/~mmalte/rcps/ are integrated into our model. It is assumed to be 320 ppm in 1950 AD according to the existing records. In the 2100, as predicted by RCP4.5 and RCP8.5, pCO_{2atm} will reach 538 ppm and 945 ppm, respectively.

Runoff variation estimation by climate and land-use change. In our prior CCSF modeling studies, long-term runoff changes were calculated by resolving the balance equation between precipitation and evapotranspiration[12]. During the past few decades, the historical global water cycle seems to have strengthened[36]. For a long time, water yield has been mainly considered to depend on natural factors but recent studies have emphasized that anthropogenic factors, such as land-use and land-cover changes can be another factor driving runoff perturbations in areas with major human interventions[21]. Generally, in forest-dominated catchments, the evapotranspiration is higher than in grass-dominated catchments under similar climatic conditions, because of the different water consumption capacities of plants[37]. Agricultural activities and urbanization can also alter the vegetation cover, soil properties and thereby change water yield and runoff patterns. Here, we use the model recommended by Zhang et al.[37] to separately estimate the evapotranspiration of forest and of grass lands. In addition, in order to estimate the hydrological changes of other land-cover/land-use types in the LHU dataset, we additionally introduce three extended models (for crop, non forest, and urban) that are based on the standard function given by Zhang et al.[37]. Our extension functions are based on a three-year water balance study in a karst simulation test site that detects the water yields of five different land uses in karst terrain[17]. The final modified model can be expressed as:

$$ET_{sum} = fET_f + gET_g + nET_n + cET_c + uET_u \quad (6)$$

where ET_{sum} (mm) is the total annual evapotranspiration, f, g, n, c, and u are the ratios of forest, grass, non forest, crop, and urban cover in e ach pixel, respectively (f+g+n+c+u = 1), and ET_f, ET_g, ET_n, ETc, and ET_u (mm) are the corresponding annual evapotranspiration from different land uses.

Maximal potential dissolution method used for CCSF estimate. To obtain the global CCSF variations for long-time periods, we replace R in Eq. (1) by $R = P$-ET, with P the total precipitation (m yr^{-1}) and ET the evapotranspiration (m yr^{-1}). We assume that the total dissolved carbon can be approximated by the bicarbonate alone, [DIC] = [HCO_3^-], which is valid for pH values around 8. In this pH range, reduced electroneutrality states that for each bicarbonate molecule, two calcium atoms are present, thus $[HCO_3^-] = 2[Ca^{2+}]$. Thus, after multiplying Eq. (1) with the atomic mass of carbon, 12 g mol^{-1}, Eq. (1) can be reformulated to the annual CCSF (t C km^{-2} yr^{-1}; refs. [11,12]):

$$CCSF = 12(P - ET)[Ca^{2+}]_{eq} \quad (7)$$

where $[Ca^{2+}]_{eq}$ is the concentration of calcium ion at equilibrium (mol m^{-3}). The annual TCS (t C yr^{-1}) for a given karst area can be calculated by:

$$TCS = 12(P - ET)S[Ca^{2+}]_{eq} \quad (8)$$

where S [km^2] is the land surface area of the carbonate outcrops.

Data availability

The authors declare that the data supporting the findings of this study are publicly available in the web pages provided in the article. The equilibrium model and all relevant data are available from the corresponding author upon request. The source data underlying Figs. 1, 3–6 are provided as a Source Data file.

Received: 22 August 2019; Accepted: 26 November 2019;
Published online: 17 December 2019

References

1. Schimel, D. S. Terrestrial ecosystems and the carbon cycle. *Glob. Change Biol.* **1**, 77–91 (1995).
2. Arora, V. K. & Boer, G. J. Uncertainties in the 20th century carbon budget associate with land use change. *Glob. Change Biol.* **16**, 3327–3348 (2010).
3. Gislason, S. R. et al. Direct evidence of the feedback between climate and weathering. *Earth Planet. Sci. Lett.* **277**, 213–2222 (2009).
4. Raymond, P. A., Oh, N. H., Turner, R. E. & Broussard, W. Anthropogenically enhanced fluxes of water and carbon from the Mississippi River. *Nature* **451**, 449–452 (2008).
5. Liu, Z., Dreybrodt, W. & Wang, H. A new direction in effective accounting for the atmospheric CO_2 budget: Considering the combined action of carbonate dissolution, the global water cycle and photosynthetic uptake of DIC by aquatic organisms. *Earth-Sci. Rev.* **99**, 162–172 (2010).
6. Gaillardet, J., Calmels, D., Romero-Mujalli, G. Z. & Hartmann, J. Global climate control on carbonate weathering intensity. *Chem. Geol.* https://doi.org/10.1016/j.chemgeo.2018.05.009 (2018).
7. Gaillardet, J., Dupre, B., Louvat, P. & Allegre, C. J. Global silicate weathering and CO_2 consumption rates deduced from the chemistry of large rivers. *Chem. Geol.* **159**, 3–30 (1999).
8. Gombert, P. Role of karstic dissolution in global carbon cycle. *Glob. Planet. Change* **33**, 177–184 (2002).
9. Dreybrodt, W. *Processes in Karst Systems* (Springer, Berlin, 1988).

10. Liu, Z., Dreybrodt, W. & Liu, H. Atmospheric CO_2 sink: silicate weathering or carbonate weathering? *Appl. Geochem.* **26**, 292–294 (2011).
11. Zeng, C., Liu, Z., Zhao, M. & Yang, R. Hydrologically-driven variations in the karst-related carbon sink fluxes: Insights from high-resolution monitoring of three karst catchments in Southwest China. *J. Hydrol.* **533**, 74–90 (2016).
12. Zeng, S., Jiang, Y. & Liu, Z. Assessment of climate impacts on the karst-related carbon sink in SW China using MPD and GIS. *Glob. Planet. Change* **144**, 171–181 (2016).
13. Goddéris, Y., Williams, J. Z., Schott, J., Pollard, D. & Brantley, S. L. Time evolution of the mineralogical composition of Mississippi Valley loess over the last 10kyr: Climate and geochemical modelling. *Geochim. Cosmochim. Acta* **74**, 6357–6374 (2010).
14. Andrews, J. A. & Schlesinger, W. H. Soil CO_2 dynamics, acidification, and chemical weathering in a temperate forest with experimental CO_2 enrichment. *Glob. Biogeochem. Cy* **15**, 149–162 (2001).
15. Romero-Mujalli, G. J. & Hartmann, B. Temperature and CO_2 dependency of global carbonate weathering fluxes - Implications for future carbonate weathering research. *Chem. Geol.* https://doi.org/10.1016/j.chemgeo.2018.08.010 (2018).
16. Macpherson, G. L., Sullivan, P. L., Stotler, R. L. & Norwood, B. S. Increasing groundwater CO_2 in a mid-continent tallgrass prairie: controlling factors. *E3S Web Conf.* **98**, 06008 (2019).
17. Zeng, Q. et al. Carbonate weathering-related carbon sink fluxes under different land uses: A case study from the Shawan Simulation Test Site, Puding, Southwest China. *Chem. Geol.* **474**, 58–71 (2017).
18. Beaulieu, E., Goddéris, Y., Donnadieu, Y., Labat, D. & Roelandt, C. High sensitivity of the continental-weathering carbon dioxide sink to future climate change. *Nat. Clim. Change* **5**, 346–349 (2012).
19. Perrin, A. S., Probst, A. & Probst, J. L. Impact of nitrogenous fertilizer on carbonate dissolution in small agricultural catchment: implications for weathering CO_2 uptake at regional and global scales. *Geochim. Cosmochim. Acta* **72**, 3015–3213 (2008).
20. Drake, T. W. et al. Increasing alkalinity export from large Russian arctic river. *Environ. Sci. Tech.* **52**, 8302–8308 (2018).
21. Piao, S. et al. Changes in climate and land use have a larger direct impact than rising CO_2 on global river runoff trends. *Proc. Natl Acad. Sci. USA* **104**, 15242–15247 (2007).
22. Fekete, B. M., Vörösmarty, C. & Grabs, W. High-resolution fields of global runoff combining observed river discharge and simulated water balances. *Glob. Biogeochem. Cycles* **16**, 15–1 (2002).
23. Riebesell, U. et al. Enhanced biological carbon consumption in a high CO_2 ocean. *Nature* **450**, 545–548 (2007).
24. Norby, R. J., DeLucia, E. H. & Gielen, B. Forest response to elevated CO_2 is conserved across a broad range of productivity. *Proc. Natl Acad. Sci. USA* **102**, 18052–18056 (2005).
25. Lerman, A. L., Wu, L. & Mackenzie, F. T. CO_2 and H_2SO_4 consumption in weathering and material transport to the ocean, and their role in the global carbon balance. *Mar. Chem.* **106**, 326–350 (2007).
26. Thrasher, B. et al. Downscaled climate projections suitable for resource management. *Eos Trans. AGU* **94**, 321–321 (2013).
27. Hurtt, G. C. et al. Harmonization of land-use scenarios for the period 1500–2100: 600 years of global gridded annual land-use transitions, wood harvest, and resulting secondary lands. *Climatic Change* **109**, 117 (2011).
28. Gwiazda, R. H. & Broecker, W. S. The separate and combined effects of temperature, soil pCO_2 and organic acidity on silicate weathering in the soil environment: formulation of a model and results. *Glob. Biogeochem. Cycles* **8**, 141–155 (1994).
29. Schenk, H. & J. Jackson, R. B. The global biogeography of roots. *Ecol. Monogr.* **72**, 311–328 (2002).
30. Schulze, E.-D., Mooney, H. A., Sala, O. E., Jobbagy, E. & Buchmann, N. Rooting depth, water availability, and vegetation cover along an aridity gradient in Patagonia. *Oecologia* **108**, 503–5511 (1996).
31. Jiao, F., Wen, Z. M. & An, S. S. Changes in soil properties across a chronosequence of vegetation restoration on Loess Plateau of China. *Catena* **86**, 100–166 (2011).
32. Khaledian., Y., Kiana, F., Ebrahimi, S., Brevik, E. & Aitkenhead-Peterson, J. Assessment and monitoring of soil degradation during land use change using multivariate analysis. *Land Degrad. Dev.* **28**, 128–141 (2016).
33. Jin, Y. & Jury, W. A. Characterizing the dependence of gas diffusion coefficient on soil properties. *Soil Sci. Soc. Am. J.* **60**, 66–71 (1996).
34. Lieth, H. Modeling the primary productivity of the world. In *Primary Productivity of the Biosphere* 237–263 (Springer, Berlin Heidelberg, 1975).
35. Del Grosso, S. et al. Global potential net primary production predicted from vegetation class, precipitation, and temperature. *J. Ecol.* **89**, 2117–2126 (2008).
36. Gedney, N. et al. Detection of a direct carbon dioxide effect in continental river runoff records. *Nature* **439**, 835–838 (2006).
37. Zhang, L., Dawes, W. R. & Walker, G. R. Response of mean annual evapotranspiration to vegetation changes at catchment scale. *Water Resour. Res.* **37**, 701–708 (2001).
38. Xu, Z. & Liu, C. Chemical weathering in the upper reaches of Xijiang River draining the Yunnan-Guizhou Plateau, Southwest China. *Chem. Geol.* **239**, 83–895 (2007).
39. Ferguson, P. R., Dubois, K. D. & Veizer, J. Fluvial carbon fluxes under extreme rainfall conditions: inferences from the Fly River, Papua New Guinea. *Chem. Geol.* **281**, 283–292 (2011).
40. Pitman, J. I. Carbonate chemistry of groundwater from tropical tower karst in south Thailand. *Water Resour. Res.* **14**, 961–967 (1978).
41. Giusti, E. V. *Hydrogeology of the Karst of Puerto Rico,* Vol. 1012 (US Govt. Print. Off, 1978).
42. Moore, P. J., Martin, J. B. & Screaton, E. J. Geochemical and statistical evidence of recharge, mixing, and controls on spring discharge in an eogenetic karst aquifer. *J. Hydrol.* **376**, 443–455 (2009).
43. Szramek, K. et al. Weathering intensity of calcite versus dolomite in carbonate-bearing temperate zone watersheds: carbonate geochemistry and fluxes from catchments within the St. Lawrence and Danube river basins. *Geochem. Geophys. Geosyst.* **8**, Q04002 (2007).
44. Sarazin, G. & Ciabrini, J. P. Water geochemistry of three mountain streams from carbonate watersheds in the Southern French Alps. *Aquat. Geochem.* **3**, 233–265 (1997).
45. Huh, Y., Tsoi, M. Y., Zaitsev, A. & Edmond, J. M. The fluvial geochemistry of the rivers of Eastern Siberia: I. Tributaries of the Lena River draining the sedimentary platform of the Siberian Craton. *Geochim. Cosmochim. Acta* **62**, 1657–1676 (1998).
46. Millot, R., Gaillardet, J., Dupré, B. & Allègre, C. J. Northern latitude chemical weathering rates: clues from the Mackenzie River Basin, Canada. *Geochim. Cosmochim. Acta* **67**, 1305–1329 (2003).

Acknowledgements

We thank Prof. Dr. Derek Ford for insightful comments on previous versions of this manuscript. This study has been financially supported by the National Natural Science Foundation of China (41430753, U1612441, and 41921004) and the Strategic Priority Research Program of Chinese Academy of Sciences.

Author contributions

Z.L. was the leader of the project financially supported by NSFC. G.K. and Z.L. designed the modelling. S.Z. ran the model and wrote the paper.

Competing interests

The authors declare no competing interests.

Additional information

Supplementary information is available for this paper at https://doi.org/10.1038/s41467-019-13772-4.

Correspondence and requests for materials should be addressed to Z.L. or G.K.

Peer review information *Nature Communications* thanks Yves Godderis and other, anonymous, reviewers for their contributions to the peer review of this work. Peer review reports are available.

Reprints and permission information is available at http://www.nature.com/reprints

Publisher's note Springer Nature remains neutral with regard to jurisdictional claims in published maps and institutional affiliations.

Pages 811–821 of Paper 4 are not included in the online version.